

1 **Mid-latitude mixed-phase stratocumulus clouds and their interactions with aerosols:**  
2 **how ice processes affect microphysical, dynamic and thermodynamic development in**  
3 **those clouds and interactions?**

4

5 Seoung Soo Lee<sup>1,2</sup>, Kyung-Ja Ha<sup>2,3,4</sup>, Manguttathil. G. Manoj<sup>5</sup>, Mohammad  
6 Kamruzzaman<sup>6,7</sup>, Hyungjun Kim<sup>8,9,10</sup>, Nobuyuki Utsumi<sup>11</sup>, Youtong Zheng<sup>12</sup>, Byung-Gon  
7 Kim<sup>13</sup>, Chang-Hoon Jung<sup>14</sup>, Junshik Um<sup>15</sup>, Jianping Guo<sup>16</sup>, Kyoung Ock Choi<sup>17,18</sup>, Go-Un  
8 Kim<sup>19</sup>

9

10 <sup>1</sup>Earth System Science Interdisciplinary Center, University of Maryland, College Park,  
11 Maryland, USA

12 <sup>2</sup>Research Center for Climate Sciences, Pusan National University, Busan, Republic of  
13 Korea

14 <sup>3</sup>Center for Climate Physics, Institute for Basic Science, Busan, Republic of Korea

15 <sup>4</sup>BK21 School of Earth and Environmental Systems, Pusan National University, Busan,  
16 Republic of Korea

17 <sup>5</sup>Advanced Centre for Atmospheric Radar Research, Cochin University of Science and  
18 Technology, Kerala, India

19 <sup>6</sup>School of Mathematical Sciences, University of Adelaide, Adelaide, Australia

20 <sup>7</sup>Natural and Built Environments Research Centre, Division of Information Technology,  
21 Engineering and the Environment (ITEE), University of South Australia, Adelaide,  
22 Australia

23 <sup>8</sup>Institute of Industrial Science, University of Tokyo, Tokyo, Japan

24 <sup>9</sup>Moon Soul Graduate School of Future Strategy, Korea Advanced Institute of Science  
25 and Technology, Daejeon, Republic of Korea

26 <sup>10</sup>Department of Civil and Environmental Engineering, Korea Advanced Institute of  
27 Science and Technology, Daejeon, Republic of Korea

28 <sup>11</sup>Nagomori Institute of Actuators, Kyoto University of Advanced Science, Japan

29 <sup>12</sup>The Program in Atmospheric and Oceanic Sciences, Princeton University,  
30 and National Oceanic and Atmospheric Administration/Geophysical Fluid Dynamics  
31 Laboratory, Princeton, New Jersey, USA

32 <sup>13</sup>Department of Atmospheric Environmental Sciences, Gangneung–Wonju National  
33 University, Gangneung, Gang-Won do, Republic of Korea

34 <sup>14</sup>Department of Health Management, Kyungin Women’s University, Incheon, Republic of  
35 Korea

36 <sup>15</sup>Department of Atmospheric Sciences, Division of Earth Environmental System, Busan,  
37 Republic of Korea

38 <sup>16</sup>State Key Laboratory of Severe Weather, Chinese Academy of Meteorological  
39 Sciences, Beijing 100081, China

40 <sup>17</sup>Department of Atmospheric Sciences, Yonsei University, Seoul, Republic of Korea

41 <sup>18</sup>Department of Atmospheric Sciences, University of Washington, Seattle, Washington,  
42 USA

43 <sup>19</sup>Marine Disaster Research Center, Korea Institute of Ocean Science and Technology,  
44 Pusan, Republic of Korea

45  
46  
47  
48

49 Corresponding author: Seoung Soo Lee  
50 Office: (303) 497-6615  
51 Cell: (609) 375-6685  
52 Fax: (303) 497-5318  
53 E-mail: [cumulss@gmail.com](mailto:cumulss@gmail.com), [slee1247@umd.edu](mailto:slee1247@umd.edu)

54

55

56

57

58

59

60

61

62

63

64

65

66

67

68

69

70

71

72

73

74

75

76 **Abstract**

77

78 Mid-latitude mixed-phase stratocumulus clouds and their interactions with aerosols remain  
79 poorly understood. This study examines the roles of ice processes in those clouds and their  
80 interactions with aerosols using a large-eddy simulation (LES) framework. Cloud mass  
81 becomes much lower in the presence of ice processes and the Wegener-Bergeron-Findeisen  
82 (WBF) mechanism in the mixed-phase clouds as compared to that in warm clouds. This is  
83 because while the WBF mechanism enhances the evaporation of droplets, the low  
84 concentration of aerosols acting as ice nucleating particles (INP) and cloud ice number  
85 concentration (CINC) prevent the efficient deposition of water vapor. Note that the INP  
86 concentration in this study is based on the observed spatiotemporal variability of aerosols.  
87 This results in the lower CINC as compared to that with empirical dependence of the INP  
88 concentrations on temperature in a previous study. In the mixed-phase clouds, the  
89 increasing concentration of aerosols that act as cloud condensation nuclei (CCN) decreases  
90 cloud mass by increasing the evaporation of droplets through the WBF mechanism and  
91 decreasing the intensity of updrafts. In contrast to this, in the warm clouds, the absence of  
92 the WBF mechanism makes the increase in the evaporation of droplets inefficient,  
93 eventually enabling cloud mass to increase with the increasing concentration of aerosols  
94 acting as CCN. Here, the results show that when there is an increasing concentration of  
95 aerosols that act as INP, the deposition of water vapor is more efficient than when there is  
96 the increasing concentration of aerosols acting as CCN, which in turn enables cloud mass  
97 to increase in the mixed-phase clouds.

98

99

100

101

102

103

104

105

106

## 1. Introduction

107

108

109 Stratiform clouds such as the stratus and stratocumulus clouds play an important role in  
110 global hydrologic and energy circulations (Warren et al. 1986, 1988; Stephens and  
111 Greenwald 1991; Hartmann et al. 1992; Hahn and Warren 2007; Wood, 2012). Aerosol  
112 concentrations have increased significantly as a result of industrialization. Increasing  
113 aerosols are known to decrease droplet size and thus increase the albedo of stratiform  
114 clouds (Twomey, 1974, 1977). Increasing aerosols may also suppress precipitation and,  
115 hence, alter the mass and lifetime of those clouds (Albrecht, 1989; Guo et al., 2016). These  
116 aerosol effects strongly depend on how increasing aerosols affect entrainment at the tops  
117 of the planetary boundary layer (PBL) (Ackerman et al., 2004) and disrupt global  
118 hydrologic and energy circulations. However, these effects are highly uncertain and thus  
119 act to cause the highest uncertainty in the prediction of future climate (Ramaswamy et al.,  
120 2001; Forster et al., 2007). Most of the previous studies on stratiform clouds and their  
121 interactions with aerosols to reduce the uncertainty have dealt with warm stratiform clouds  
122 and have seldom considered ice-phase cloud particles (e.g., ice crystals) (Ramaswamy et  
123 al., 2001; Forster et al., 2007; Wood, 2012). In reality, especially during wintertime when  
124 the surface temperature approaches the freezing temperature, stratiform clouds frequently  
125 involve ice particles and associated processes such as deposition and freezing. Since  
126 particularly in midlatitudes, stratiform clouds are generally way below the altitude of  
127 homogeneous freezing, in these clouds, liquid and ice particles usually co-exist.

128 The water-vapor equilibrium saturation (or saturation pressure) is lower for ice particles  
129 than for liquid particles. In mixed-phase clouds where liquid- and ice-phase hydrometeors  
130 coexist, when a given water-vapor pressure is higher than the equilibrium pressure for  
131 liquid particles, ice and liquid particles grow together via deposition and condensation,  
132 respectively, while competing for water vapor. When a given water-vapor pressure is lower  
133 than or equal to the equilibrium pressure for liquid particles, ice (liquid) particles can  
134 experience supersaturation (undersaturation or saturation). In this situation, liquid particles  
135 evaporate, while water vapor is deposited onto ice crystals. Water vapor in the air, which  
136 is depleted by the deposition onto ice crystals, is re-supplied by water vapor that is  
137 produced by the evaporation of droplets. The re-supplied water vapor in turn deposits onto

138 ice crystals. In other words, due to differences in the water-vapor equilibrium saturation  
139 pressure between ice and liquid particles, ice particles eventually grow at the expense of  
140 liquid particles. This is so-called Wegener-Bergeron-Findeisen (WBF) mechanism  
141 (Wegener 1911; Bergeron 1935; Findeisen 1938).

142 The occurrence of the WBF mechanism depends on updrafts, humidity, associated  
143 supersaturation and microphysical factors such as cloud-particle concentrations and sizes  
144 (Korolev, 2007). Also, it needs to be pointed out that when the WBF mechanism starts and  
145 how long it lasts depend on how a timescale for updrafts and associated supersaturation is  
146 compared to that for phase-transition processes as a part of microphysical processes  
147 (Pruppacher and Klett, 1978). Korolev (2007) have utilized a parcel-model concept to  
148 come up with conditions of updrafts and microphysical factors where the WBF mechanism  
149 is operative.

150 The evolution of cloud particles as well as their interactions with aerosols is strongly  
151 dependent on thermodynamic and dynamic conditions such as humidity, temperature and  
152 updraft intensity (Pruppacher and Klett, 1978; Khain et al., 2008). Interactions between ice  
153 and liquid particles in mixed-phase clouds, which include the WBF mechanism, change  
154 thermodynamic and dynamic conditions where cloud particles grow. Impacts of these  
155 changes on the development of mixed-phase clouds and their interactions with aerosols  
156 have not been understood well.

157 Over the last decades, numerous studies have been performed to improve our  
158 understanding of mixed-phase clouds by focusing on clouds in the Arctic and over the  
159 Southern Ocean. It has been found that the prevalence of mixed-phase clouds over the  
160 Arctic enables them to have a substantial impact on radiative and hydrologic circulations  
161 (e.g., Shupe et al., 2001, 2005; Intrieri et al., 2002; Dong and Mace, 2003; Zuidema et al.,  
162 2005; Hu et al., 2010; Kanitz et al., 2011; Morrison et al., 2011; Huang et al., 2012). In  
163 addition, Rangno and Hobbs (2001), Lohmann (2002) and Borys et al. (2003) have  
164 proposed not only cloud condensation nuclei (CCN) but also ice nucleating particles (INP)  
165 affect mixed-phase clouds by altering microphysical variables (e.g., number concentrations  
166 and sizes of cloud particles) and dynamic variables (e.g., updrafts). However, Lance et al.  
167 (2010) and Jackson et al. (2012) have indicated that these aerosol effects on mixed-phase  
168 clouds have not been clearly identified due to lack of data of meteorological and cloud

169 conditions in which aerosols influence those clouds. Naud et al. (2014) and Bodas-Salcedo  
170 et al. (2016) have reported that climate models have not been able to represent mixed-  
171 phased clouds and their interactions with aerosols reasonably well and this has been one  
172 important reason why climate models have produced large errors in simulating energy and  
173 hydrologic budgets and circulations. Young et al. (2017) have reported that the  
174 parametrization of ice-crystal nucleation can be a key reason for the misrepresentation of  
175 mixed-phase clouds in models.

176 This study aims to gain a better understanding of mixed-phase stratocumulus clouds  
177 and interactions between those clouds and aerosols. The better understanding enables us to  
178 gain a more general understanding of stratiform clouds and their interactions with aerosols,  
179 which better elucidates roles of clouds and aerosol-cloud interactions in climate. This in  
180 turn provides valuable information to better parameterize stratiform clouds and interactions  
181 for climate models. To fulfill the aim, this study focuses on effects of the interplay between  
182 ice crystals and droplets on those clouds, and interactions of these effects with aerosols  
183 using a large-eddy simulation (LES) Eulerian framework. The LES framework reasonably  
184 resolves microphysical and dynamic processes at turbulence scales and thus we can obtain  
185 process-level understanding of those effects and interactions. Note that with the Eulerian  
186 framework, instead of tracking down individual air parcels, which can be pursued with the  
187 Lagrangian framework, this study looks at updrafts, microphysical factors, phase-transition  
188 processes and their evolution, which are averaged over grid points in a domain, to examine  
189 the overall interplay between ice and liquid particles over the whole domain. Also, in the  
190 LES framework, air parcels go through various updrafts, microphysical factors and  
191 feedbacks between them. Thus, unlike in Korolev (2007), an air parcel in the LES  
192 framework can repeatedly experience conditions where the WBF mechanism does not  
193 work and those where the mechanism works as it moves around three-dimensionally.  
194 Hence, chasing down air parcels in terms of conditions (e.g., updrafts and microphysical  
195 factors) for processes such as the WBF mechanism is enormous task and not that viable.  
196 This motivates us to embrace the approach that adopts the averaged updrafts, microphysical  
197 factors and phase-transition processes to examine the overall interplay between ice and  
198 liquid particles which includes the WBF mechanism. To help this approach to identify the

199 overall interplay between ice and liquid particles clearly, this study utilizes sensitivity  
200 simulations.

201 Mixed-phase stratiform clouds have been formed frequently over the Korean  
202 Peninsula in midlatitudes. These clouds have been affected by the advection of aerosols  
203 from East Asia (e.g., Lee et al., 2013; Oh et al., 2015; Eun et al., 2016; Ha et al., 2019).  
204 However, we do not have a clear understanding of those clouds and impacts of those  
205 aerosols, which are particularly associated with the industrialization of East Asia, on them  
206 in the Peninsula (Eun et al., 2016). Motivated by this, we examine those clouds and effects  
207 of the advected aerosols from East Asia on them over an area in the Korean Peninsula as a  
208 way of better understanding those clouds and aerosol-cloud interactions in them.

209

## 210 **2. Case description**

211

212 A system of mixed-phase stratocumulus clouds was observed in the Seoul area in Korea  
213 over a period between 00:00 LST (local solar time) on January 12<sup>th</sup> and 00:00 LST on  
214 January 14<sup>th</sup> in 2013. The Seoul area is a conurbation area composed of the Seoul capital  
215 city and adjacent highly populated cities. The population of the Seoul area is estimated at  
216 twenty-five million. Coincidentally, during this period, there is advection of an aerosol layer  
217 from the west of the Seoul area (or from East Asia) to it and this lifts aerosol concentrations  
218 in the Seoul area. This type of advection has been monitored by island stations in the  
219 Yellow Sea (Eun et al., 2016; Ha et al., 2019). For this study, the advection is monitored  
220 and identified by comparisons in PM<sub>10</sub> and PM<sub>2.5</sub>, representing aerosol mass, between a  
221 ground station in Baekryongdo island, located in the Yellow Sea, and ground stations in  
222 and around the Seoul area. These stations observe and measure PM<sub>10</sub> and PM<sub>2.5</sub> using the  
223 beta-ray attenuation method (Eun et al., 2016; Ha et al., 2019). PM stands for particulate  
224 matter and PM<sub>10</sub> (PM<sub>2.5</sub>) is the total mass of aerosol particles whose diameter is smaller  
225 than 10 (2.5)  $\mu\text{m}$  per unit volume of the air. In Figure 1, the island and the Seoul area are  
226 included in a rectangle that represents an area of interest in terms of the advection of the  
227 aerosol layer. Figure 2a shows the time series of PM<sub>10</sub> and PM<sub>2.5</sub>, observed and measured  
228 by the ground station on the island and a representative ground station in the Seoul area,  
229 between January 10<sup>th</sup> and 19<sup>th</sup> in 2013 when there is strong advection of aerosols from East



230 Asia to the Seoul area. Around 00:00 LST on January 12<sup>th</sup>, aerosol mass starts to increase  
231 and reaches its peak at 09:00 LST on January 12<sup>th</sup> on the island. Then, there is a subsequent  
232 increase in aerosol mass in the Seoul area, which starts around 05:00 LST on January 12<sup>th</sup>,  
233 and it reaches its peak at 18:00 LST on January 12<sup>th</sup> in the Seoul area due to the advection  
234 of aerosols from East Asia to the Seoul area through the island. Figures 2b and 2c show  
235 observed and measured aerosol mass distribution in the rectangle in Figure 1 at 05:00 LST  
236 and 18:00 LST on January 12<sup>th</sup>, respectively. To construct Figures 2b and 2c, observed and  
237 measured aerosol mass concentrations by the ground stations are interpolated into  
238 equidistant points in the rectangle. Consistent with the time series, there is the high aerosol  
239 mass in and around the island due to the advection of aerosols from the East-Asia continent  
240 at 05:00 LST on January 12<sup>th</sup> (Figure 2b). Then, the advection continues to move aerosol  
241 mass eastward further to the Seoul area, resulting in a subsequent decrease in aerosol mass  
242 in and around the island and an increase in aerosol mass in the Seoul area at 18:00 LST on  
243 January 12<sup>th</sup> (Figure 2c).

244 With the advection of aerosols, there is the advection of meteorological conditions.  
245 To identify this advection of meteorological conditions in the Seoul area, the vertical  
246 distributions of the radiosonde-observed potential temperature and humidity at 03:00 and  
247 15:00 LST on January 12<sup>th</sup> in the Seoul area are obtained and shown in Figure 3. At 03:00  
248 LST on January 12<sup>th</sup> just before when aerosol concentrations start to increase due to the  
249 aerosol advection in the Seoul area, there is a stable layer in the PBL whose top is around  
250 1.0 km (Figure 3a). This stable layer is not favorable for the formation of a deck of  
251 stratiform clouds. However, after 03:00 LST on January 12<sup>th</sup>, the PBL becomes a well-  
252 mixed layer and its top height increases to 1.5 km as seen in comparisons between 03:00  
253 LST and 15:00 LST on January 12<sup>th</sup> in the Seoul area (Figures 3a and 3b). Hence, with  
254 advection-induced increases in aerosol concentrations and the associated advection of  
255 meteorological conditions, meteorological conditions become favorable for the formation  
256 of a deck of stratocumulus clouds in the Seoul area. In this study, we examine how the  
257 advection of aerosols affects the observed mixed-phase stratocumulus clouds in the Seoul  
258 area and impacts of the advection of meteorological conditions on those clouds are out of  
259 scope of this study.

260

### 3. LES and simulations

#### 3.1 LES

As a LES Eulerian model, we use the Advanced Research Weather Research and Forecasting (ARW) model (version 3.3.1), which is a nonhydrostatic compressible model (Michalakes et al., 2001; Klemp et al., 2007). Prognostic microphysical variables are transported with a 5th-order monotonic advection scheme (Wang et al., 2009). Shortwave and longwave radiation is parameterized by the Rapid Radiation Transfer Model (RRTM; Mlawer et al., 1997; Fouquart and Bonnel, 1980). The effective sizes of hydrometeors are calculated in an adopted microphysics scheme and the calculated sizes are transferred to the RRTM to consider effects of the effective sizes on radiation.

To represent microphysical processes, the LES model adopts a bin scheme based on the Hebrew University Cloud Model described by Khain et al. (2011). The bin scheme solves a system of kinetic equations for the size distribution functions of water drops, ice crystals or cloud ice (plate, columnar and branch types), snow aggregates, graupel and hail, as well as CCN and INP. Water drops whose size is smaller than  $80\ \mu\text{m}$  in diameter are classified to be cloud droplets (or cloud liquid), while drops whose size is greater than  $80\ \mu\text{m}$  in diameter are classified to be rain drops (or rain). Each size distribution is represented by 33 mass doubling bins, i.e., the mass of a particle  $m_k$  in the  $k$ th bin is determined as  $m_k = 2m_{k-1}$ .

A cloud-droplet nucleation parameterization based on Köhler theory represents cloud-droplet nucleation. Arbitrary aerosol mixing states and aerosol size distributions can be fed to this parameterization. To represent heterogeneous ice-crystal nucleation, the parameterizations by Lohmann and Diehl (2006) and Möhler et al. (2006) are used. In these parameterizations, contact, immersion, condensation-freezing, and deposition nucleation paths are all considered by taking into account the size distribution of INP, temperature and supersaturation. Homogeneous aerosol (or haze particle) and droplet freezing is also considered following the theory developed by Koop et al. (2000).

#### 3.2 Control run

292

293 For a three-dimensional simulation of the observed case of mixed-phase stratocumulus  
294 clouds, i.e., the control run, a domain with a 100-m resolution just over the Seoul area as  
295 shown in Figure 1 is adopted. The control run is for a period between 00:00 LST on January  
296 12<sup>th</sup> and 00:00 LST on January 14<sup>th</sup> in 2013. The length of the domain in the east-west  
297 (north-south) direction is 220 (180) km. In the vertical domain, the resolution coarsens with  
298 height. The resolution in the vertical domain is 20 m just above the surface and 100 m at  
299 the model top that is at  $\sim 5$  km in altitude.

300 Initial and boundary conditions of potential temperature, specific humidity, and  
301 wind for the simulation are provided by reanalysis data. These data are produced by the  
302 Met Office Unified Model (Brown et al., 2012) every 6 hours on a  $0.11^\circ \times 0.11^\circ$  grid. These  
303 data represent the synoptic-scale environment. An open lateral boundary condition is  
304 employed for the control run. Surface heat fluxes are predicted by the Noah land surface  
305 model (LSM; Chen and Dudhia, 2001). When clouds start to form around 08:00 LST on  
306 January 12<sup>th</sup>, the average temperature over all grid points at cloud tops and bottoms is 252.0  
307 and 263.9 K, respectively.

308 The horizontally homogeneous aerosol properties are assumed in the current version  
309 of the ARW model. To consider the advection of aerosols and the associated  
310 spatiotemporal variation of aerosol properties such as composition and number  
311 concentration, this assumption of the aerosol homogeneity is abandoned. For this  
312 consideration, an aerosol preprocessor is developed to represent the variability of aerosol  
313 properties. Observed background aerosol properties such as aerosol mass (e.g., PM<sub>10</sub> and  
314 PM<sub>2.5</sub>) at observation sites are interpolated into model grid points and time steps by this  
315 aerosol preprocessor.

316 Surface sites that measure PM<sub>2.5</sub> and PM<sub>10</sub> in the domain observe the variability of  
317 aerosol properties. Here, we assume that PM<sub>2.5</sub> and PM<sub>10</sub> represent the mass of aerosols  
318 that act as CCN. These sites resolve the variability with high spatiotemporal resolutions,  
319 since they are distributed with about 1 km distance between them and measure aerosol  
320 mass every  $\sim 10$  minutes. However, they do not measure other aerosol properties such as  
321 aerosol composition and size distributions. There are additional sites of the aerosol robotic  
322 network (AERONET; Holben et al., 2001) in the domain with distances of  $\sim 10$  km between

323 them. Hence, these AERONET sites provide data with coarser resolutions as compared to  
324 those of the  $PM_{2.5}$  and  $PM_{10}$  data, although information on aerosol composition and size  
325 distributions are provided by the AERONET sites. In this study, the variability of properties  
326 of aerosols that act as CCN over the domain is represented by using data from the high-  
327 resolution  $PM_{2.5}/PM_{10}$  sites, while the relatively low-resolution data from the AERONET  
328 sites are used to represent aerosol composition and size distributions.

329 According to AERONET measurements during the period with the observed  
330 stratocumulus clouds, aerosol particles, on average, are an internal mixture of 70 %  
331 ammonium sulfate and 30 % organic compound. This organic compound is assumed to be  
332 water soluble and composed of (by mass) 18 % levoglucosan ( $C_6H_{10}O_5$ , density =  $1600 \text{ kg m}^{-3}$ ,  
333  $\text{van't Hoff factor} = 1$ ), 41 % succinic acid ( $C_6O_4H_6$ , density =  $1572 \text{ kg m}^{-3}$ ,  $\text{van't Hoff}$   
334  $\text{factor} = 3$ ), and 41 % fulvic acid ( $C_{33}H_{32}O_{19}$ , density =  $1500 \text{ kg m}^{-3}$ ,  $\text{van't Hoff factor} = 5$ )  
335 based on a simplification of observed chemical composition. Aerosol chemical  
336 composition in this study is assumed to be represented by this mixture in all parts of the  
337 domain during the whole simulation period, based on the fact that aerosol composition does  
338 not vary significantly over the domain during the whole period with the observed clouds.  
339 Aerosols before their activation can affect radiation by changing the reflection, scattering,  
340 and absorption of shortwave and longwave radiation. However, these impacts on radiation  
341 are not considered in this study, since the mixture does not include a significant amount of  
342 radiation absorbers such as black carbon. Based on the AERONET observation, the size  
343 distribution of background aerosols acting as CCN is assumed to follow the tri-modal log-  
344 normal distribution as shown in Figure 4. Stated differently, the size distribution of  
345 background aerosols acting as CCN in all parts of the domain during the whole simulation  
346 period is assumed to follow size distribution parameters or the shape of distribution as  
347 shown in Figure 4; by averaging size distribution parameters (i.e., modal radius and  
348 standard deviation of each of nuclei, accumulation and coarse modes, and the partition of  
349 aerosol number among those modes) over the AERONET sites and the period with the  
350 stratocumulus clouds, the assumed shape of the size distribution of background aerosols in  
351 Figure 4 is obtained. Since the AERONET observation shows that the shape of the size  
352 distribution does not vary significantly over the domain during the simulation period, we  
353 believe that this assumption is reasonable. With the assumption above,  $PM_{2.5}$  and  $PM_{10}$  are

354 converted to the background number concentrations of aerosols acting as CCN. These  
355 background number concentrations, associated aerosol size distribution and composition  
356 are interpolated or extrapolated to grid points immediately above the surface and time steps  
357 in the simulation. Background aerosol concentrations are assumed not to vary with height  
358 from immediately above the surface to the PBL top, however, above the PBL top, they are  
359 assumed to reduce exponentially with height. Aerosol size distribution and composition do  
360 not vary with height. Once background aerosol properties (i.e., aerosol number  
361 concentrations, size distribution and composition) are put into each grid point and time step,  
362 those properties at each grid point and time step do not change during the course of the  
363 simulation.

364 For the control run, aerosol properties of INP and CCN are assumed to be identical  
365 except for the concentration of background aerosols. The concentration of background  
366 aerosols acting as INP is assumed to be 100 times lower than the concentration of  
367 background aerosols acting as CCN at each of time steps and grid points. This is based on  
368 a general difference in concentration between CCN and INP (Pruppacher and Klett, 1978).

369 Once clouds form and background aerosols start to be in clouds, those aerosols are  
370 not background aerosols anymore and the size distribution and concentrations of those  
371 aerosols begin to evolve through aerosol sinks and sources. These sinks and sources include  
372 advection and aerosol activation (Fan et al., 2009). For example, activated particles are  
373 emptied in the corresponding bins of the aerosol spectra. In clouds, aerosol mass included  
374 in hydrometeors, after activation, is moved to different classes and sizes of hydrometeors  
375 through collision-coalescence and removed from the atmosphere once hydrometeors that  
376 contain aerosols reach the surface. In non-cloudy areas, aerosol size and spatial  
377 distributions are set to follow background counterparts. In other words, for this study, we  
378 use “the aerosol recovery method” where immediately after clouds disappear completely  
379 at any grid points, aerosol size distributions and number concentrations at those points  
380 recover to background properties that background aerosols at those points have before  
381 those points are included in clouds. In this method, there is no time interval between the  
382 cloud disappearance and the aerosol recovery. Here, when the sum of mass of all types of  
383 hydrometeors (i.e., water drops, ice crystals, snow aggregates, graupel and hail) is not zero

384 at a grid point, that grid point is considered to be in clouds. When this sum becomes zero,  
385 clouds are considered to disappear.

386 It is notable that in clouds, processes such as aerosol activation, which is related to  
387 aerosol-cloud interactions and the nucleation scavenging, and aerosol transportation by  
388 wind and turbulence, and impacts of these processes on aerosol size distribution and  
389 concentrations are considered in this study as in other models that explicitly predict aerosol  
390 size distribution and concentrations such as the chemistry version of the Weather Research  
391 and Forecasting (WRF) model (WRF-Chem) (Grell et al., 2005; Skamarock et al., 2008).  
392 When clouds disappear, in those other models, without nudging aerosols to observed  
393 background counterparts, aerosols just evolve based on the emissions of aerosols around  
394 the surface, aerosol chemical and physical processes, aerosol transportation and so on.  
395 However, in the ARW model used here, aerosols are forced to be nudged into observed  
396 background aerosols and this may act as a weakness of the aerosol recovery (or nudging)  
397 method.

398 Numerous CSRM studies have adopted this aerosol recovery method and proven that  
399 it is able to simulate overall cloud and precipitation properties reasonably well (e.g.,  
400 Morrison and Grabowski, 2011; Lebo and Morrison, 2014; Lee et al., 2016; Lee et al.,  
401 2018). These properties include cloud fraction, cloud-top height, cloud-bottom height,  
402 cumulative precipitation, precipitation frequency distribution, mean precipitation rate,  
403 cloud-system organization and precipitation spatiotemporal distributions. These studies  
404 have shown that there is good consistency between those simulated properties and observed  
405 counterparts. The good consistency means that the percentage difference in those  
406 properties between simulations and corresponding observation is  $\sim 10$  to 20% or less.

407 The recovery of aerosols to their background counterparts is mainly to keep aerosol  
408 concentrations outside clouds in the simulation at observed counterparts. Other models that  
409 explicitly predict aerosol concentrations with no use of the aerosol recovery method are  
410 not able to simulate aerosol spatiotemporal distributions and their evolutions which are  
411 identical to those observed, although those models require a much larger amount of  
412 computational resources and time than the aerosol recovery method. This is mainly because  
413 there are uncertainties in the representation of aerosol chemical and physical processes and  
414 these processes consume a large amount of computational resources and time in those

415 models. For this study, particularly to simulate the variation of aerosol concentrations over  
416 grid points and time steps induced by the aerosol advection as observed with the minimized  
417 use of computational resources and time, observed aerosol concentrations, based on the  
418 observed PM data and the assumed aerosol size distribution and composition, are applied  
419 to grid points and time steps in the simulation directly via the aerosol preprocessor in  
420 association with the aerosol recovery method. In this way, background aerosol  
421 concentrations (or background aerosols or aerosols outside clouds) in the simulation are  
422 exactly identical to those observed, in case we neglect possible errors from the assumption  
423 on aerosol size distribution and composition, and the interpolation or extrapolation of  
424 observed data to grid points and time steps in the simulation. In addition, those background  
425 aerosols from observation are results of processes related to aerosols in real nature (e.g.,  
426 aerosol emissions, cloud impacts on aerosols via scavenging processes, aerosol chemical  
427 and physical processes and aerosol transportation by wind and turbulence). Hence, by  
428 adopting background aerosols, as they are in observation, for the simulation, not only we  
429 are able to consider the transportation of background aerosols by wind (or aerosol  
430 advection) and associated aerosol evolutions as observed but also we are able to consider  
431 the evolution of background aerosols induced by the other aerosol-related processes as  
432 observed in the simulation. We believe that this balances out the weakness of the aerosol  
433 recovery method to result in the reasonable simulation of the selected case, as is evidently  
434 shown by the fact that simulated cloud properties are in a good agreement with observed  
435 counterparts as described below.

436

437

### 3.3 Additional runs

438

439 To examine effects of the aerosol advection on the observed stratocumulus clouds over the  
440 Seoul area, the control run is repeated by removing the increase in aerosol concentrations  
441 due to the aerosol advection. This repeated run is referred to as the low-aerosol run

442

443 In the low-aerosol run, to remove the increase in aerosol concentrations, background  
444 aerosol concentrations after 05:00 LST on January 12<sup>th</sup> do not evolve with the aerosol  
445 advection and are assumed to have background aerosol concentrations at 05:00 LST on  
January 12<sup>th</sup> at every time step and grid point only for the concentration of background

446 aerosols acting as CCN. Here, the time- and domain-averaged concentration of background  
447 aerosols acting as CCN after 05:00 LST on January 12<sup>th</sup> in the low-aerosol run is lower  
448 than that in the control run by a factor of  $\sim 3$ . It is notable that there are no differences in  
449 the concentration of background aerosols acting as INP between the control and low-  
450 aerosol runs. This is to isolate effects of CCN, which accounts for most of aerosols, on  
451 clouds from those effects of INP via comparisons between the runs. Via the comparisons,  
452 we are able to identify how advection-induced increases in the concentration of aerosols  
453 acting as CCN affect clouds. The ratio of the concentration of background aerosols acting  
454 as CCN at 05:00 LST on January 12<sup>th</sup> to that after 05:00 LST on January 12<sup>th</sup> varies among  
455 grid points and time steps, since the concentration varies spatiotemporally throughout the  
456 simulation period in the control run. This means that a factor by which the concentration  
457 of background aerosols acting as CCN varies after 05:00 LST on January 12<sup>th</sup> between the  
458 control and low-aerosol runs is different for each of the time steps and grid points.

459 As mentioned above, impacts of the advection of meteorological conditions, which  
460 accompanies the advection of aerosols and associated increases in aerosol concentrations,  
461 on the stratocumulus clouds in the Seoul area are out of scope of this study. Hence, there  
462 are no differences in synoptic-scale environment or meteorological conditions between the  
463 control and low-aerosol runs. This enables the isolation of impacts of the aerosol advection  
464 through comparisons between the runs. If impacts of the advection of meteorological  
465 conditions were investigated by repeating the control run, with an assumption that  
466 meteorological conditions after 03:00 LST on January 12<sup>th</sup> do not evolve and are fixed at  
467 03:00 LST on January 12<sup>th</sup>, for the purpose of comparing the control run to this repeated  
468 run, there would be no or nearly no formation of stratocumulus clouds in this repeated run;  
469 this is because there is a stable layer at 03:00 LST on January 12<sup>th</sup>, which is just before the  
470 advection of aerosols affects aerosol concentrations in the Seoul area and not favorable for  
471 the formation of clouds as described in Section 2. As mentioned in Section 2, the advection  
472 of meteorological conditions, which are with advection-induced increases in aerosol  
473 concentrations, enables the formation of the stratocumulus clouds in the Seoul area. This  
474 study examines impacts of the aerosol advection on those clouds for this given advection  
475 of meteorological conditions.



476 To examine effects of the interplay between ice crystals and droplets on the adopted  
477 system of stratocumulus clouds and its interactions with aerosols, the control and low-  
478 aerosol runs are repeated by removing ice processes. These repeated runs are referred to as  
479 the control-noice and low-aerosol-noice runs. In the control-noice and low-aerosol-noice  
480 runs, only aerosols acting as CCN, droplets (i.e., cloud liquid), raindrops and associated  
481 phase-transition processes (e.g., condensation and evaporation) exist, and aerosols acting  
482 as INP, all solid hydrometeors (i.e., ice crystals, snow, graupel, and hail) and associated  
483 phase-transition processes (e.g., deposition and sublimation) are turned off, regardless of  
484 temperature. Via comparisons between the control and control-noice runs, we aim to  
485 identify effects of the interplay between ice crystals and droplets on the adopted system.  
486 Via comparisons between a pair of the control and low-aerosol runs and that of the control-  
487 noise and low-aerosol-noice runs, we aim to identify effects of the interplay between ice  
488 crystals and droplets on interactions between the system and aerosols. Henceforth, the pair  
489 of the control and low-aerosol runs is referred to as the ice runs, while the pair of the  
490 control-noice and low-aerosol-noice runs is referred to as the noise runs.

491 To better understand findings in Section 4.1.1, which explain how the interplay between  
492 ice crystals and droplets affects stratocumulus clouds, the control run is repeated by  
493 increasing the concentration of background aerosols acting as INP by a factor of 10 and  
494 100 at each time step and grid point. These repeated runs are detailed in Section 4.1.2 and  
495 referred to as the INP-10 and INP-100 runs, respectively. To better understand findings in  
496 Section 4.2.1, which explain how aerosols acting as CCN affect the interplay between ice  
497 crystals and droplets, the control run is repeated by reducing the concentration of  
498 background aerosols acting as INP in the same way as the concentration of background  
499 aerosols acting as CCN is reduced in the low-aerosol-run as compared to that in the control  
500 run. This repeated run is referred to as the INP-reduced run and detailed in Section 4.2.2.  
501 To see the roles played by the sedimentation of ice particles (i.e., ice crystals, snow  
502 aggregates, graupel and hail) in stratiform clouds and their interactions with aerosols, the  
503 control, INP-10, INP-100, low-aerosol and INP-reduced runs are repeated with the  
504 sedimentation of ice particles turned off. These repeated runs are referred to as the control-  
505 no-sedim, INP-10-no-sedim, INP-100-no-sedim, low-aerosol-no-sedim and INP-reduced-  
506 no-sedim runs, and detailed in Sections 4.1.3 and 4.2.3. To examine roles played by the

507 sedimentation of both of ice and liquid particles (i.e., droplets and rain drops) in stratiform  
508 clouds, the control run is repeated again with the sedimentation of both of ice and liquid  
509 particles turned off. This repeated run is referred to as the control-no-sedim-ice-liq run.  
510 Table 1 summarizes all of the simulations in this study.

511

## 512 **4. Results**

513

### 514 **4.1 Effects of the interplay between ice crystals and droplets on clouds**

515

#### 516 **4.1.1 The control and control-noice runs**

517

518 Figure 5a shows the time series of the domain-averaged liquid-water path (LWP), ice-water  
519 path (IWP) and water path (WP), which is the sum of LWP and IWP, for the control run,  
520 and LWP for the control-noice run. Since in the control-noice run, there are no ice particles,  
521 LWP acts as WP in the run. WP is higher in the control-noice run than in the control run  
522 throughout the whole simulation period. This higher WP in the control-noice run  
523 accompanies the higher average cloud fraction over time steps with non-zero cloud fraction.  
524 The average cloud fraction is 0.98 and 0.92 in the control-noice and control runs,  
525 respectively. At the initial stage before 20:00 LST on January 12<sup>th</sup>, differences in WP  
526 between the runs are not as significant as those after 20:00 LST on January 12<sup>th</sup> (Figure  
527 5a). The differences in WP between the runs are greatest around 00:00 LST on January  
528 13<sup>th</sup> when WP reaches its maximum value in each of the runs (Figure 5a). These differences  
529 decrease as time goes by after around 00:00 LST on January 13<sup>th</sup> (Figure 5a). The time-  
530 and domain-averaged WP over the period between 00:00 LST (local solar time) on January  
531 12<sup>th</sup> and 00:00 LST on January 14<sup>th</sup> is 18 and 55 g m<sup>-2</sup> in the control and control-noice  
532 runs, respectively. Associated with this, the WP peak value reaches 83 g m<sup>-2</sup> in the control  
533 run, while the value reaches 230 g m<sup>-2</sup> in the control-noice run (Figure 5a). Over most of  
534 the simulation period, IWP is greater than LWP in the control run except for the period  
535 between ~22:00 LST on January 12<sup>th</sup> and ~01:00 LST on January 13<sup>th</sup> (Figure 5a). In the  
536 control run, the time- and domain-averaged IWP and LWP are 11 and 7 g m<sup>-2</sup>, respectively.  
537 Results here indicate that when solid and liquid particles coexist, cloud mass, represented

538 by WP, reduces a lot as compared to that when liquid particles alone exist. To evaluate the  
539 control run, satellite and ground observations can be utilized. In the case of the Moderate  
540 Resolution Imaging Spectroradiometer, one of representative polar orbiting image sensors  
541 on board satellites, it passes the Seoul area only at 10:30 am and 1:30 pm every day, hence,  
542 the sensor is not able to provide reliable data that cover the whole simulation period.  
543 Multifunctional Transport Satellites (MTSAT), which are geostationary satellites and  
544 available in the East Asia, do not provide reliable data of LWP and IWP, although they  
545 provide comparatively reliable data of cloud fraction and cloud-top height throughout the  
546 whole simulation period (Faller, 2005). Ground observations provide data of cloud fraction  
547 and cloud-bottom height throughout the whole simulation period. Here, the simulated cloud  
548 fraction and cloud-bottom height are compared to those from ground observations, while  
549 the simulated cloud-top height is compared to that from the MTSAT. The average cloud  
550 fraction over time steps with non-zero cloud fraction is 0.92 and 0.86 in the control run and  
551 observation, respectively. The average cloud-bottom height over grid columns and time  
552 steps with non-zero cloud-bottom height is 230 (250) m in the control run (observation).  
553 The average cloud-top height over grid columns and time steps with non-zero cloud-top  
554 height is 2.2 (2.0) km in the control run (observation). For this comparison between the  
555 control run and observation, observation data are interpolated into grid points and time  
556 steps in the control run. The percentage difference in each of cloud fraction, cloud-bottom  
557 and -top heights between the control run and observations is  $\sim 10\%$  and thus the control  
558 run is considered performed reasonably well for these variables.

559       Condensation and deposition are the main sources of cloud mass in the control run.  
560 Since in the control-noice run, there are no ice particles, deposition is absent, and thus,  
561 condensation alone acts as the main source of cloud mass. As seen in Figure 5b,  
562 condensation rates in the control-noice run are much higher than the sum of condensation  
563 and deposition rates in the control run. Associated with this, there is greater cloud mass in  
564 the control-noice run than in the control run, although deposition is absent in the control-  
565 noice run. However, at the initial stage before 20:00 LST on January 12<sup>th</sup>, differences  
566 between the sum in the control run and condensation rate in the control-noice run are not  
567 as significant as compared to those after 20:00 LST on January 12<sup>th</sup> (Figure 5b). Hence,  
568 those differences increase as time progresses after the initial stage. Those differences are

569 greatest around 00:00 LST on January 13<sup>th</sup> when the sum in the control run or condensation  
570 rate in the control-noise run reaches its maximum value. The differences decrease as time  
571 goes by after around 00:00 LST on January 13<sup>th</sup>. Condensation rate, deposition rate in the  
572 control run, and condensation rate in the control-noise run are similar to LWP, IWP in the  
573 control run, and LWP in the control-noise run, respectively, in terms of their temporal  
574 evolutions (Figures 5a and 5b). This similarity confirms that deposition and condensation  
575 are the main sources of IWP and LWP, respectively, and control cloud mass. Thus,  
576 understanding the evolutions of condensation and deposition is equivalent to understanding  
577 those of LWP and IWP, respectively. Hence, in the following, to understand evolutions of  
578 cloud mass and its differences between the simulations in this study, we analyze evolutions  
579 of condensation, deposition, and their differences between the runs.

580 The qualitative nature of differences in WP, which represents cloud mass, over the  
581 whole simulation period between the control and control-noise runs is initiated and  
582 established during the initial stage of cloud development before 20:00 LST on January 12<sup>th</sup>  
583 (Figures 5a and 5b). Hence, to understand mechanisms that initiate differences in WP  
584 between the control and control-noise runs, deposition, condensation and associated  
585 variables are analyzed for the initial stage. Note that synoptic or environmental conditions  
586 such as humidity and temperature are identical between the control and control-noise runs.  
587 These conditions act as initial and boundary conditions for the simulations and thus initial  
588 and boundary conditions are identical between the runs. Also, during the initial stage,  
589 feedbacks between dynamics (e.g., updrafts) and microphysics just start to form and thus  
590 are not fully established as compared to those feedbacks after the initial stage. This enables  
591 us to perform analyses of deposition and condensation during the initial stage by reasonably  
592 excluding a large portion of complexity caused by those feedbacks. Hence, those analyses  
593 during the initial stage can provide a clearer picture of either microphysical or dynamic  
594 mechanisms that control differences in results between the runs.

595 During the initial stage before 20:00 LST on January 12<sup>th</sup>, evaporation rates, averaged  
596 over the cloud layer, are higher in the control run than in the control-noise run and this is  
597 contributed by the WBF mechanism which facilitates evaporation of droplets and  
598 deposition onto ice crystals (Figure 5c). In addition, it should be noted that ice crystals  
599 consume water vapor that is needed for droplet nucleation. This makes it difficult for

600 droplets to be activated in the control run as compared to a situation in the control-noise  
601 run. Associated with the more evaporation and difficulty in droplet activation, droplets  
602 disappear more and form less, leading to a situation where cloud droplet number  
603 concentration (CDNC) starts to be lower in the control run during the initial stage (Figure  
604 5d). This is despite the higher entrainment rate at the PBL tops and associated more  
605 evaporation in the control-noise run than in the control run. The average entrainment rate  
606 over all grid points at the PBL tops and over the initial stage is 0.18 and 0.08 cm s<sup>-1</sup> in the  
607 control-noise and control runs, respectively. In this study, the entrainment rate is calculated  
608 as follows:

609

$$610 \text{ The entrainment rate} = dz_i/dt - w_{sub}$$

611

612 Here,  $z_i$  is the PBL height and  $w_{sub}$  is the large-scale subsidence rate at the PBL top. Then,  
613 during the initial stage, the reduction in CDNC contributes to a reduction in condensation  
614 in the control run as compared to that in the control-noise run (Figure 5b). Fewer droplets  
615 mean that there is a less integrated droplet surface area where condensation occurs and this  
616 contributes to less condensation in the control run. As seen in Figures 5c and 5d, the cloud  
617 layer is between ~200 m and ~1.5 km in the control run, while it is between ~200 m and  
618 ~2.5 km in the control-noise run. Hence, air parcels go up higher, which also contribute to  
619 more condensation in the control-noise run than in the control run. However, aided by the  
620 fact that the water-vapor equilibrium saturation pressure is lower for ice particles than for  
621 liquid particles, deposition is facilitated at the initial stage in the control run whether the  
622 water-vapor pressure is higher than the equilibrium pressure for liquid particles or not as  
623 long as the water-vapor pressure is higher than the equilibrium pressure for ice particles.  
624 This leads to greater deposition than condensation in the control run at the initial stage  
625 (Figure 5b). This deposition is inefficient and the subsequent increase in deposition is not  
626 sufficient, so, the sum of condensation and deposition rates in the control run is slightly  
627 lower than condensation rate in the control-noise run at the initial stage (Figure 5b); this  
628 contributes to slightly lower WP in the control run than in the control-noise run during the  
629 initial stage (Figure 5a). Hence, slightly greater latent heating, which is associated with  
630 condensation, in the control-noise run than that, which is associated with the sum of

631 deposition and condensation, in the control run develops during the initial stage. This  
632 initiates stronger feedbacks between updrafts and latent heating in the control-noise run  
633 than in the control run during the initial stage and these stronger feedbacks are fully  
634 established after the initial stage. This in turn results in much stronger updrafts after the  
635 initial stage in the control-noise run than in the control run. Mainly due to these much  
636 stronger updrafts after the initial stage, the time- and domain-averaged updrafts over the  
637 whole simulation period are also much greater in the control-noise run than in the control  
638 run (Figure 6a). The much stronger updrafts produce much larger WP and associated larger  
639 cloud fraction in the control-noise run than in the control run after the initial stage (Figure  
640 5a).

641 Results here indicate that the reduced cloud mass, due to the reduced condensation,  
642 is not efficiently compensated by the gain of solid mass via deposition in the control run.  
643 If the reduced mass is efficiently compensated by deposition, that would lead to much  
644 smaller differences in WP between the control and control-noise runs. Here, we  
645 hypothesize that the inefficient deposition is related to cloud ice number concentration  
646 (CINC) as seen in Figure 6b. Note that the surface of ice crystals is where deposition occurs  
647 and the more surface area of ice crystals favors more deposition. We hypothesize that CINC  
648 and the associated integrated surface area of ice crystals are not large enough to induce a  
649 large amount of deposition that can potentially make WP similar between the control and  
650 control-noise runs. Stated differently, it is hypothesized that water vapor is not able to find  
651 enough surface area of ice crystals for the large amount of deposition.

652

#### 653 **a. LWP and IWP frequency distributions**

654

655 As seen in Figure 7a, the control-noise run has the lower (higher) WP cumulative frequency  
656 for WP below (above)  $\sim 100 \text{ g m}^{-2}$  than the control run at the last time step. This means  
657 that the lower average WP in the control run is mainly due to a reduction in WP above  
658  $\sim 100 \text{ g m}^{-2}$  in the control run. The LWP frequency reduces substantially in the control run  
659 as compared to that in the control-noise run (Figure 7b). With this reduction, LWP above  
660  $\sim 800 \text{ g m}^{-2}$  disappears and there is in general two to three orders of magnitude lower LWP

661 frequency for LWP below  $\sim 800 \text{ g m}^{-2}$  in the control run than in the control-noise run  
662 (Figure 7b).

663 As seen in Figure 7b, at the last time step, there is the presence of IWP frequency in  
664 addition to the LWP frequency in the control run. Through the facilitated deposition, the  
665 IWP frequency is greater than the LWP frequency for IWP below  $\sim 200 \text{ g m}^{-2}$  in the control  
666 run. Particularly for IWP below  $\sim 100 \text{ g m}^{-2}$ , the IWP frequency in the control run is greater  
667 than the LWP frequency in the control-noise run. This enables the greater WP frequency  
668 in the control run than in the control-noise run for WP below  $\sim 100 \text{ g m}^{-2}$  in spite of the  
669 lower LWP frequency below  $\sim 100 \text{ g m}^{-2}$  in the control run (Figures 7a and 7b). However,  
670 the lower IWP frequency for IWP above  $\sim 100 \text{ g m}^{-2}$  in the control run than the LWP  
671 frequency for LWP above  $\sim 100 \text{ g m}^{-2}$  in the control-noise run contributes to the lower WP  
672 frequency for WP above  $\sim 100 \text{ g m}^{-2}$  in the control run (Figures 7a and 7b). The lower WP  
673 frequency for WP above  $\sim 100 \text{ g m}^{-2}$  in the control run is also contributed by the lower  
674 LWP frequency for LWP above  $\sim 100 \text{ g m}^{-2}$  in the control run (Figures 7a and 7b).

675

#### 676 **4.1.2 The INP-10 and INP-100 runs**

677

678 To test above-mentioned hypothesis about the CINC-related inefficient deposition, the  
679 control run is compared with the INP-10 and INP-100 runs (Table 1). In particular, in the  
680 INP-100 run, the concentration of background aerosols acting as INP becomes that of  
681 background aerosols acting as CCN. This may be unrealistic. However, the main purpose  
682 of the INP-10 and INP-100 runs is to test the hypothesis and it is believed that the high  
683 concentrations of background aerosols acting as INP in the INP-10 and INP-100 runs are  
684 able to clearly isolate the role of the INP concentration and CINC in WP by making a stark  
685 contrast in the INP concentration and CINC between the control, INP-10 and INP-100 runs.

686 As seen in Figure 8a, CINC averaged over grid points and time steps with non-zero  
687 CINC increases by a factor of  $\sim 5$  ( $\sim 60$ ), when the concentration of background aerosols  
688 acting as INP increases by a factor of 10 (100) from the control run to the INP-10 (INP-  
689 100) run. With these increases in CINC, the average radius of ice crystals over grid points  
690 and time steps with non-zero CINC decreases by  $\sim 15\%$  and  $25\%$  in the INP-10 and INP-  
691 100 runs, respectively. This induces increases in the integrated surface area of ice crystals

692 and thus deposition in the INP-10 and INP-100 runs as compared to those in the control  
693 run (Figures 5b, 8b and 8c). These increases in deposition are more, because of greater  
694 increases in the integrated surface area in the INP-100 run than in the INP-10 run (Figures  
695 8b and 8c). Of interest is that the increase in deposition accompanies a decrease in  
696 condensation in the INP-10 and the INP-100 runs as compared to that in the control run  
697 (Figures 5b, 8b and 8c). This is because due to more deposition, more water vapor is  
698 transferred from air to ice crystals, which leaves less water vapor for droplet activation and  
699 condensation in the INP-10 run and INP-100 runs than in the control run when the water-  
700 vapor pressure is higher than the water-vapor saturation pressure for liquid particles in air  
701 parcels. Greater deposition leaves less water vapor for droplet activation and condensation,  
702 leading to less activation and condensation in the INP-100 run than in the INP-10 run when  
703 the water-vapor pressure is higher than the water-vapor saturation pressure for liquid  
704 particles in air parcels. When the water-vapor pressure is lower than the water-vapor  
705 saturation pressure for liquid particles, increasing deposition induces the increasing  
706 evaporation of droplets and decreasing CDNC among the control, INP-10 and INP-100  
707 runs in air parcels. This subsequently contributes to decreasing condensation among those  
708 runs when the water-vapor pressure becomes higher than the water-vapor saturation  
709 pressure for liquid particles in those air parcels.

710 Associated with increases in deposition and decreases in condensation, IWP increases  
711 and LWP decreases in both of the INP-10 and INP-100 runs as compared to those in the  
712 control run. The time- and domain-averaged IWP, LWP and WP are 24 (47), 5 (3), and 29  
713 (50)  $\text{g m}^{-2}$  in the INP-10 (INP-100) run. Since there are greater increases in deposition and  
714 greater decreases in condensation, these increases in IWP and decreases in LWP are greater  
715 in the INP-100 run than in the INP-10 run. The increasing deposition and IWP contribute  
716 to increases in WP, while the decreasing condensation and LWP contribute to decreases in  
717 WP in the INP-10 and INP-100 runs. Figure 9a shows that there are increases in WP in  
718 the INP-10 and INP-100 runs as compared to WP in the control run and those increases are  
719 greater in the INP-100 run than in the INP-10 run. This means that the increases in  
720 deposition and IWP outweigh the decreases in condensation and LWP, respectively, in the  
721 INP-10 and INP-100 runs. This outweighing is greater and leads to greater increases in WP  
722 in the INP-100 run than in the INP-10 run (Figure 9a). As seen in Figure 9a, the enhanced



723 average WP in the INP-100 (INP-10) run reaches 91% (53%) of that in the control-noice  
724 run, while the average WP in the control run accounts for only ~30% of that in the control-  
725 noise run. Associated with the enhanced average WP, the average cloud fraction over time  
726 steps with non-zero cloud fraction increases from 0.92 in the control run to 0.97 (0.94) in  
727 the INP-100 (INP-10) run. Accompanying this is that the time- and domain-averaged  
728 updraft mass flux in the INP-100 (INP-10) run over the whole simulation period reaches  
729 95% (78%) of that in the control-noice run, while the average updraft mass flux in the  
730 control run accounts for only ~50% of that in the control-noice run. The average cloud-top  
731 height over grid columns and time steps with non-zero cloud-top height in the INP-100  
732 (INP-10) run, particularly over the initial stage between 00:00 LST and 20:00 LST on  
733 January 12<sup>th</sup>, reaches 92% (80%) of that in the control-noice run. Hence, the increasing  
734 deposition in the INP-10 and INP-100 runs involves its positive feedbacks with dynamics  
735 (i.e., updrafts). This eventually enables air parcels in the INP-100 run to have stronger  
736 updrafts than those in the control run and thus to go up nearly as high as those in the control-  
737 noise run. Through the positive feedbacks between the increasing deposition and dynamics,  
738 increasing dynamic intensity with the increasing vertical extent of air parcels or clouds in  
739 turn enables deposition and IWP to further increase, resulting in the similar WP and cloud  
740 fraction between the INP-100 and control-noice runs. Here, comparisons among the control,  
741 INP-10 and INP-100 runs confirm the hypothesis that ascribes much lower WP in the  
742 control run than in the control-noice run to the CINC-related inefficient deposition in the  
743 control run.

744

#### 745 **a. LWP and IWP frequency distributions**

746

747 With the increasing concentration of aerosols acting as INP and CINC from the control run  
748 to the INP-10 run to the INP-100 run, there are substantial increases in the IWP cumulative  
749 frequency, while there are substantial decreases in the LWP cumulative frequency at the  
750 last time step (Figure 9b). These increases in the IWP frequency accompany increases in  
751 the IWP maximum value from ~200 g m<sup>-2</sup> in the control run to ~1200 g m<sup>-2</sup> in the INP-100  
752 run through ~500 g m<sup>-2</sup> in the INP-10 run (Figure 9b). These decreases in the LWP  
753 frequency accompany decreases in the LWP maximum value from ~700 g m<sup>-2</sup> in the control

754 run to  $\sim 100 \text{ g m}^{-2}$  in the INP-100 run through  $\sim 300 \text{ g m}^{-2}$  in the INP-10 run (Figure 9b).  
 755 The increases in the IWP frequency outweigh decreases in the LWP frequency between the  
 756 INP-10 and INP-100 runs (the INP-10 and control run), leading to the greater average WP  
 757 in the INP-100 run than in the INP-10 run (in the INP-10 run than in the control run).

758

### 759 **4.1.3 Sedimentation of hydrometeors**

760

761 With increasing concentrations of aerosols acting as INP between the control, INP-10 and  
 762 INP-100 runs, there are changes in the sedimentation of ice particles and this induces  
 763 changes in the precipitation rate at cloud bases. The average precipitation rate over all grid  
 764 points at cloud bases and over the whole simulation period is 0.004, 0.002, and 0.0006  $\text{g}$   
 765  $\text{m}^{-2} \text{ s}^{-1}$  in the control, INP-10 and INP-100 runs, respectively. As mentioned above, there  
 766 are also changes in the deposition rate among those simulations. The time- and column-  
 767 averaged deposition rate is 0.027, 0.059 and 0.125  $\text{g m}^{-2} \text{ s}^{-1}$  in the control, INP-10 and INP-  
 768 100 runs, respectively. As a first step to obtain the column average of a variable, at each  
 769 time step, the average value of the variable over each column is obtained by summing up  
 770 the value of the variable over the vertical domain in each of all columns in the domain and  
 771 dividing the sum by the total number of grid points in each column. This sum of the value  
 772 is obtained over all grid points in the vertical domain whether they have zero values of the  
 773 variable or not. The column average in this study is the average value (in each column) that  
 774 is summed up over all columns and divided by the total number of columns in the domain.

775 We see that the change in deposition rate from the control run to the INP-10 run (to the  
 776 INP-100 run) is 16 (29) times greater than that in the cloud-base precipitation rate. Hence,  
 777 the varying sedimentation of ice particles and associated precipitation is likely to play an  
 778 insignificant role in the varying cloud mass among the runs as compared to the varying  
 779 deposition. To confirm this, the control, INP-10 and INP-100 runs are repeated by setting  
 780 the fall velocity of ice particles to zero. These repeated runs are the control-no-sedim and  
 781 INP-10-no-sedim and INP-100-no-sedim runs. The time- and domain-averaged IWP, LWP  
 782 and WP are 11 (14), 7 (5) and 18 (19)  $\text{g m}^{-2}$ , respectively, in the control (control-no-sedim)  
 783 run. The time- and domain-averaged IWP, LWP and WP are 26 (49), 4 (2) and 30 (51)  $\text{g}$   
 784  $\text{m}^{-2}$ , respectively, in the INP-10-no-sedim (INP-100-no-sedim) run. Remember that the

785 time- and domain-averaged IWP, LWP and WP are 24 (47), 5 (3) and 29 (50)  $\text{g m}^{-2}$ ,  
786 respectively, in the INP-10 (INP-100) run. The presence of the sedimentation decreases  
787 IWP and increases LWP as compared to the situation with no sedimentation for each of the  
788 runs. However, the average WP in the control-no-sedim run is still much lower than that in  
789 the control-noice run. The average WP in the INP-100-no-sedim run (the INP-10-no-sedim  
790 run) reaches 93% (55%) of that in the control-noice run and this is similar to the situation  
791 among the INP-10, INP-100 and control-noice runs. This demonstrates that the  
792 sedimentation of ice particles and associated precipitation are not main factors that control  
793 the variation of cloud mass among the control, INP-10, INP-100 and control-noice runs.

794 To further examine the role played by the sedimentation of hydrometeors particularly  
795 in the lower WP in the control run than that in the control-noice run, the control run is  
796 repeated again by setting the fall velocity of both of ice and liquid particles to zero. The  
797 repeated run is the control-no-sedim-ice-liq run. The time- and domain-averaged IWP,  
798 LWP and WP are 11 (15), 7 (9) and 18 (24)  $\text{g m}^{-2}$ , respectively, in the control (control-no-  
799 sedim-ice-liq) run. The presence of the sedimentation of both of ice and liquid particles  
800 decreases both of IWP and LWP as compared to the situation with no sedimentation of  
801 both of ice and liquid particles. However, the average WP in the control-no-sedim-ice-liq  
802 run is still much lower than that in the control-noice run. Hence, the lower WP in the control  
803 run than that in the control-noice run does not depend on whether the sedimentation of both  
804 of ice and liquid particles is present in the control run. This indicates that the sedimentation  
805 of both of ice and liquid particles is not a factor that causes the lower WP in the control run  
806 than in the control-noice run.

807

## 808 **4.2 Aerosol-cloud interactions**

809

### 810 **4.2.1 CCN**

811

812 With advection-induced increases in aerosol concentrations between the control and  
813 low-aerosol runs, there are aerosol-induced increases and decreases in IWP and LWP,  
814 respectively (Figure 10a). The increases in IWP are outweighed by the decreases in LWP,  
815 leading to aerosol-induced decreases in the average WP between the ice runs. This involves

816 aerosol-induced decreases in the average cloud fraction over time steps with non-zero  
817 cloud fraction from 0.93 in the low-aerosol run to 0.92 in the control run. As seen in Figure  
818 10b, the WP frequency is greater particularly for  $WP < \sim 300 \text{ g m}^{-2}$ , leading to the higher  
819 average WP in the low-aerosol run than in the control run. As seen in Figure 10c,  
820 particularly for WP below  $\sim 200 \text{ g m}^{-2}$ , the IWP frequency increases, while the LWP  
821 frequency decreases with increasing aerosols between the ice runs. The increase in the IWP  
822 frequency is not able to outweigh the decrease in the LWP frequency, leading to aerosol-  
823 induced decreases in the average WP between the ice runs. Results here are contrary to  
824 the conventional wisdom that increasing concentrations of aerosols acting as CCN tend to  
825 increase WP in stratiform clouds (Albrecht, 1989).

826       Between the noise runs, there is an increase in LWP (i.e., WP) with the increasing  
827 concentration of aerosols acting as CCN (Figure 10a). This involves aerosol-induced  
828 increases in the average cloud fraction over time steps with non-zero cloud fraction from  
829 0.96 in the low-aerosol-noise run to 0.98 in the control-noise run. The greater LWP  
830 frequency, concentrated in the LWP range between  $\sim 100$  and  $\sim 600 \text{ g m}^{-2}$ , leads to the  
831 greater average LWP or WP in the control-noise run than in the low-aerosol-noise run  
832 (Figures 10b and 10c).

833

834       a. Ice runs

835

836               1) Condensation and evaporation

837

838       The qualitative nature of aerosol-induced differences in deposition, IWP, condensation and  
839 LWP over the whole simulation period between the ice runs is initiated and established  
840 during the initial stage of cloud development before 20:00 LST on January 12<sup>th</sup> (Figure  
841 10a). To understand mechanisms that control aerosol-induced differences in deposition and  
842 condensation as a way of understanding mechanisms that control those differences in IWP  
843 and LWP, the time series of deposition rate, condensation rate and associated variables in  
844 each of the ice runs and differences in these variables between the ice runs is obtained for  
845 the initial stage. Since this study focuses on these differences in the variables as a  
846 representation of aerosol effects on clouds, in the following, the description of the

847 differences is given in more detail by involving both figures and text as compared to the  
848 description of the variables in each of the ice runs, involving text only for the sake of  
849 brevity.

850

851 i. CDNC and its relation to condensation and evaporation

852

853 Evaporation and condensation rates are higher in the control run than in the low-aerosol  
854 run throughout the initial stage and up to ~15:30 LST on January 12<sup>th</sup>, respectively (Figure  
855 11a). Increases in evaporation tend to make more droplets disappear, while increases in  
856 aerosol activation and resultant condensation counteract the disappearance more. The  
857 average CDNC over grid points and time steps with non-zero CDNC is larger in the control  
858 run than in the low-aerosol run not only over the initial stage but also over the whole  
859 simulation period (Figures 11a and 12a). This means that on average, the evaporatively-  
860 driven increases in the disappearance of droplets are outweighed by the activation- and/or  
861 condensationally-enhanced counteraction particularly during the initial stage with  
862 increasing aerosol concentrations between the ice runs. As marked by a green-dashed box  
863 in Figure 11a, there are steady and rapid temporal increases in the CDNC differences  
864 between the ice runs over a period from 12:50 to 13:20 LST on January 12<sup>th</sup>. This is due to  
865 steady and rapid temporal increases in CDNC, which are larger in the control run than in  
866 the low-aerosol run, over the period. More droplets or higher CDNC provides a larger  
867 integrated surface area of droplets where evaporation and condensation of droplets occur,  
868 and thus acts as more sources of evaporation and condensation. With steady and rapid  
869 temporal increases in CDNC as a source of evaporation and condensation, temporal  
870 increases in both evaporation and condensation show a jump (or a surge or a rapid increase)  
871 in them for the period between 12:50 and 13:20 LST on January 12<sup>th</sup> in each of the ice runs  
872 (Supplementary Figure 1). Here, evaporation occurs at grid points where the water-vapor  
873 pressure is lower than the water-vapor equilibrium saturation pressure for liquid particles  
874 and thus WBF mechanism can occur, while condensation occurs at grid points where the  
875 water-vapor pressure is higher than the water-vapor equilibrium saturation pressure for  
876 liquid particles. This jump is higher associated with the larger temporal increase in CDNC  
877 in the control run than in the low-aerosol run (Supplementary Figure1). This induces

878 differences in each of evaporation and condensation between the ice runs to jump, as also  
879 marked by the green-dashed box in Figure 11a, during the time period.

880 The jump in differences in condensation between the ice runs is not as high as that in  
881 differences in evaporation between the ice runs (Figure 11a). This situation accompanies  
882 the fact that in each of the ice runs, the jump in evaporation is higher than that in  
883 condensation (Supplementary Figure 1). This means that differences in the jump between  
884 evaporation and condensation are greater in the control run than in the low-aerosol run  
885 (Supplementary Figure 1). Hence, evaporation-driven jump in the disappearance of  
886 droplets outweighs condensation-driven jump in counteraction against the disappearance  
887 in each of the ice runs. Due to this, the increasing temporal trend of CDNC turns to its  
888 decreasing trend in each of the ice runs around 13:30 LST on January 12<sup>th</sup>. If the rate of  
889 this decrease in CDNC with time is equal between the ice runs, there is no decreasing trend  
890 in differences in CDNC between the runs. However, remember that differences in the jump  
891 between evaporation and condensation are greater in the control run than in the low-aerosol  
892 run. Hence, when the jumps occur, evaporation-induced disappearance of droplets is  
893 counteracted by condensation “less” in the control run than in the low-aerosol run. This  
894 induces the rate of the CDNC decrease to be greater in the control run than in the low-  
895 aerosol run. This in turn turns the increasing temporal trend of the CDNC differences  
896 between the ice runs to their decreasing trend around 13:30 LST on January 12<sup>th</sup> (Figure  
897 11a).

898 The decreasing temporal trend of CDNC contributes to a decreasing temporal trend  
899 of each evaporation and condensation, starting around 13:30 LST on January 12<sup>th</sup>, by  
900 reducing the integrated surface area of droplets in each of the ice runs. This decreasing  
901 trend of each evaporation and condensation is larger associated with the larger decreasing  
902 trend of CDNC in the control run than in the low-aerosol run (Supplementary Figure 1).  
903 This induces the increasing temporal trend of differences in each evaporation and  
904 condensation between the ice runs to change into their decreasing temporal trend around  
905 13:30 LST on January 12<sup>th</sup> (Figure 11a). The decreasing trend of evaporation in each of the  
906 ice runs is smaller than that in condensation (Supplementary Figure 1). Associated with  
907 this, the decreasing trend of differences in evaporation between the ice runs is smaller than  
908 that in condensation (Figure 11a). Stated differently, the temporal reduction in evaporation

909 in each of the ice runs and its differences between the runs from 13:30 LST on January 12<sup>th</sup>  
910 onwards during the initial stage occurs to a less extent as compared to that in condensation  
911 and its differences.

912

913 ii. Evaporation and condensation efficiency

914

915 For a given humidity, the increase in the surface-to-volume ratio of droplets increases the  
916 evaporation (condensation) efficiency by increasing the integrated surface area of droplets  
917 per unit volume or mass of droplets. Here, evaporation (condensation) efficiency is defined  
918 to be the mass of droplets that are evaporated (condensed) per unit volume or mass of  
919 droplets. Aerosol-induced increases in the surface-to-volume ratio and thus evaporation  
920 and condensation efficiency are caused by aerosol-induced increases in CDNC and  
921 associated decreases in the droplet size. Increasing CDNC, in turn, increases competition  
922 among droplets for given water vapor needed for their condensational growth, leading to  
923 decreases in the droplet size. The average droplet radius over grid points and time steps  
924 with non-zero CDNC is 7.3, 9.8, 8.7, and 10.5  $\mu\text{m}$  in the control, low-aerosol, control-noise  
925 and low-aerosol-noise runs, respectively. It is notable that the WBF-mechanism-induced  
926 evaporation per unit volume of droplets when the water-vapor pressure is lower than or  
927 equal to the water-vapor equilibrium saturation pressure for liquid particles but higher than  
928 the equilibrium pressure for ice particles is also strongly proportional to the surface-to-  
929 volume ratio of droplets (Pruppacher and Klett, 1978). Hence, between the ice runs,  
930 enhanced evaporation efficiency by aerosol-induced increases in the surface-to-volume  
931 ratio accompanies aerosol-enhanced WBF-mechanism-associated efficiency of  
932 evaporation in addition to aerosol-enhanced efficiency of evaporation when the water-  
933 vapor pressure is lower than the water-vapor equilibrium pressure for ice particles.

934 With the steady and rapid temporal increase in CDNC, there is a steady and rapid  
935 temporal enhancement of the surface-to-volume ratio of droplets and evaporation  
936 efficiency in each of the ice runs between 12:50 and 13:20 LST on January 12<sup>th</sup>. Remember  
937 that these increases in CDNC are larger in the control run than in the low-aerosol run. This  
938 induces the greater temporal enhancement of the ratio and evaporation efficiency in the  
939 control run than in the low-aerosol run. The temporal enhancement of the ratio and

940 evaporation efficiency accompanies the temporally enhancing WBF-mechanism-related  
941 efficiency of evaporation. This accompaniment boosts evaporation and enables the jump  
942 in temporal increases in evaporation to be greater than that in condensation in each of the  
943 ice runs. In association with the larger steady and rapid temporal increase in CDNC in the  
944 control run than in the low-aerosol run, the temporally enhancing WBF-mechanism-related  
945 efficiency of evaporation and its boost on evaporation enhance with increasing aerosol  
946 concentrations. This, in turn, enables greater aerosol-induced increases in evaporation than  
947 in condensation or the greater jump in differences in evaporation between the ice runs  
948 than that in condensation over the period between 12:50 and 13:20 LST on January 12<sup>th</sup>  
949 (Figure 11a). For the period between 12:50 and 13:20 LST, there is no steady and rapid  
950 temporal increase in differences in the entrainment rate at the PBL tops unlike the situation  
951 with CDNC differences between the ice runs (Figure 11b). Hence, the greater jump in  
952 differences in evaporation between the ice runs is not likely to be induced by entrainment.

953 Even when both evaporation and condensation rates decrease with time in association  
954 with the decreasing temporal trend of CDNC and the surface-to-volume ratio of droplets  
955 over a period after 13:30 LST on January 12<sup>th</sup> during the initial stage in each of the ice  
956 runs, evaporation (condensation) rates are maintained higher throughout the initial stage  
957 (up to ~15:30 LST) in association with the higher CDNC and surface-to-volume ratio of  
958 droplets in the control run than in the low-aerosol run (Figure 11a). The presence of the  
959 WBF mechanism and entrainment facilitates evaporation and this acts against the temporal  
960 decrease in evaporation with time over the period in each of the ice runs. This counteraction  
961 by the WBF mechanism and entrainment reduces the temporal decrease in evaporation and  
962 enables evaporation to reduce temporally to a less extent as compared to condensation in  
963 each of the ice runs for the period (Supplementary Figure 1). This accompanies the  
964 differences in the temporal reduction between evaporation and condensation that are larger  
965 in the control run than in the low-aerosol run (Supplementary Figure 1). This, in turn,  
966 enables differences in evaporation between the ice runs to reduce to a less extent as  
967 compared to those in condensation over the period (Figure 11a). Due to this, differences  
968 (or aerosol-induced increases) in evaporation and associated aerosol-induced increases in  
969 evaporation-driven negative buoyancy between the ice runs are higher than those in  
970 condensation and condensation-driven positive buoyancy, respectively, for the period



971 (Figure 11a). This induces the decreasing temporal trend of differences or aerosol-induced  
972 increases in updraft mass fluxes between the ice runs over the period (Figure 11a). The  
973 decreasing temporal trend of aerosol-induced increases in updraft mass fluxes eventually  
974 leads to lower updraft mass fluxes in the control run than in the low-aerosol run, as  
975 represented by negative differences in updraft mass fluxes between the ice runs from  
976 ~15:30 LST onwards during the initial stage (Figure 11a). Associated with this,  
977 condensation becomes smaller in the control run, as represented by negative differences in  
978 condensation between the ice runs from ~15:30 LST onwards during the initial stage  
979 (Figure 11a).

980 The role of the WBF mechanism described in this section can be clearly seen by  
981 comparing the ice runs in this section to the noise runs, with no WBF mechanism, detailed  
982 in the following Section b.

983

## 984 2) Deposition and condensation

985

986 The difference in deposition between the ice runs is negligible and does not vary much  
987 with time up to ~15:30 LST on January 12<sup>th</sup> when the difference starts to show its  
988 significant increase (Figure 11a). With the start of the decreasing temporal trend of  
989 condensation around 13:30 LST on January 12<sup>th</sup>, more water vapor, not used by  
990 condensation, becomes available for deposition as compared to that before 13:30 LST on  
991 January 12<sup>th</sup> in each of the ice runs. Remember that this decreasing trend is greater in the  
992 control run than in the low-aerosol run. Hence, from 13:30 LST on January 12<sup>th</sup> onwards,  
993 more water vapor is available for deposition in the control run than in the low-aerosol run.  
994 This leads to the start of larger aerosol-induced increases in deposition between the ice runs  
995 around 13:30 LST on January 12<sup>th</sup> as compared to those increases before ~ 13:30 LST on  
996 January 12<sup>th</sup> (Figure 11a). The decrease in condensation in the control run continues and  
997 its differences between the runs grow even after the negative differences in condensation  
998 between the runs start to appear around 15:30 LST on January 12<sup>th</sup>. Hence, aerosol-induced  
999 increases in the amount of water vapor, which is not used by condensation and available  
1000 for deposition, continue even after 15:30 LST on January 12<sup>th</sup>. This enables aerosol-  
1001 induced increases in deposition between the ice runs to continue even after 15:30 LST on

1002 January 12<sup>th</sup> (Figure 11a). This is despite the evaporation-driven lower updraft mass fluxes  
1003 in the control run than in the low-aerosol run from ~ 15:30 LST on January 12<sup>th</sup> onwards  
1004 (Figure 11a). This indicates that after ~ 15:30 LST on January 12<sup>th</sup>, the microphysical  
1005 process which is related to the competition between deposition and condensation and tends  
1006 to increase deposition with increasing aerosol concentrations outweighs dynamic processes  
1007 (i.e., updraft mass fluxes) which tend to reduce deposition with increasing aerosol  
1008 concentrations.

1009         The increasing temporal trend of aerosol-induced increases in deposition is not able  
1010 to outweigh the increasing trend of aerosol-induced decreases in condensation between the  
1011 ice runs after ~ 15:30 LST on January 12<sup>th</sup> (Figure 11a). Remember that there is no change  
1012 in the background concentration of aerosols acting as INP between the ice runs. Hence, as  
1013 seen in Figure 11a, there are negligible differences in CINC between the ice runs, although  
1014 more water vapor starts to be available for deposition in the control run than in the low-  
1015 aerosol run around 13:30 LST on January 12<sup>th</sup>. This indicates that CINC per unit water  
1016 vapor available for deposition is lower in the control run. Hence, the available water vapor  
1017 has more difficulty in finding the surface area of ice crystals for deposition in the control  
1018 run. The more difficulty in finding the surface area of ice crystals for deposition makes the  
1019 deposition of the more available water vapor less efficient in the control run than in the  
1020 low-aerosol run. This damps down the increase in deposition particularly after ~ 13:30 LST  
1021 on January 12<sup>th</sup> in the control run. Then, aerosol-induced increases in deposition are not  
1022 large enough to overcome aerosol-induced decreases in condensation in the control run  
1023 particularly after ~ 15:30 LST on January 12<sup>th</sup> (Figure 11a). This in turn leads to the lower  
1024 average WP in the control run than in the low-aerosol run over the whole simulation period.

1025

1026         b. Noice runs

1027

1028         As between the ice runs, between the noice runs, the activation- and condensationally-  
1029 enhanced counteraction outweighs the evaporation-induced decreases in CDNC, leading  
1030 to increases in CDNC with increasing aerosol concentrations (Figures 11a, 11c, and 12b).  
1031 However, in the noice runs, ice processes, the associated WBF mechanism and increase in  
1032 the WBF-mechanism-associated efficiency of evaporation with increasing aerosol

1033 concentrations are absent, although aerosol-induced increases in entrainment at the PBL  
 1034 tops and surface-to-volume ratio of droplets are present. The average entrainment rate over  
 1035 all grid points at the PBL tops and over the whole simulation period is 0.71 and 0.60 cm s<sup>-1</sup>  
 1036 in the control-noise and low-aerosol-noise runs, respectively. The average entrainment  
 1037 rate over all grid points at the PBL tops and over the whole simulation period is 0.13 and  
 1038 0.15 cm s<sup>-1</sup> in the control and low-aerosol runs. There are aerosol-induced decreases in the  
 1039 average entrainment over the whole simulation period between the ice runs. The boost of  
 1040 evaporation by the WBF mechanism in each of the ice runs leads to greater evaporation  
 1041 efficiency by outweighing the lower entrainment rate in the control run than in the control-  
 1042 noise run and in the low-aerosol run than in the low-aerosol-noise run. Aerosol-induced  
 1043 increases in the boost lead to aerosol-induced greater increases in evaporation efficiency  
 1044 between the ice runs than between the noise runs despite aerosol-induced decreases  
 1045 (increases) in the entrainment rate between the ice (noise) runs for the whole simulation  
 1046 period. Particularly for the initial stage, evaporation efficiency in the control, low-aerosol,  
 1047 control-noise, and low-aerosol-noise runs is 1.61, 0.90, 0.21, and 0.12 %, respectively.  
 1048 Here, to obtain evaporation efficiency, the cumulative values of evaporation and cloud-  
 1049 liquid mass at the last time step of the initial stage are calculated as follows:

1050

$$1051 \text{ A cumulative value of an arbitrary variable "A"} = \iint AdVdt \quad (1)$$

1052

1053 Here,  $dV = dxdydz$  and  $t$  represents time.  $x$ ,  $y$  and  $z$  represent displacement in east-west,  
 1054 north-south and vertical directions, respectively. Evaporation rate in a unit volume of air,  
 1055 which is in a unit of kg m<sup>-3</sup> s<sup>-1</sup>, at each grid point and time step is put into Eq. (1) as "A" to  
 1056 obtain the cumulative value of evaporation. To obtain the cumulative value of cloud-liquid  
 1057 mass, cloud-liquid mass in a unit volume of air at each grid point and time step is first  
 1058 divided by the time step. This divided cloud-liquid mass, which is also in a unit of kg m<sup>-3</sup>  
 1059 s<sup>-1</sup>, represents cloud-liquid mass per unit time and volume and is put into Eq. (1) as "A" to  
 1060 obtain the cumulative value of cloud-liquid mass. Then, the cumulative evaporation is  
 1061 divided by the cumulative cloud-liquid mass to obtain the evaporation efficiency for each  
 1062 of the runs.

1063           With temporal increases in CDNC, which are larger in the control-noice run than in  
1064 the low-aerosol-noice run, leading to those in CDNC differences between the noise runs,  
1065 there are temporal increases in condensation and evaporation, which are larger in the  
1066 control-noice run than in the low-aerosol-noice run, and thus in their differences between  
1067 the noise runs (Figure 11c). Associated with aerosol-induced smaller increases in  
1068 evaporation efficiency between the noise runs, aerosol-induced increases in condensation  
1069 are always greater than aerosol-induced increases in evaporation between the noise runs  
1070 during the initial stage (Figure 11c). This maintains aerosol-induced increases in updraft  
1071 mass fluxes between the noise runs and leads to aerosol-induced increases in WP between  
1072 the noise runs. Also, with higher CDNC and associated smaller sizes of droplets, there is  
1073 suppressed autoconversion in the control-noice run as compared to that in the low-aerosol-  
1074 noise run. Here, autoconversion is the process of droplets colliding with and coalescing  
1075 each other to grow into raindrops. Due to this, the average precipitation rate over all grid  
1076 points at cloud bases and over the whole simulation period is lower in the control-noice  
1077 run. The average cloud-base precipitation rate is 0.009 and 0.019  $\text{g m}^{-2} \text{s}^{-1}$  in the control-  
1078 noise and low-aerosol-noice runs, respectively. The difference in this average precipitation  
1079 rate between the noise runs is  $\sim$  two times smaller than that in the time- and column-  
1080 averaged condensation rate. Hence, while aerosol-induced precipitation suppression  
1081 contributes to higher WP in the control-noice run, this contribution is not as significant as  
1082 that of aerosol-enhanced condensation.

1083           In contrast to the situation in the noise runs, in the ice runs, after  $\sim$ 12:50 LST on January  
1084 12<sup>th</sup>, aerosol-induced increases in condensation become lower than those in evaporation,  
1085 leading to aerosol-induced lower updrafts and WP (Figure 11a). This comparison between  
1086 the ice and noise runs confirms that the presence of ice processes and the associated WBF  
1087 mechanism plays a critical role in the lower aerosol-induced increases in condensation than  
1088 in evaporation in the ice runs. Figure 13 schematically depicts the flow of processes that  
1089 are described in Section 4.2.1.

1090

#### 1091           **4.2.2 INP**

1092

1093 So far, we have examined effects of the increasing concentration of aerosols acting as CCN.  
1094 However, unlike situations in warm stratocumulus clouds that have garnered most of  
1095 attention in terms of aerosol-cloud interactions, not only aerosols acting as CCN but also  
1096 those acting as INP can affect mixed-phase stratocumulus clouds (Rangno and Hobbs, 2001;  
1097 Lohmann, 2002; Borys et al., 2003). The above-described INP-10 and INP-100 runs as  
1098 compared to the control run identifies how the increasing concentration of aerosols acting  
1099 as INP affects mixed-phase clouds. As seen in this comparison, the increasing  
1100 concentration of aerosols acting as INP causes WP to increase, contrary to effects of the  
1101 increasing concentration of aerosols acting as CCN. However, at each time step and grid  
1102 point, a factor by which the concentration of background aerosols acting as CCN varies  
1103 between the control and low-aerosol runs is different from that by which the concentration  
1104 of background aerosols acting as INP varies among the control, INP-10 and INP-100 runs.  
1105 For better comparisons between CCN and INP effects, it is better to make consistency in  
1106 the factors between simulations for CCN effects and those for INP effects. For this  
1107 consistency, the INP-reduced run is performed as the repeated control run by reducing the  
1108 concentration of background aerosols acting as INP (but not CCN) at each time step and  
1109 grid point by the same factor as used for the reduction in the concentration of background  
1110 aerosols acting as CCN in the low-aerosol run as compared to that in the control run. The  
1111 INP-reduced run is compared to the control run to examine the INP effects. The INP-  
1112 reduced run is identical to the low-aerosol run except that the concentration of background  
1113 aerosols acting as INP but not CCN at every time step and grid point after 05:00 LST on  
1114 January 12<sup>th</sup> is assumed to have that at 05:00 LST on January 12<sup>th</sup>.

1115 Figure 11d shows the time series of differences in deposition rate, condensation rate  
1116 and related variables between the control and INP-reduced runs. With the increasing  
1117 concentration of background aerosols acting as INP, there are more increases in CINC  
1118 between those runs than between the control and low-aerosol runs (Figures 11a and 11d).  
1119 During the initial stage before 20:00 LST on January 12<sup>th</sup>, overall, there is an increasing  
1120 temporal trend in differences in CINC between the control and INP-reduced runs due to  
1121 the larger increasing temporal trend in CINC in the control run than in the INP-reduced run  
1122 (Figure 11d). Increasing CINC provides the increasing integrated surface area of ice  
1123 crystals for deposition. This leads to the increasing temporal trend in deposition, which is

1124 larger in the control run, and in differences in deposition between the control and INP-  
1125 reduced runs (Figure 11d). However, due to no changes in the concentration of the  
1126 background aerosols acting as CCN between the control and INP-reduced runs, there are  
1127 negligible differences in CDNC between the control and INP-reduced runs as compared to  
1128 those between the control and low-aerosol runs (Figures 11a and 11d). More evaporation  
1129 occurs in the control run than in the INP-reduced run and this is contributed by the more  
1130 deposition and associated WBF mechanism (Figure 11d). Also, more entrainment  
1131 contributes to the more evaporation in the control run (Figure 11b). Between the INP-  
1132 reduced and control runs, with no increases in the concentration of background aerosols  
1133 acting as CCN, increases in the surface-to-volume ratio of droplets and the associated  
1134 enhancement in the WBF-mechanism-related efficiency of evaporation are negligible as  
1135 compared to those between the control and low-aerosol runs. Note that there are overall  
1136 larger increases in entrainment and associated evaporation between the control and INP-  
1137 reduced runs than between the control and low-aerosol runs (Figure 11b). The negligible  
1138 enhancement in the WBF-mechanism-related efficiency of evaporation overshadows the  
1139 overall larger increases in entrainment and associated evaporation between the control and  
1140 INP-reduced runs. This leads to aerosol-induced overall smaller increases in evaporation  
1141 between the control and INP-reduced runs than between the control and low-aerosol runs  
1142 (Figures 11a and 11d).

1143       Mainly due to the increase in evaporation, there is more negative buoyancy and  
1144 updraft mass fluxes start to reduce in the control run as compared to those in the INP-  
1145 reduced run around 12:50 LST on January 12<sup>th</sup> (Figure 11d). Eventually, updraft mass  
1146 fluxes in the control run become smaller than those in the INP-reduced run around 15:50  
1147 LST on January 12<sup>th</sup> (Figure 11d). This decrease occurs to a lesser extent mainly due to  
1148 overall smaller aerosol-induced increases in evaporation between the control and INP-  
1149 reduced runs than between the control and low-aerosol runs (Figures 11a and 11d).  
1150 Associated with weaker updrafts in the control run, condensation in the control run  
1151 becomes smaller than that in the INP-reduced run around 15:50 LST on January 12<sup>th</sup> but  
1152 to a lesser degree as compared to that between the control and low-aerosol runs (Figures  
1153 11a and 11d).

1154           When there is aerosol-induced reduction in condensation, there starts to be more  
1155 available water vapor for deposition and thus aerosol-induced increases in deposition  
1156 between the control and INP-reduced runs jump around 15:50 LST on January 12<sup>th</sup> (Figure  
1157 11d). This is similar to the situation between the control and low-aerosol runs. However,  
1158 due to greater aerosol-induced increases in CINC and the associated integrated surface area  
1159 of ice crystals, after ~ 15:50 LST on January 12<sup>th</sup>, there are greater aerosol-induced  
1160 increases in deposition between the control and INP-reduced runs than between the control  
1161 and low-aerosol runs (Figures 11a and 11d). Remember that the decrease in condensation,  
1162 starting around 15:50 LST on January 12<sup>th</sup>, between the control and INP-reduced runs is  
1163 smaller than that between the control and low-aerosol runs. This enables the increase in  
1164 deposition to overcome the decrease in condensation between the control and INP-reduced  
1165 runs. The larger increase in deposition than the decrease in condensation between the  
1166 control and INP-reduced runs eventually makes updrafts in the control run greater than  
1167 those in the INP-reduced run around 18:50 LST on January 12<sup>th</sup> (Figure 11d).

1168           Initiated by aerosol-induced greater increase in deposition during the initial stage,  
1169 there is aerosol-induced greater increase in IWP between the control and INP-reduced runs  
1170 than between the control and low-aerosol runs over the whole simulation period (Figure  
1171 14). Initiated by aerosol-induced smaller decrease in condensation during the initial stage,  
1172 there is aerosol-induced smaller decrease in LWP between the control and INP-reduced  
1173 runs than between the control and low-aerosol runs over the whole simulation period  
1174 (Figure 14). This greater increase in IWP dominates over the smaller decrease in LWP  
1175 between the control and INP-reduced runs, leading to an increase in WP in the control run  
1176 as compared to that in the INP-reduced run with an increase in the average cloud fraction  
1177 over time steps with non-zero cloud fraction from 0.89 in the INP-reduced run to 0.92 in  
1178 the control run. This is in contrast to the situation between the control and low-aerosol runs.  
1179 Hence, comparisons between the control, INP-reduced and the low-aerosol runs  
1180 demonstrate that whether there is an increasing concentration of aerosols acting as INP or  
1181 CCN has substantial impacts on how WP responds to the increasing concentration of  
1182 aerosols.

1183

1184           **4.2.3 Sedimentation of ice particles**

1185  
1186 With increasing concentrations of aerosols acting as CCN between the control and low-  
1187 aerosol runs, the size and fall velocity of ice crystals do not change significantly at the  
1188 initial stage. The average ice-crystal radius over grid points and time steps with non-zero  
1189 CINC for the initial stage is 54 and 52  $\mu\text{m}$  in the control and low-aerosol runs, respectively.  
1190 This means that aerosol-induced changes in the sedimentation of ice crystals do not affect  
1191 CINC, the associated integrated surface area of ice crystals and deposition significantly.  
1192 Moreover, as described in Section 4.2.1, the CDNC evolution (but not the CINC evolution)  
1193 plays a critical role in the different evolution of evaporation, condensation, and deposition  
1194 at the initial stage between the runs. Hence, it is not likely that aerosol-induced changes in  
1195 the sedimentation of ice crystals and associated ice particles such as snow, and associated  
1196 CINC have a significant impact on aerosol-induced changes in those phase-transition  
1197 processes at the initial stage and subsequently at later stages. To check this out, the control  
1198 and low-aerosol runs are repeated by setting the fall velocity of ice particles (including ice  
1199 crystals) to zero. These repeated runs are the control-no-sedim and low-aerosol-no-sedim  
1200 runs. Hence, in these repeated runs, there are no aerosol-induced changes in the  
1201 sedimentation of ice particles. The time- and domain-averaged IWP, LWP and WP are 14  
1202 (12), 5 (8) and 19 (20)  $\text{g m}^{-2}$ , respectively, in the control-no-sedim (low-aerosol-no-sedim)  
1203 run. The time- and domain-averaged IWP, LWP and WP are 11 (10), 7 (9), 18 (19)  $\text{g m}^{-2}$ ,  
1204 respectively, in the control (low-aerosol) run. The presence of the sedimentation decreases  
1205 IWP and increases LWP as compared to the situation with no sedimentation for each of the  
1206 control and low-aerosol runs. The differences in IWP and LWP between the control-no-  
1207 sedim and low-aerosol-no-sedim runs is slightly greater than that between the control and  
1208 low-aerosol runs. Hence, the presence of impacts of aerosols acting as CCN on the  
1209 sedimentation reduces aerosol impacts on IWP and LWP. However, results here show that  
1210 the qualitative nature of impacts of aerosols acting as CCN on cloud mass does not vary,  
1211 whether there are changes in the sedimentation of ice particles with increasing  
1212 concentrations of aerosols acting as CCN. This indicates that the presence of the  
1213 sedimentation and its aerosol-induced changes is not a factor that controls the qualitative  
1214 nature of impacts of aerosols acting as CCN on cloud mass.



1215 With increasing concentrations of aerosols acting as INP between the control and INP-  
1216 reduced runs, the size and fall velocity of ice crystals change at the initial stage. The  
1217 average ice-crystal radius over grid points and time steps with non-zero CINC for the initial  
1218 stage is 54 and 59  $\mu\text{m}$  in the control and INP-reduced runs, respectively. To see the effect  
1219 of these changes in the size and associated sedimentation of ice particles on the qualitative  
1220 nature of results between the control and INP-reduced runs, the INP-reduced run is  
1221 repeated by setting the fall velocity of ice particles to zero. This repeated run is referred to  
1222 as the INP-reduced-no-sedim run. The time- and domain-averaged IWP, LWP and WP are  
1223 14 (11), 5 (6) and 19 (17)  $\text{g m}^{-2}$ , respectively, in the control-no-sedim (INP-reduced-no-  
1224 sedim) run, while the time- and domain-averaged IWP, LWP and WP are 11 (7), 7 (8) and  
1225 18 (15)  $\text{g m}^{-2}$ , respectively, in the control (INP-reduced) run. The presence of the  
1226 sedimentation decreases IWP and increases LWP as compared to the situation with no  
1227 sedimentation for each of the control and INP-reduced runs. The difference in IWP  
1228 between the control-no-sedim and INP-reduced-no-sedim runs is smaller than that between  
1229 the control and INP-reduced runs. The difference in LWP between the control-no-sedim  
1230 and INP-reduced-no-sedim runs is not different from that between the control and INP-  
1231 reduced runs. Hence, the presence of impacts of aerosols acting as INP on the  
1232 sedimentation enhances aerosol impacts on IWP, although the presence does not affect  
1233 aerosol impacts on LWP. However, the qualitative nature of impacts of aerosols acting as  
1234 INP on cloud mass also does not vary, whether there are changes in the sedimentation of  
1235 ice particles with increasing concentrations of aerosols acting as INP. This indicates that  
1236 the presence of the sedimentation and its aerosol-induced changes is not a factor that  
1237 controls the qualitative nature of impacts of aerosols acting as INP on cloud mass.

1238

## 1239 **5. Summary and conclusions**

1240

1241 When it comes to stratocumulus clouds and their interactions with aerosols, warm clouds,  
1242 which are composed of liquid particles only, have garnered most of the attention. However,  
1243 in mid-latitudes, particularly during the wintertime, there are frequent occurrences of  
1244 mixed-phase stratocumulus clouds, which are composed of both liquid and solid particles.  
1245 The level of understanding of mechanisms that control the development of these mixed-

1246 phase clouds and their interactions with aerosols has been low. Motivated by this, this study  
1247 aims to improve our understanding of the development of these mixed-phase stratocumulus  
1248 clouds and their interactions with aerosols by focusing on roles of ice particles and  
1249 processes in the development and interactions.

1250 Ice crystals (i.e., cloud ice) and their interactions with droplets (i.e., cloud liquid) in a  
1251 selected system of mixed-phase stratocumulus clouds lower cloud mass substantially as  
1252 compared to that in warm stratocumulus clouds. This is due to insufficient compensation  
1253 of the reduced condensation and LWP by deposition and IWP in the mixed-phase clouds.  
1254 This insufficient compensation is related to low CINC and associated low integrated  
1255 surface area of ice crystals in the mixed-phase clouds. As the concentration of aerosols  
1256 acting as INP and CINC increase, deposition enhances and this enables cloud mass in the  
1257 mixed-phase clouds to be similar to that in the warm clouds.

1258 In the mixed-phase clouds, with the increasing concentration of aerosols acting as  
1259 CCN, there are decreases in cloud mass. In the mixed-phase clouds, aerosol-induced  
1260 increases in the evaporation of droplets, which involve the WBF mechanism, and their  
1261 impacts on updrafts outweigh aerosol-intensified feedbacks between condensation and  
1262 updrafts. This leads to aerosol-induced decreases in cloud mass. However, in the warm  
1263 clouds, with the increasing concentration of aerosols acting as CCN, there are increases in  
1264 cloud mass. Due to the absence of the WBF mechanism, in the warm clouds, aerosol-  
1265 induced increases in the evaporation of droplets are not as efficient as in the mixed-phase  
1266 clouds. This enables aerosol-intensified feedbacks between condensation and updrafts to  
1267 induce aerosol-induced increases in cloud mass in the warm clouds. With the increases in  
1268 the concentration of aerosols acting as INP, there are aerosol-induced greater increases in  
1269 CINC and deposition than with the increases in the concentration of aerosols acting as  
1270 CCN. This enables the increasing concentration of aerosols acting as INP to induce  
1271 increases in cloud mass, which is in contrast to the situation with the increasing  
1272 concentration of aerosols acting as CCN.

1273 It is generally true that the conventional wisdom of stratiform clouds and aerosol  
1274 effects on them has been established mostly by relying on warm clouds (Ramaswamy et  
1275 al., 2001; Forster et al., 2007; Wood, 2012). For example, this wisdom generally indicates  
1276 that increasing concentrations of aerosols acting as CCN increase cloud mass (Albrecht,

1277 1989). However, in contrast to this, this study shows that in the mixed-phase stratiform  
1278 clouds, the increasing concentration of aerosols acting as CCN can reduce cloud mass via  
1279 CCN-induced changes in interactions between ice and liquid particles. It is also shown that  
1280 the increasing concentration of aerosols acting as INP enhances cloud mass via INP-  
1281 induced changes in interactions between ice and liquid particles, in contrast to roles of the  
1282 increasing concentration of aerosols acting as CCN in cloud mass. In addition, this study  
1283 finds that the presence of ice particles and its interactions with liquid particles reduce cloud  
1284 mass in the mixed-phase clouds as compared to that in warm clouds. Mid-latitude winter  
1285 stratiform clouds and high-latitude clouds such as the Arctic stratiform clouds frequently  
1286 involve ice particles as well as liquid particles. As discussed in Stevens and Feingold  
1287 (2009), our lack of understanding of these clouds and their interactions with aerosols has  
1288 made a significant contribution to the high uncertainty in the prediction of climate change.  
1289 Hence, to reduce this uncertainty especially by reducing the related uncertainty in climate  
1290 models, we have to go beyond the warm-cloud-based traditional parameterizations of  
1291 clouds and their interactions with aerosols in climate models. For this, this study indicates  
1292 that it is imperative to develop new parameterizations that consider impacts of interactions  
1293 between ice and liquid particles on clouds, and the interplay of those impacts with varying  
1294 concentrations of aerosols acting not only as CCN but also as INP.

1295 The average CINC in the control run in this study is on the order of magnitude of  $\sim 0.1$   
1296  $\text{cm}^{-3}$  and this is an order of magnitude lower than that in the control run in Lohmann and  
1297 Diehl (2006) for similar temperature and CDNC ranges between the runs. Remember that  
1298 this study uses parameterizations by Lohmann and Diehl (2006) for the heterogeneous INP  
1299 activation. In the control run in Lohmann and Diehl (2006), the INP concentrations, which  
1300 are dependent only on temperature, are used for the INP activation. However, in the control  
1301 run in this study, instead of obtaining the INP concentrations empirically using the  
1302 temperature as in Lohmann and Diehl (2006), the observed spatiotemporal variation of the  
1303 INP concentration is considered for the INP activation. Lohmann and Diehl (2006) have  
1304 shown that using the INP concentrations, which are empirically obtained based only on  
1305 temperature, for the INP activation can increase CINC by a factor of  $\sim 10$  as compared to  
1306 that when the spatiotemporal variation of the INP concentration, as a result of above-  
1307 mentioned processes related to aerosols, is considered for the activation. It is believed that

1308 this explains the discrepancy in CINC between the control in this study and that in  
1309 Lohmann and Diehl (2006).

1310 Note that many of the previous studies of mixed-phase stratocumulus clouds (e.g.,  
1311 Ovchinnikov et al., 2011; Possner et al., 2017) have focused on roles of cloud-top radiative  
1312 cooling, entrainment and sedimentation of ice particles in mixed-phase stratocumulus  
1313 clouds and their interactions with aerosols. However, there have not been many studies that  
1314 focus on roles of microphysical interactions, which involve microphysical processes (e.g.,  
1315 evaporation, condensation and deposition) and factors (e.g., cloud-particle concentrations  
1316 and sizes), between ice and liquid particles in those clouds and their interplay with aerosols.  
1317 Hence, we believe that this study contributes to the more general understanding of mixed-  
1318 phase clouds and their interactions with aerosols.

1319

1320

1321

1322

1323

1324

1325

1326

1327

1328

1329

1330

1331

1332

1333

1334

1335

1336

1337

1338

1339 **Code/Data availability**

1340

1341 The Code/data used are currently private and stored in our private computer system.  
1342 Opening the data to the public requires approval from funding sources. Since funding  
1343 projects associated with this work are still going on, these sources do not allow the data to  
1344 be open to the public; 2–3 years after these project ends, the data can be open to the public.  
1345 However, if there is any inquiry about the data, contact the corresponding author Seoung  
1346 Soo Lee (slee1247@umd.edu).

1347

1348 **Author contributions**

1349 SSL, KJH and BGK established essential initiative ideas to start this work. While SSL  
1350 worked on the analysis of simulation data, KJH and MGM worked on the analysis of  
1351 observation data. MK, HK, NU and JG participated in the preliminary analysis of  
1352 simulation and observation data, and provided ideas to improve the presentation of results  
1353 by reviewing the manuscript. YZ, KOC and GUK provided ideas to deal with reviewers’  
1354 comments, while CHJ and JU performed additional simulations and associated analysis to  
1355 handle those comments.

1356

1357 **Competing interests**

1358 The authors declare that they have no conflict of interest.

1359

1360 **Acknowledgements**

1361

1362 This study is supported by the National Research Foundation of Korea (NRF) grant funded  
1363 by the Korea government (MSIT) (No. NRF2020R1A2C1003215), the “Construction of  
1364 Ocean Research Stations and their Application Studies” project funded by the Ministry of  
1365 Oceans and Fisheries, South Korea, and the FRIEND (Fine Particle Research Initiative in  
1366 East Asia Considering National Differences) Project through the National Research  
1367 Foundation of Korea (NRF) funded by the Ministry of Science and ICT  
1368 (2020M3G1A1114617).

1369

1370

1371 **References**

1372

1373 Ackerman, A. S., Kirkpatrick, M. P., Stevens, D. E., and Toon, O. B.: The impact of  
1374 humidity above stratiform clouds on indirect aerosol climate forcing, *Nature*, 432,  
1375 1014-1017, 2004.

1376 Albrecht, B. A.: Aerosols, cloud microphysics, and fractional cloudiness, *Science*, 245,  
1377 1227-1230, 1989.

1378 Bergeron, T.: On the physics of clouds and precipitation. *Proces Verbaux de l'Association*  
1379 *de Meteorologie, International Union of Geodesy and Geophysics*, 156–178, 1935.

1380 Bodas-Salcedo, A., Hill, P. G., Furtado, K., Williams, K. D., Field, P. R., Manners, J. C.,  
1381 Hyder, P., and Kato, S.: Large contribution of supercooled liquid clouds to the solar  
1382 radiation budget of the Southern Ocean, *J. Climate*, 29, 4213–4228,  
1383 doi:10.1175/JCLI-D-15-0564.1, 2016.

1384 Borys, R. D., Lowenthal, D. H., Cohn, S. A. and Brown, W. O. J.: Mountaintop and radar  
1385 measurements of anthropogenic aerosol effects on snow growth and snowfall rate.  
1386 *Geophys. Res. Lett.*, 30, 1538, doi:10.1029/2002GL016855 ,2003.

1387 Brown, A., Milton, S., Cullen, M., Golding, B., Mitchell, J., and Shelly, A.: Unified  
1388 modeling and prediction of weather and climate: A 25-year journey, *Bull. Am*  
1389 *Meteorol. Soc.* 93, 1865–1877, 2012.

1390 Chen, F., and Dudhia, J.: Coupling an advanced land-surface hydrology model with the  
1391 Penn State-NCAR MM5 modeling system. Part I: Model description and  
1392 implementation, *Mon. Wea. Rev.*, 129, 569–585, 2001.

1393 Dong, X., and Mace, G. G.: Arctic stratus cloud properties and radiative forcing derived  
1394 from ground-based data collected at Barrow, Alaska. *J. Climate*, 16, 445–461,  
1395 doi:10.1175/1520-0442(2003)016,0445:ASCPAR.2.0.CO;2, 2003.

1396 Eun, S.-H., Kim, B.-G., Lee, K.-M., and Park, J.-S.: Characteristics of recent severe haze  
1397 events in Korea and possible inadvertent weather modification, *SOLA*, 12, 32-36,  
1398 2016.

1399 Faller, K: MTSAT-1R: A multifunctional satellite for Japan and the Asia-Pacific region,  
1400 *Proceedings of the 56th IAC 2005*, Fukuoda, Japan, Oct. 17-21, 2005, IAC-05-  
1401 B3.2.04

- 1402 Fan, J., Yuan, T., Comstock, J. M., et al.: Dominant role by vertical wind shear in regulating  
1403 aerosol effects on deep convective clouds, *J. Geophys. Res.*, 114,  
1404 doi:10.1029/2009JD012352, 2009.
- 1405 Findeisen, W.: Kolloid-meteorologische Vorgänge bei Neiderschlagsbildung. *Meteor. Z.*,  
1406 55, 121–133, 1938.
- 1407 Forster, P., et al., Changes in atmospheric constituents and in radiative forcing, in: *Climate*  
1408 *change 2007: the physical science basis*, Contribution of working group I to the Fourth  
1409 *Assessment Report of the Intergovernmental Panel on Climate Change*, edited by  
1410 Solomon, S., et al., Cambridge Univ. Press, New York, 2007.
- 1411 Fouquart, Y., and Bonnel, B.: Computation of solar heating of the Earth's atmosphere: a  
1412 new parameterization, *Beitr. Phys. Atmos.*, 53, 35-62, 1980.
- 1413 Grell, G. A., Peckham, S. E., Schmitz, R., McKeen, S. A., Frost, G., Skamarock, W. C.,  
1414 and Eder, B.: Fully coupled online chemistry in the WRF model, *Atmos.*  
1415 *Environ.*, 39, 6957– 6976, 2005.
- 1416 Guo, J., M. Deng, S. S. Lee, F. Wang, Z. Li, P. Zhai, H. Liu, W. Lv, W. Yao, and X. Li:  
1417 Delaying precipitation and lightning by air pollution over the Pearl River Delta. Part  
1418 I: Observational analyses, *J. Geophys. Res. Atmos.*, 121, 6472–6488,  
1419 doi:10.1002/2015JD023257, 2016.
- 1420 Ha, K.-J., Nam, S., Jeong, J.-Y., et al., Observations utilizing Korean ocean research  
1421 stations and their applications for process studies, *Bull. Amer. Meteor. Soc.*, 100,  
1422 2061-2075, 2019.
- 1423 Hahn, C. J., and Warren, S. G.: A gridded climatology of clouds over land (1971–96) and  
1424 ocean (1954–97) from surface observations worldwide. *Numeric Data Package NDP-*  
1425 *026EORNL/CDIAC-153*, CDIAC, Department of Energy, Oak Ridge, TN, 2007.
- 1426 Hartmann, D. L., Ockert-Bell, M. E., and Michelsen, M. L.: The effect of cloud type on  
1427 earth's energy balance—Global analysis, *J. Climate*, 5, 1281–1304, 1992.
- 1428 Holben, B. N., Tanré, D., Smirnov, et al.: An emerging ground-based aerosol climatology:  
1429 Aerosol optical depth from AERONET, *J. Geophys. Res.*, 106, 12067–12097, 2001.
- 1430 Hu, Y., Rodier, S., Xu, K.-M., Sun, W., Huang, J., Lin, B., Zhai, P., and Josset, D.:  
1431 Occurrence, liquid water content and fraction of supercooled water clouds from  
1432 combined CALIOP/IIR/MODIS measurements, *J. Geophys. Res.*, 115, D00H34,

- 1433 doi:10.1029/2009JD012384, 2010.
- 1434 Huang, Y., Siems, S. T., Manton, M. J., Protat, A. and Delanöe, J.: A study on the low-  
1435 altitude clouds over the Southern Ocean using the DARDAR-MASK, *J. Geophys.*  
1436 *Res.*, 117, D18204, doi:10.1029/2012JB009424, 2012.
- 1437 Intrieri, J. M., Shupe, M. D., Uttal, T. and McCarty, B. J.: An annual cycle of Arctic cloud  
1438 characteristics observed by radar and lidar at SHEBA, *J. Geophys. Res.*, 107, 8030,  
1439 doi:10.1029/2000jc000423, 2002.
- 1440 Jackson, R. C., and Coauthors: The dependence of Arctic mixed-phase stratus ice cloud  
1441 microphysics on aerosol concentration using observations acquired during ISDAC  
1442 and M-PACE, *J. Geophys. Res.*, 117, D15207, doi:10.1029/2012JD017668, 2012.
- 1443 Kanitz, T., Seifert, P., Ansmann, A., Engelmann, R., Althausen, D., Casiccia, C. and  
1444 Rohwer, E. G.: Contrasting the impact of aerosols at northern and southern  
1445 midlatitudes on heterogeneous ice formation, *Geophys. Res. Lett.*, 38,  
1446 L17802, doi:10.1029/2011GL048532, 2011.
- 1447 Khain, A., BenMoshe, N. and Pokrovsky, A.: Factors determining the impact of aerosols  
1448 on surface precipitation from clouds: Attempt of classification, *J. Atmos. Sci.*, 65,  
1449 1721 – 1748, 2008.
- 1450 Khain, A., Pokrovsky, A., Rosenfeld, D., Blahak, U., and Ryzhkoy, A.: The role of CCN in  
1451 precipitation and hail in a mid-latitude storm as seen in simulations using a spectral  
1452 (bin) microphysics model in a 2D dynamic frame, *Atmos. Res.*, 99, 129–146, 2011.
- 1453 Klemp, J. B., Skamarock, W. C., and Dudhia, J.: Conservative split-explicit time  
1454 integration methods for the compressible nonhydrostatic equations, *Mon. Weather*  
1455 *Rev.*, 135, 2897 – 2913, 2007.
- 1456 Koop, T., Luo, B. P., Tsias, A. and Peter, T.: Water activity as the determinant for  
1457 homogeneous ice nucleation in aqueous solutions, *Nature*, 406, 611-614, 2000.
- 1458 Lance, S., Brock, C. A., Rogers, D. and Gordon, J. A.: Water droplet calibration of the  
1459 Cloud Droplet Probe (CDP) and inflight performance in liquid, ice and mixed-phase  
1460 clouds during ARCPAC, *Atmos. Meas. Tech.*, 3, 1683–1706, doi:10.5194/amt-3-  
1461 1683-2010, 2010.
- 1462 Lebo, Z. J., and Morrison, H.: Dynamical effects of aerosol perturbations on simulated  
1463 idealized squall lines, *Mon. Wea. Rev.*, 142, 991-1009, 2014.



- 1464 Lee, S., Ho, C.-H., Lee, Y. G., Choi, H.-J. and Song, C.-K.: Influence of transboundary air  
1465 pollutants from China on the high-PM10 episode in Seoul, Korea for the period  
1466 October 16–20, 2008. *Atmos. Environ.*, 77, 430–439, 2013.
- 1467 Lee, S. S., Kim, B.-G., and Yum, S. S., et al.: Effect of aerosol on evaporation, freezing and  
1468 precipitation in a multiple cloud system, *Clim. Dyn.*, 48, 1069-1087, 2016.
- 1469 Lee, S. S., Donner, L. J., Phillips, V. T. J. and Ming, Y.: The dependence of aerosol effects  
1470 on clouds and precipitation on cloud-system organization, shear and stability. *J.*  
1471 *Geophys. Res.*, 113, D16202, doi:10.1029/2007JD009224, 2008.
- 1472 Lohmann, U.: Agglaciation indirect aerosol effect caused by soot aerosols, *Geophys. Res.*  
1473 *Lett.*, 29, doi:10.1029/2001GL014357, 2002.
- 1474 Michalakes, J., Chen, S., Dudhia, J., Hart, L., Klemp, J., Middlecoff, J. and Skamarock,  
1475 W.: Development of a next generation regional weather research and forecast model,  
1476 in *Developments in Teracomputing: Proceedings of the Ninth ECMWF Workshop on*  
1477 *the Use of High Performance Computing in Meteorology*, edited by W. Zwiefelhofer  
1478 and N. Kreitz, pp. 269 – 276, World Sci., Singapore, 2001.
- 1479 Mlawer, E. J., Taubman, S. J., Brown, P. D., Iacono, M. J., and Clough, S. A.: RRTM, a  
1480 validated correlated-k model for the longwave, *J. Geophys. Res.*, 102, 16663-16668,  
1481 1997.
- 1482 Morrison, A. E., Siems, S. T. and Manton, M. J.: A three year climatology of cloud-top  
1483 phase over the Southern Ocean and North Pacific, *J. Climate*, 24, 2405–  
1484 2418, doi:10.1175/2010JCLI3842.1, 2011.
- 1485 Morrison, H., and Grabowski, W. W.: Cloud-system resolving model simulations of aerosol  
1486 indirect effects on tropical deep convection and its thermodynamic environment,  
1487 *Atmos. Chem. Phys.*, 11, 10503–10523, 2011.
- 1488 Möhler, O., et al, Efficiency of the deposition mode ice nucleation on mineral dust particles,  
1489 *Atmos. Chem. Phys.*, 6, 3007-3021, 2006.
- 1490 Naud, C., Booth, J. F. and Del Genio, A. D.: Evaluation of ERA-Interim and MERRA  
1491 cloudiness in the Southern Ocean, *J. Climate*, 27, 2109–2124, doi:10.1175/JCLI-D-  
1492 13-00432.1, 2014.
- 1493 Oh, H.-R., Ho, C.-H., Kim, J., Chen, D., Lee, S., Choi, Y.-S., Chang, L.-S., and Song, C.-  
1494 K.: Long-range transport of air pollutants originating in China: A possible major cause

- 1495 of multi-day high-PM10 episodes during cold season in Seoul, Korea. *Atmos.*  
1496 *Environ.*, 109, 23–30, 2015.
- 1497 Ovchinnikov, M., Korolev, A., and Fan, J.: Effects of ice number concentration on  
1498 dynamics of a shallow mixed-phase stratiform cloud, *J. Geophys. Res.*, 116, D00T06,  
1499 doi:10.1029/2011JD015888, 2011.
- 1500 Possner, A., Ekman, A. M. L., and Lohmann, U.: Cloud response and feedback processes  
1501 in stratiform mixed-phase clouds perturbed by ship exhaust, *Geophys. Res. Lett.*, 44,  
1502 1964–1972, doi:10.1002/2016GL071358, 2017.
- 1503 Pruppacher, H. R. and Klett, J. D.: *Microphysics of clouds and precipitation*, 714pp, D.  
1504 Reidel, 1978.
- 1505 Rangno, A. L., and Hobbs, P. V.: Ice particles in stratiform clouds in the Arctic and possible  
1506 mechanisms for the production of high ice concentrations, *J. Geophys. Res.*, 106,15  
1507 065–15 075, doi:10.1029/2000JD900286, 2001.
- 1508 Ramaswamy, V., et al.: Radiative forcing of climate change, in *Climate Change 2001: The*  
1509 *Scientific Basis*, edited by J. T. Houghton et al., 349-416, Cambridge Univ. Press,  
1510 New York, 2001.
- 1511 Shupe, M. D., Uttal, T., Matrosov, S. Y. and Rrisch, A. S.: Cloud water contents and  
1512 hydrometeor sizes during the FIRE Arctic clouds experiment, *J. Geophys. Res.*, 106,  
1513 15 015–15 028, doi:10.1029/2000JD900476, 2001.
- 1514 Shupe, M. D., Uttal, T. and Matrosov, S. Y.: Arctic cloud microphysics retrievals from  
1515 surface-based remote sensors at SHEBA, *J. Appl. Meteor.*, 44, 1544–1562,  
1516 doi:10.1175/JAM2297.1, 2005.
- 1517 Skamarock, W. C., Klemp, J. B., Dudhia, J., Gill, D. O., Barker, D. M., Duda, M. G., Wang,  
1518 W., and Powers, J. G.: A description of the advanced research WRF version 3, NCAR  
1519 Tech. Note NCAR/TN-475+STR, 113 pp., Boulder, Colo., 2008.
- 1520 Stephens, G. L., and Greenwald, T. J.: Observations of the Earth's radiation budget in  
1521 relation to atmospheric hydrology. Part II: Cloud effects and cloud feedback. *J.*  
1522 *Geophys. Res.*, 96, 15 325–15 340, 1991.
- 1523 Stevens, B., and Feingold, G.: Untangling aerosol effects on clouds and precipitation in a  
1524 buffered system, *Nature*, 461, 607-613, 2009.
- 1525 Twomey, S.: The influence of pollution on the shortwave albedo of clouds, *J. Atmos. Sci.*,

- 1526 34, 1149-1152, 1977.
- 1527 Twomey, S.: Pollution and the Planetary Albedo, *Atmos. Env.*, 8,1251-1256, 1974.
- 1528 Wang, H., Skamarock, W. C., and Feingold, G.: Evaluation of scalar advection schemes in  
1529 the Advanced Research WRF model using large-eddy simulations of aerosol-cloud  
1530 interactions, *Mon. Wea. Rev.*, 137, 2547-2558, 2009.
- 1531 Warren, S. G., Hahn, C. J., London, J., Chervin, R. M., and Jenne, R. L.: Global distribution  
1532 of total cloud cover and cloud types over land. NCAR Tech. Note NCAR/TN-  
1533 273+STR, National Center for Atmospheric Research, Boulder, CO, 29 pp. + 200  
1534 maps, 1986.
- 1535 Wegener, A.: *Thermodynamik der Atmosphäre*. J. A. Barth, 311 pp, 1911.
- 1536 Wood, R.: Stratocumulus clouds, *Mon. Wea. Rev.*, 140, 2373-2423, 2012.
- 1537 Young, G., Connolly, P. J., Jones, H. M., and Choullarton, T. W.: Microphysical sensitivity  
1538 of coupled springtime Arctic stratocumulus to modelled primary ice over the ice pack,  
1539 marginal ice, and ocean, *Atmos. Chem. Phys.*, 17, 4209–4227,  
1540 <https://doi.org/10.5194/acp-17-4209-2017>, 2017.
- 1541 Zuidema, P., Westwater, E. R., Fairall, C. and Hazen, D.: Ship-based liquid water path  
1542 estimates in marine stratocumulus, *J. Geophys. Res.*, 110, D20206,  
1543 doi:10.1029/2005JD005833, 2005.
- 1544
- 1545
- 1546
- 1547
- 1548
- 1549
- 1550
- 1551
- 1552
- 1553
- 1554
- 1555
- 1556
- 1557
- 1558
- 1559
- 1560
- 1561
- 1562

1563 **FIGURE CAPTIONS**

1564

1565 Figure 1. A rectangle represents the domain of interest in terms of the aerosol advection.  
1566 A dot on the top-right corner of the rectangle marks a station that measures  $PM_{10}$  and  $PM_{2.5}$   
1567 in Baekryongdo island as detailed in Section 2. An area to the east of the yellow line in the  
1568 rectangle is the Seoul area. In the Seoul area, a dot marks a representative station that  
1569 measures  $PM_{10}$  and  $PM_{2.5}$  in the Seoul area as detailed in Section 2. A closed dotted line  
1570 marks the boundary of the Seoul city.

1571

1572 Figure 2. (a) Time series of  $PM_{10}$  and  $PM_{2.5}$  observed at the ground station in Baekryongdo  
1573 island (BN) and a representative ground station in the Seoul area (SL). The abscissa  
1574 represents days between January 10<sup>th</sup> and 19<sup>th</sup> in 2013. The blue (red) arrow marks time  
1575 when aerosol mass starts to increase in BN (SL) due to the advection of aerosols from East  
1576 Asia to the Seoul area. The spatial distribution of  $PM_{2.5}$ , which is observed and measured  
1577 by the ground stations and interpolated into grid point over the rectangle in Figure 1, at (b)  
1578 05:00 LST and (c) 18:00 LST on January 12<sup>th</sup> in 2013.

1579

1580 Figure 3. The vertical distributions of the radiosonde-observed (a) potential temperature  
1581 and (b) water-vapor mass density at 03:00 LST and 15:00 LST on January 12<sup>th</sup>.

1582

1583 Figure 4. Aerosol size distribution at the surface. N represents aerosol number  
1584 concentration per unit volume of air and D represents aerosol diameter.

1585

1586 Figure 5. Time series of (a) the domain-averaged liquid-water path (LWP), ice-water path  
1587 (IWP) and water path (WP), which is the sum of LWP and IWP, for the control run, and  
1588 LWP for the control-noise run, and (b) the domain-averaged condensation rates, deposition  
1589 rates and the sum of those rates in the control run and condensation rates in the control-  
1590 noise run. (c) Vertical distribution of the time- and domain-averaged evaporation rates and  
1591 (d) the average CDNC over grid points and time steps with non-zero CDNC for the initial  
1592 stage between 00:00 LST and 20:00 LST on January 12<sup>th</sup>.

1593

1594 Figure 6. Vertical distributions of (a) the time- and domain-averaged updraft mass fluxes  
1595 for the control and control-noise runs and (b) the average cloud ice number concentration  
1596 (CINC) over grid points and time steps with non-zero CINC (for the whole domain and  
1597 simulation period in the control run).

1598

1599 Figure 7. Cumulative frequency of (a) WP in the control run and LWP, which is WP, in  
1600 the control-noise run and (b) LWP and IWP in the control run and LWP in the control-  
1601 noise run at the last time step.

1602

1603 Figure 8. (a) Vertical distributions of the average CINC over grid points and time steps  
1604 with non-zero CINC (for the whole domain and simulation period) in the control, INP-10,  
1605 and INP-100 runs. Time series of the domain-averaged condensation rates, deposition rates  
1606 and the sum of those rates (b) in the INP-10 run and (c) in the INP-100 run. In (b) and (c),  
1607 condensation rates in the control-noise run are additionally displayed.

1608

1609 Figure 9. (a) Time series of the domain-averaged LWP, IWP and WP for the control run,  
1610 LWP for the control-noise run and WP for the INP-10 and INP-100 runs. (b) Cumulative  
1611 frequency of LWP, IWP and WP for the control, INP-10 and INP-100 runs at the last time  
1612 step.

1613

1614 Figure 10. (a) Time series of the domain-averaged LWP, IWP and WP for the control and  
1615 low-aerosol runs, and LWP, which is also WP, for the control-noise and low-aerosol-noise  
1616 runs. (b) Cumulative frequency of WP for the control, low-aerosol run, control-noise and  
1617 low-aerosol-noise runs, and (c) LWP and IWP for the control and low-aerosol runs and  
1618 LWP in the control-noise and low-aerosol-noise runs at the last time step.

1619

1620 Figure 11. (a) Time series of differences in the domain-averaged updraft mass fluxes,  
1621 deposition, condensation and evaporation rates, the average CDNC (CINC) over grid  
1622 points with non-zero CDNC (CINC) between the control and low-aerosol runs (the control  
1623 run minus the low-aerosol run). (b) Time series of differences in the average entrainment  
1624 rate over all grid points at the PBL tops between the control and low-aerosol runs (the

1625 control run minus the low-aerosol run) and between the control and INP-reduced runs (the  
1626 control run minus the INP-reduced run). (c) Same as (a) but between the control-noice and  
1627 low-aerosol-noice runs (the control-noice run minus the low-aerosol-noice run) and (d)  
1628 same as (a) but between the control and INP-reduced runs (the control run minus the INP-  
1629 reduced run). Dashed lines in (a), (b), (c) and (d) represent zero differences. In (c), due to  
1630 the absence of ice processes in the noise runs, differences in deposition rates and CINC are  
1631 absent. A green-dashed box in (a) and (b) marks a time period when steady and rapid  
1632 temporal increases in the CDNC differences and a jump in differences in each of  
1633 condensation and evaporation rates between the control and low-aerosol runs occur (see  
1634 text for details).

1635

1636 Figure 12. Vertical distributions of the average CDNC over grid points and time steps with  
1637 non-zero CDNC (for the whole domain and simulation period) (a) in the control and low-  
1638 aerosol runs, and (b) in the control-noice and low-aerosol-noice runs.

1639

1640 Figure 13. A schematic diagram that depicts the flow of processes that are described in  
1641 Section 4.2.1 and associated with responses of clouds to increasing aerosols acting as CCN.

1642

1643 Figure 14. Time series of the domain-averaged LWP, IWP and WP for the control, low-  
1644 aerosol and INP-reduced runs, and LWP, which is also WP, for the control-noice and low-  
1645 aerosol-noice runs.

1646

1647

1648

1649

1650

1651

1652

1653

1654

1655

Simulation s	Increases in the background concentration of aerosols acting as CCN due to the aerosol advection after 05:00 LST on January 12 <sup>th</sup>	Ice processes	Background concentration of aerosols acting as INP	Ice-particle Sedimentation	Liquid-particle Sedimentation
Control run	Present	Present	100 times lower than the background concentration of aerosols acting as CCN	Present	Present
Low-aerosol run	Absent	Present	Same as in the control run	Present	Present
Control-noise run	Present	Absent	Absent	Present	Present
Low-aerosol-noise run	Absent	Absent	Absent	Present	Present
INP-10 run	Present	Present	10 times higher than in the control run	Present	Present
INP-100 run	Present	Present	100 times higher than in the control run	Present	Present
INP-reduced run	Present	Present	Reduced in the same way as CCN is reduced in the low-aerosol run	Present	Present
Control-no-sedim	Present	Present	Same as in the control run	Absent	Present

Control- no-sedim- ice-liq	Present	Present	Same as in the control run	Absent	Absent
Low- aerosol-no- sedim	Absent	Present	Same as in the control run	Absent	Present
INP-10-no- sedim	Present	Present	Same as in the INP-10 run	Absent	Present
INP-100- no-sedim	Present	Present	Same as in the INP-100 run	Absent	Present
INP- reduced- no-sedim	Present	Present	Same as in the INP- reduced run	Absent	Present

1656

1657 Table 1. Summary of simulations

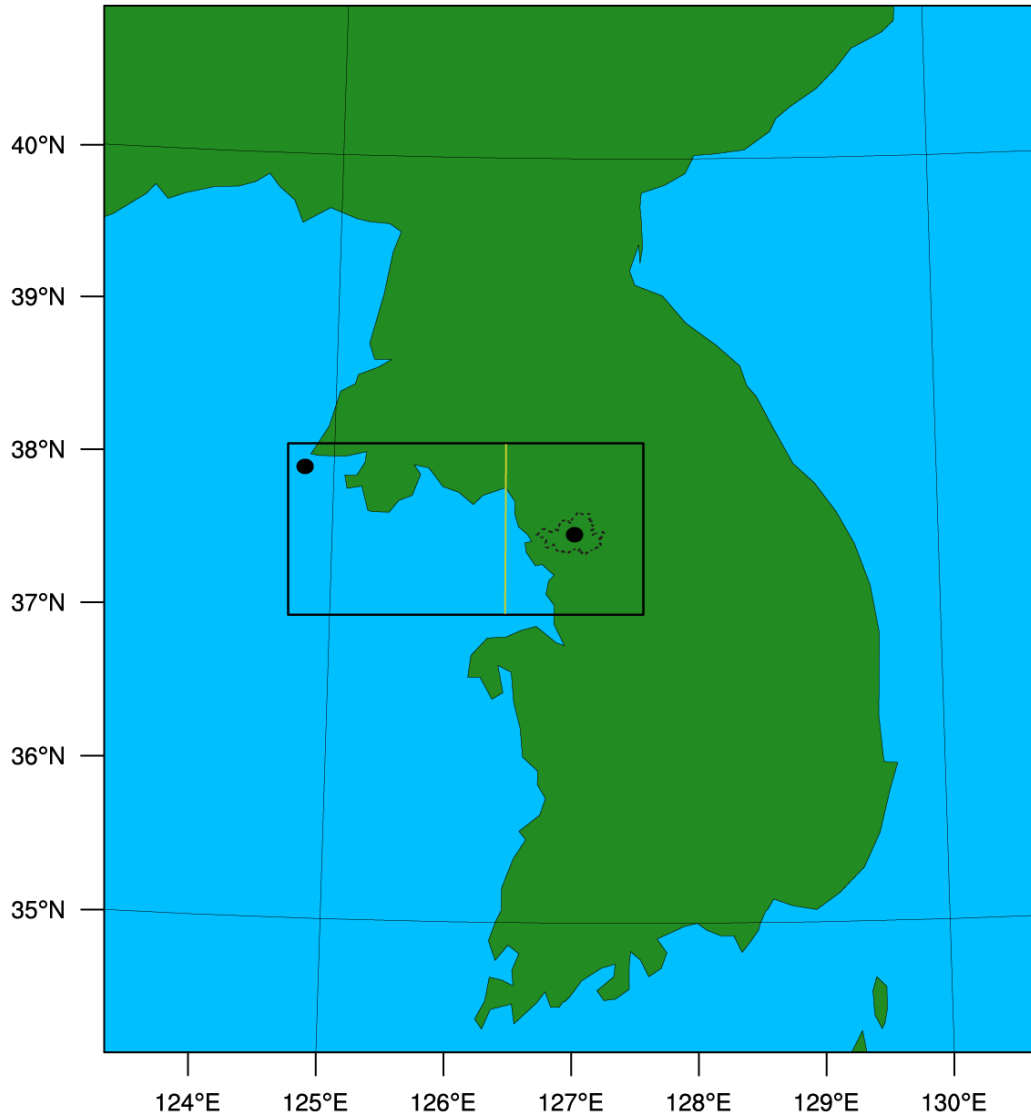
1658

1659

1660

1661





1662

1663

1664

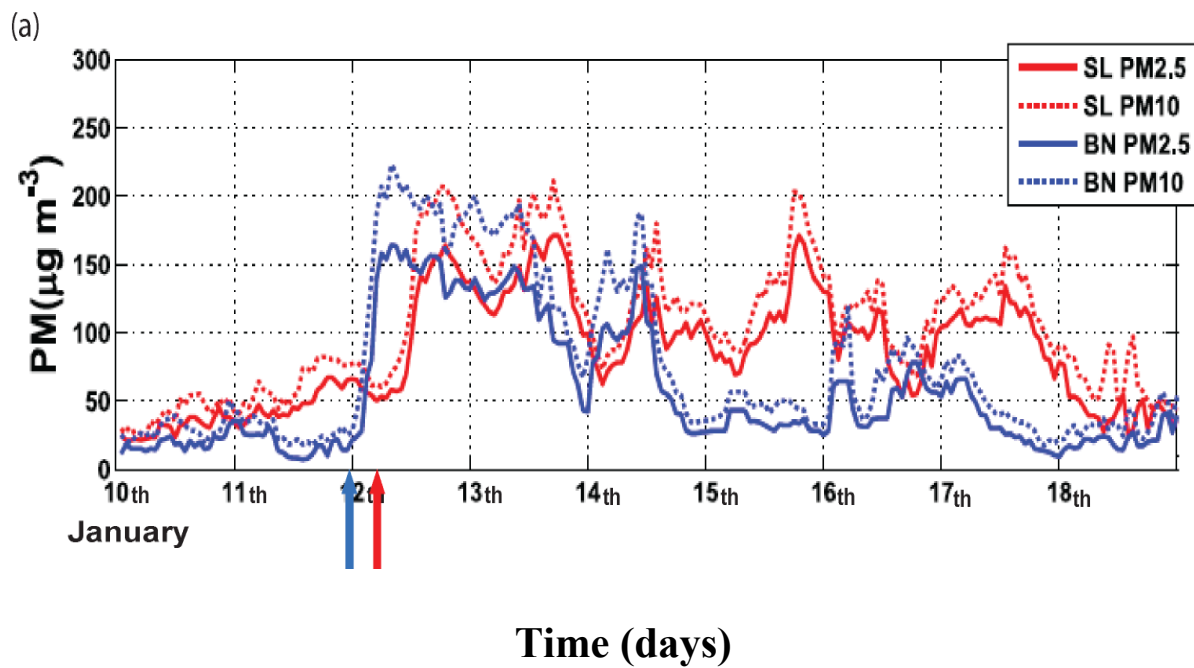
1665

1666

1667

1668

**Figure 1**



1669

1670

1671

1672

1673

1674

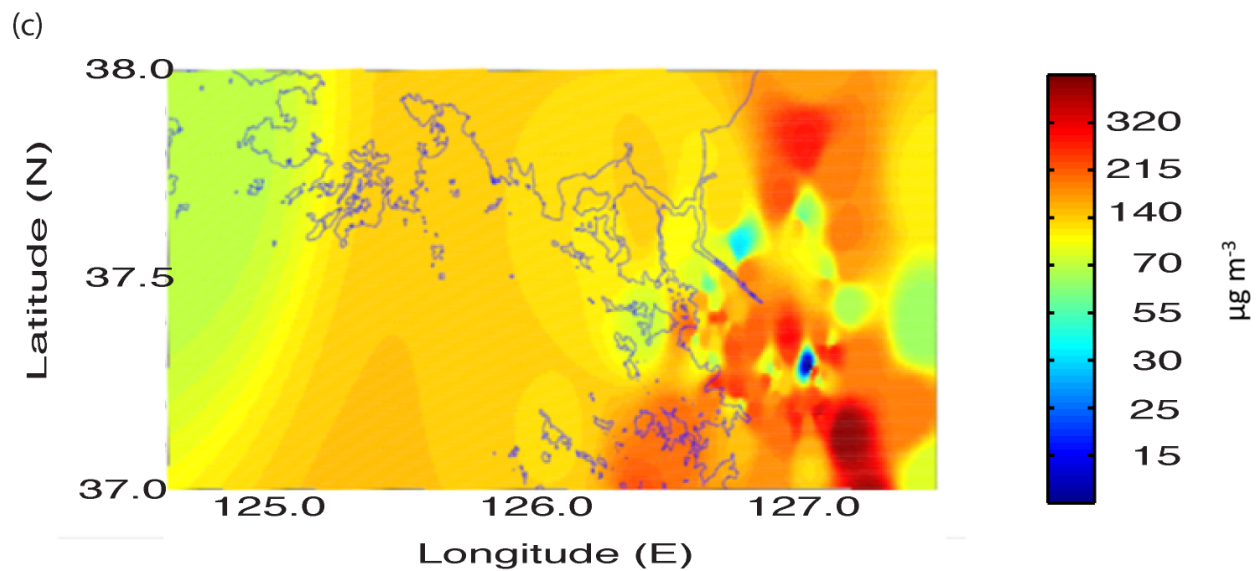
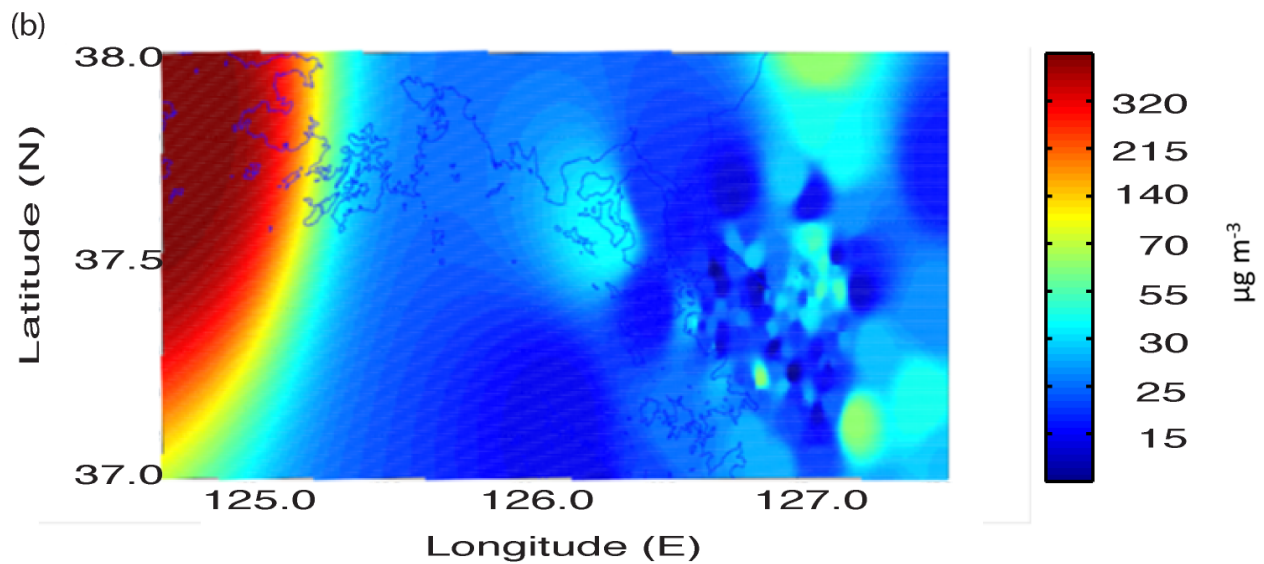
1675

1676

1677

1678

Figure 2a



1679

1680

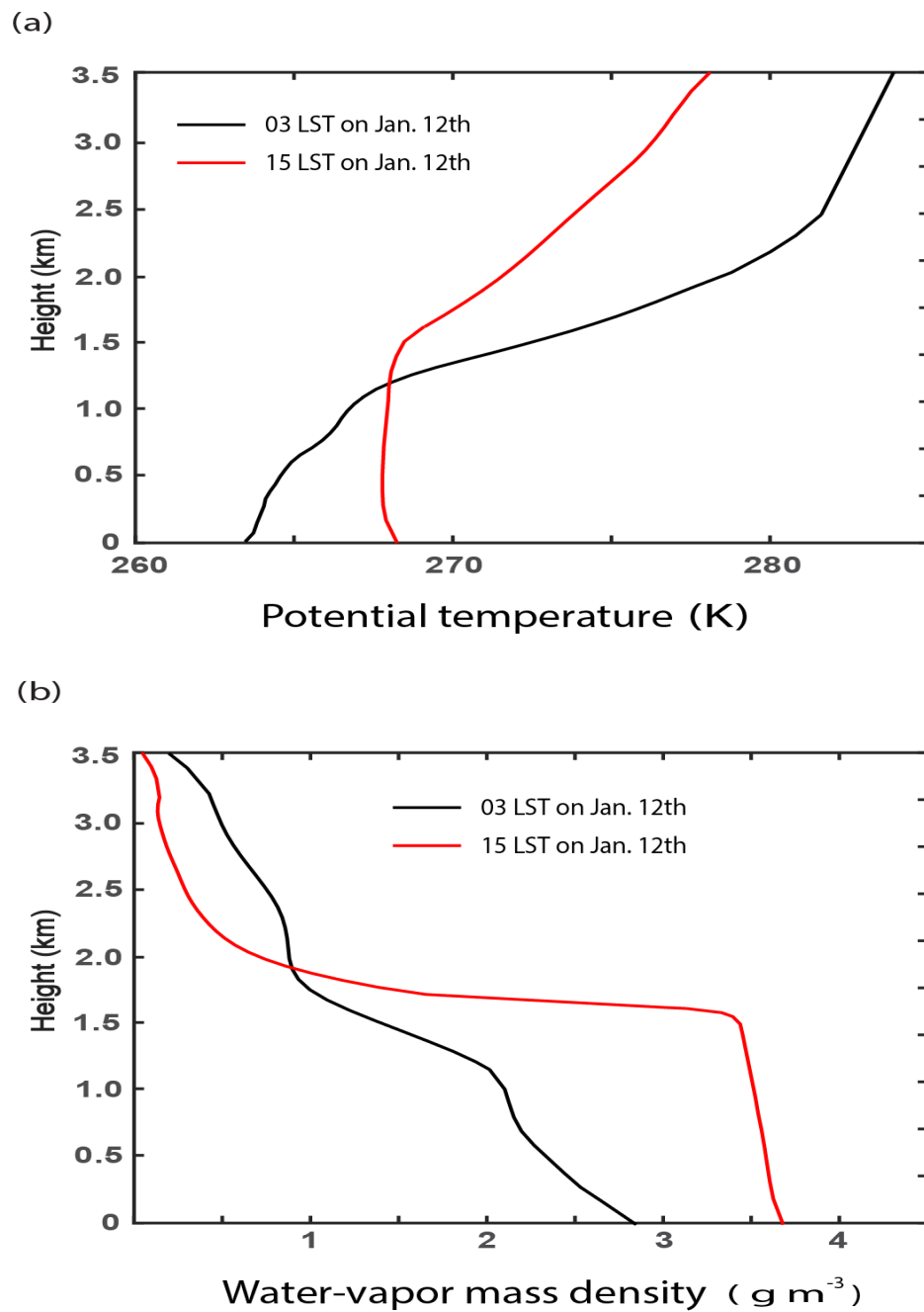
1681

1682

1683

1684

**Figures 2b and 2c**



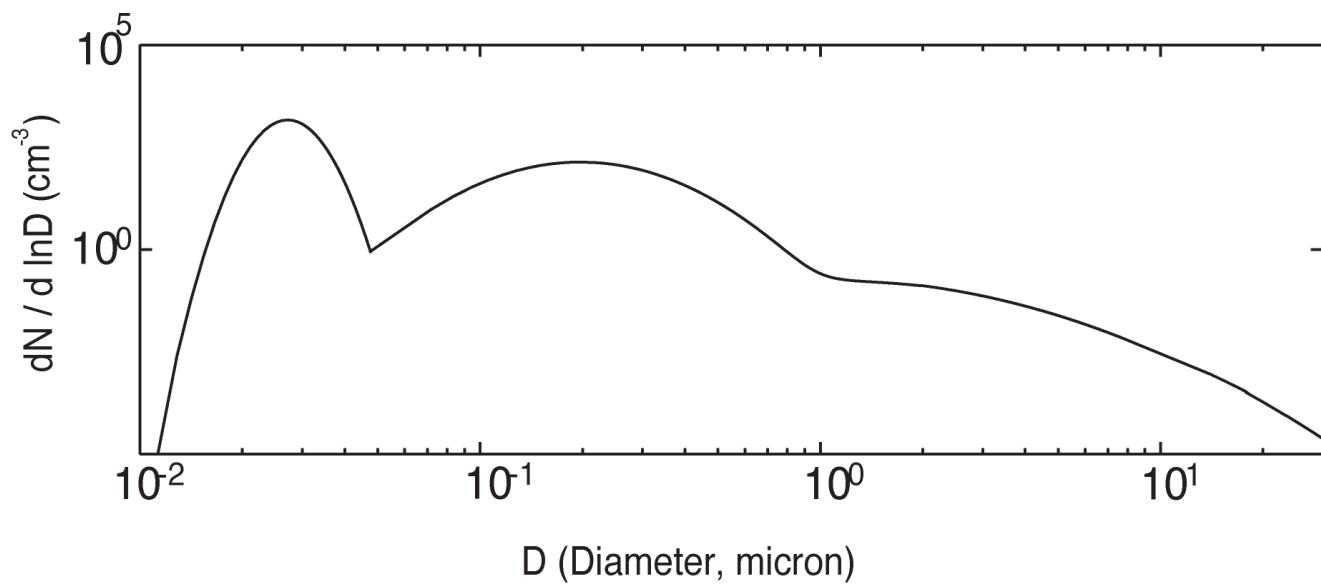
1685

1686

1687

1688

**Figure 3**



1689

1690

1691

1692

1693

1694

1695

1696

1697

1698

1699

1700

1701

1702

1703

1704

1705

1706

1707

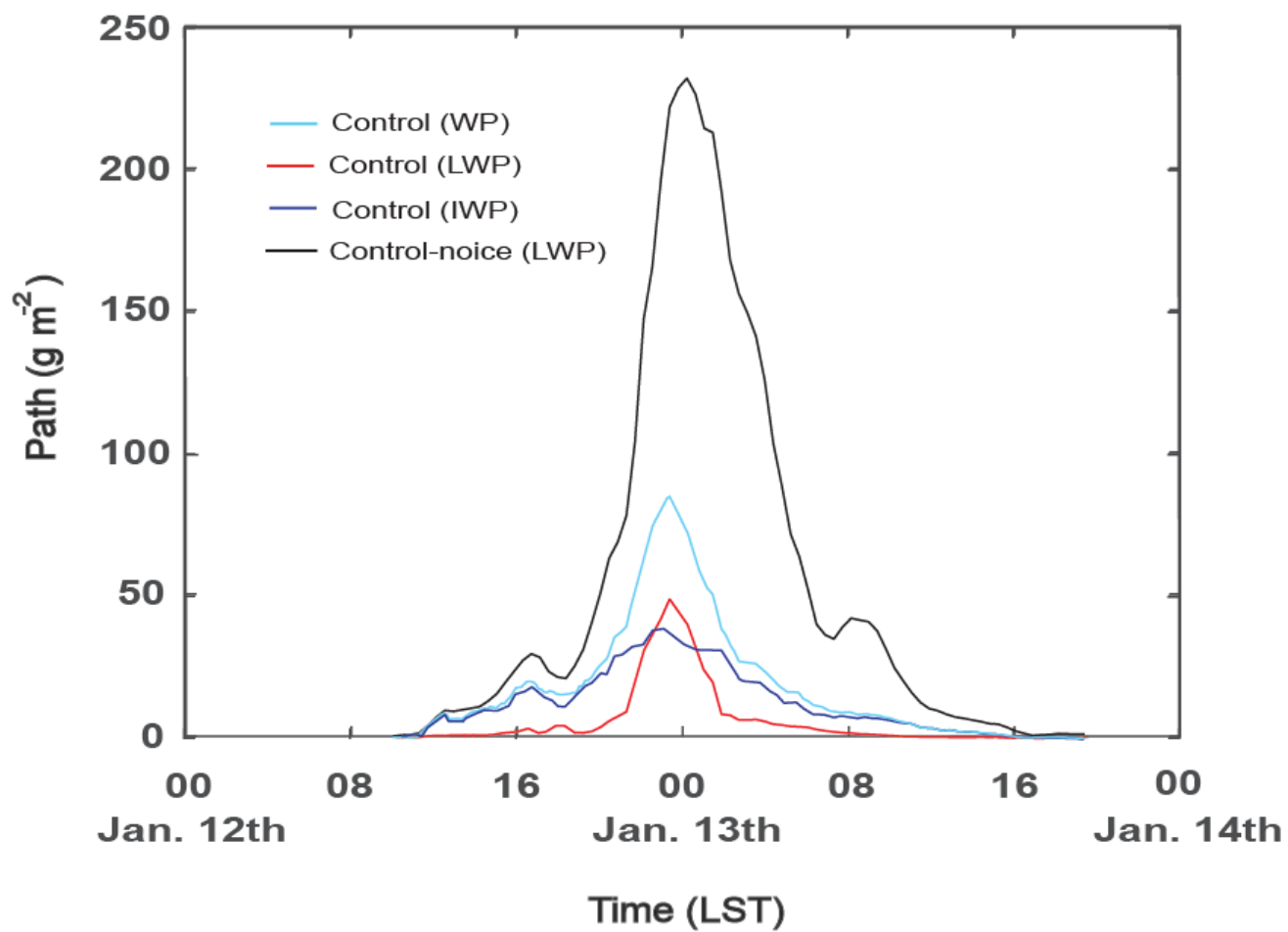
1708

1709

1710

**Figure 4**

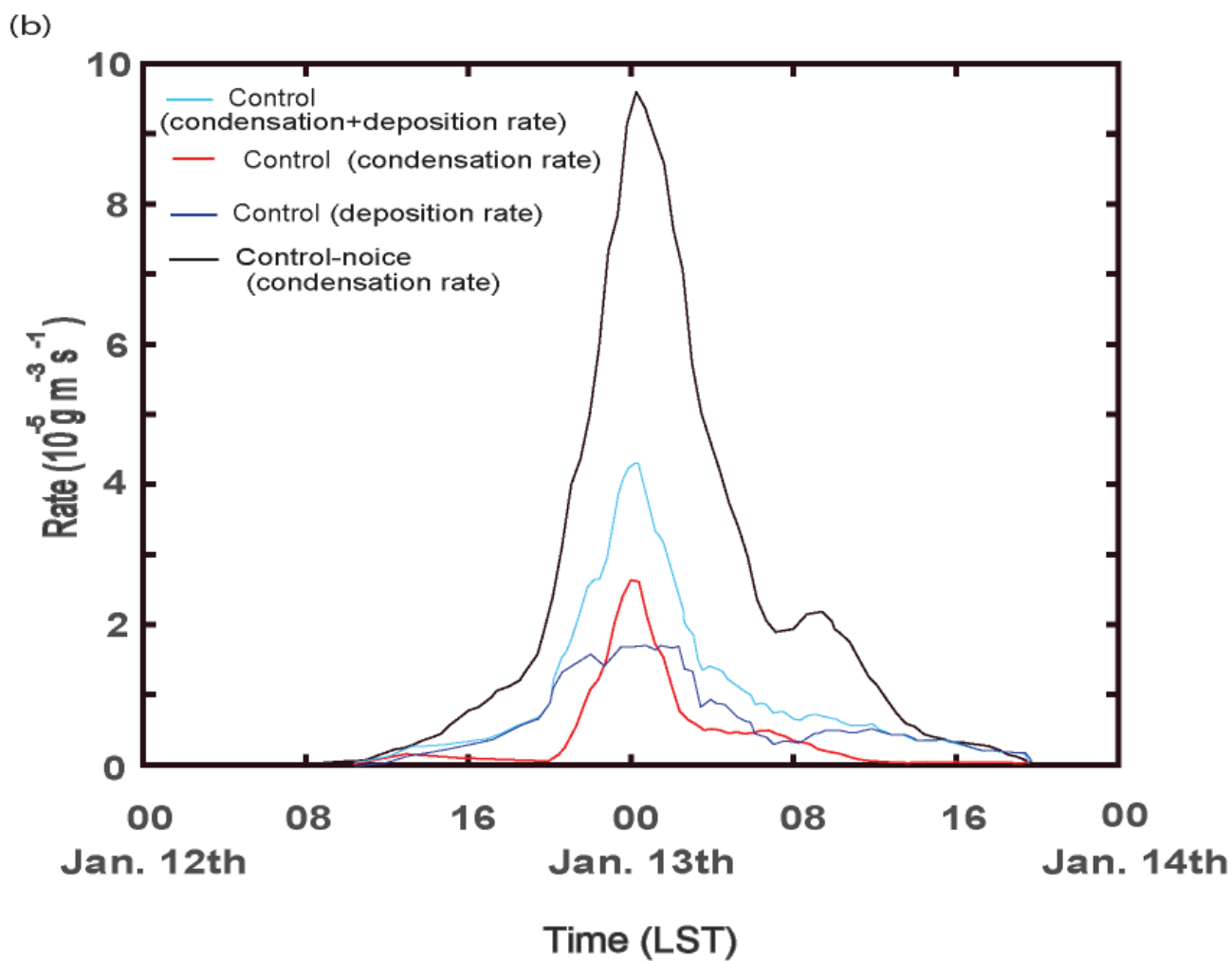
(a)

**Figure 5a**

1711  
1712  
1713  
1714  
1715  
1716  
1717  
1718  
1719  
1720  
1721  
1722  
1723

1724

1725



1726

1727

1728

1729

1730

1731

1732

1733

1734

1735

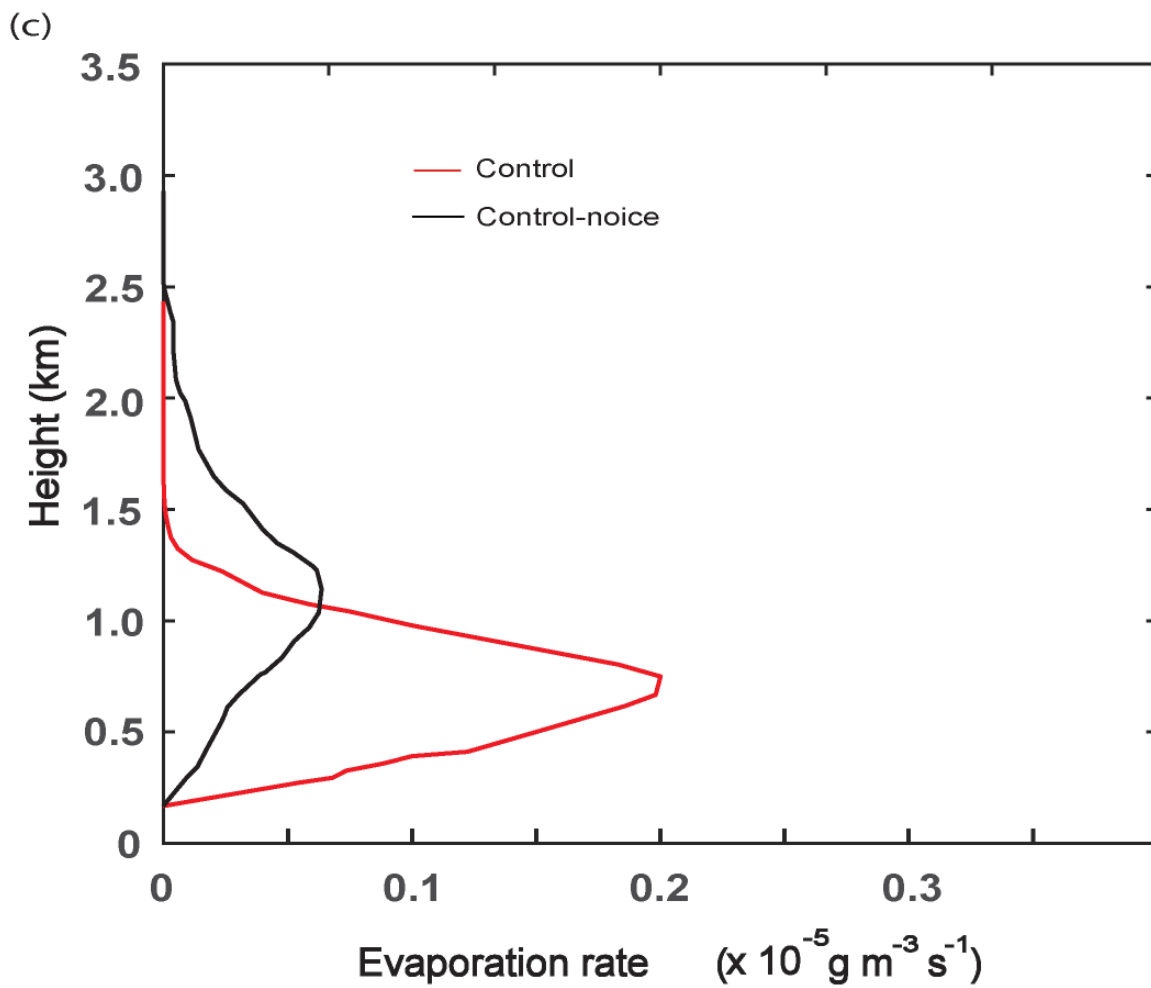
1736

1737

1738

**Figure 5b**

1739



1740

1741

1742

1743

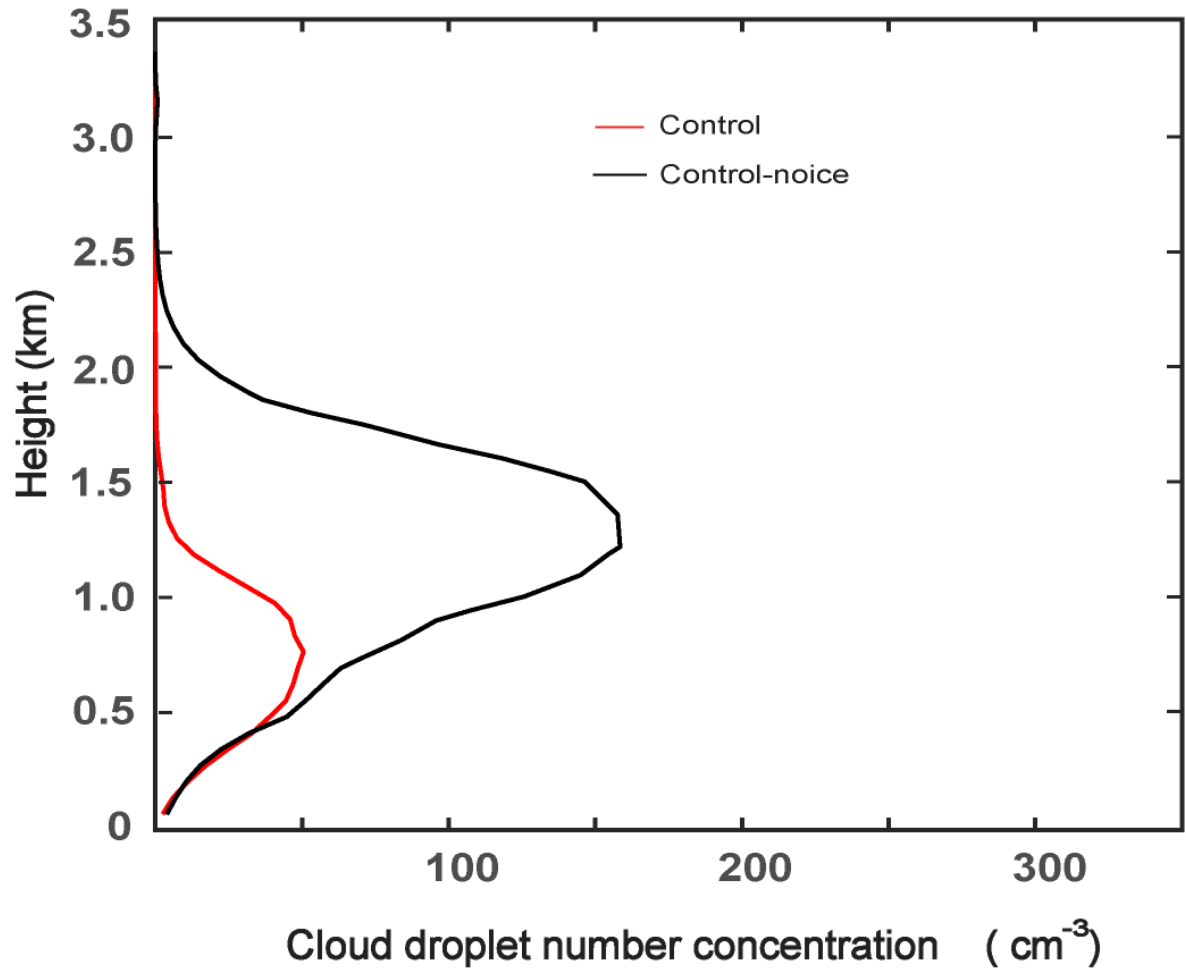
**Figure 5c**

1744

1745



(d)



1746

1747

1748

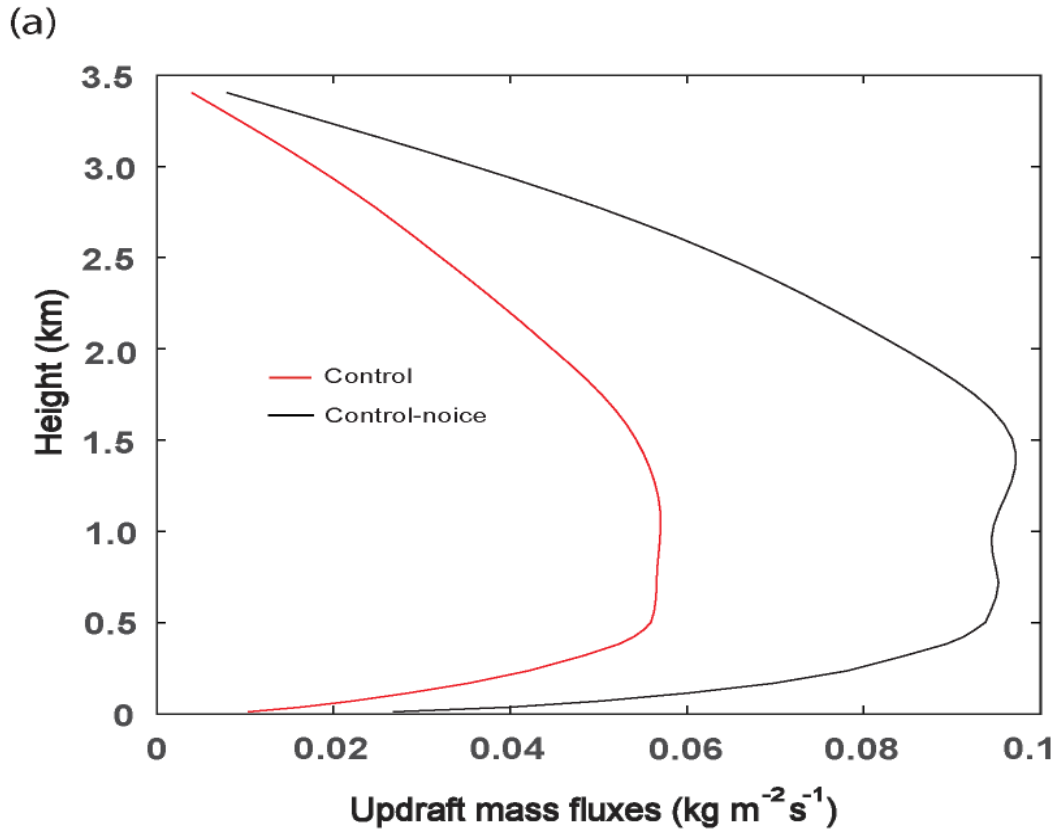
1749

1750

1751

1752

**Figure 5d**



1753

1754

**Figure 6a**

1755

1756

1757

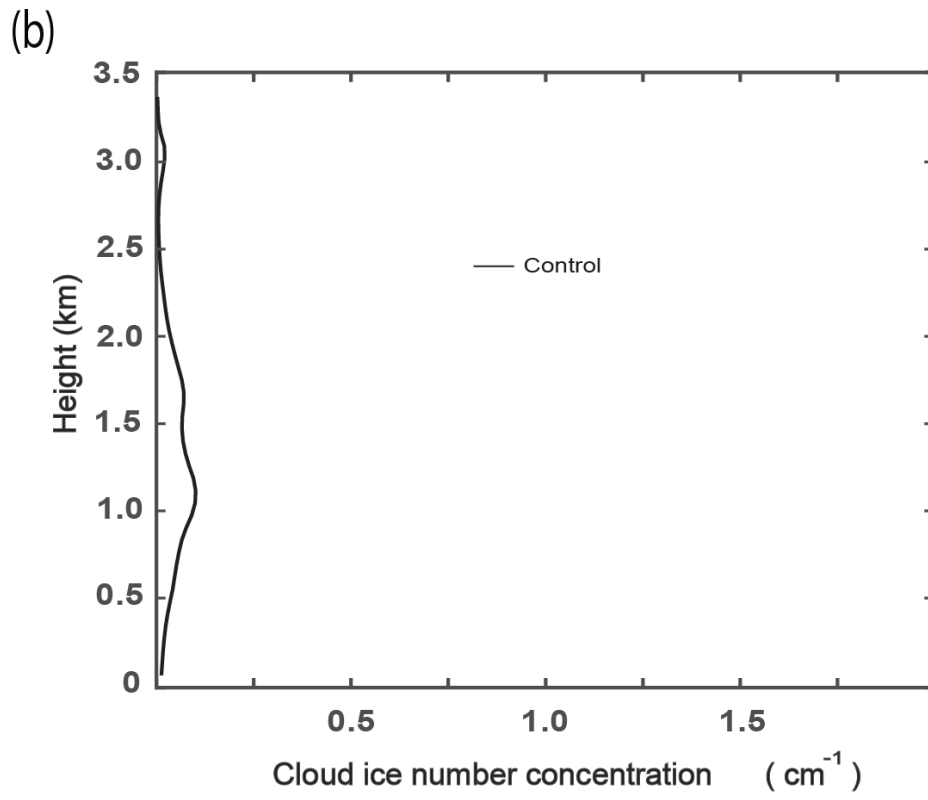
1758

1759

1760

1761

1762



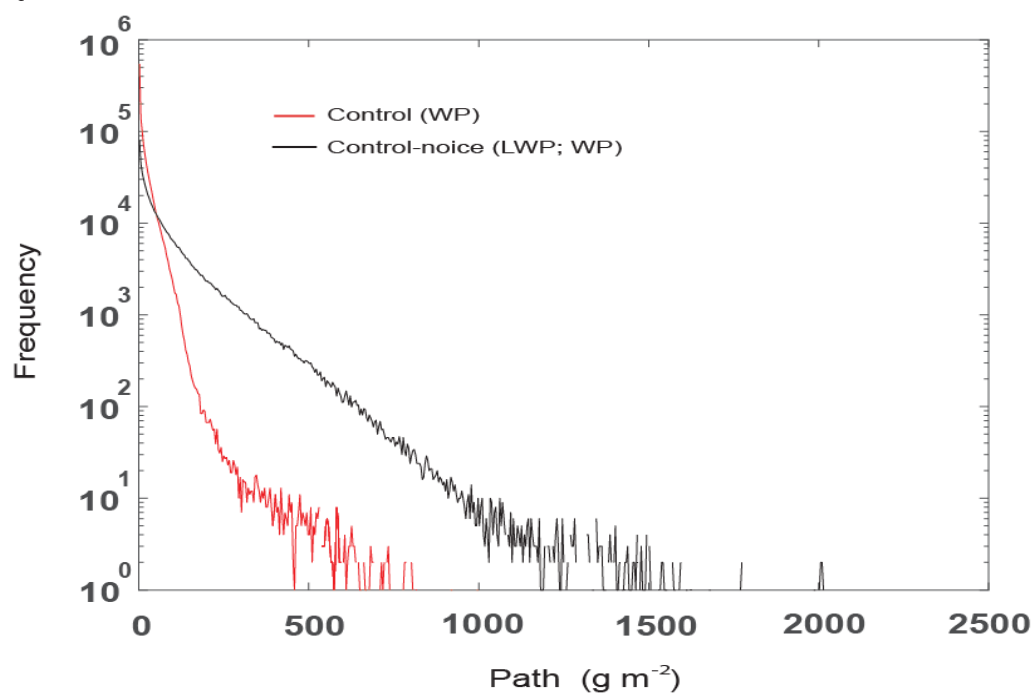
1763

1764

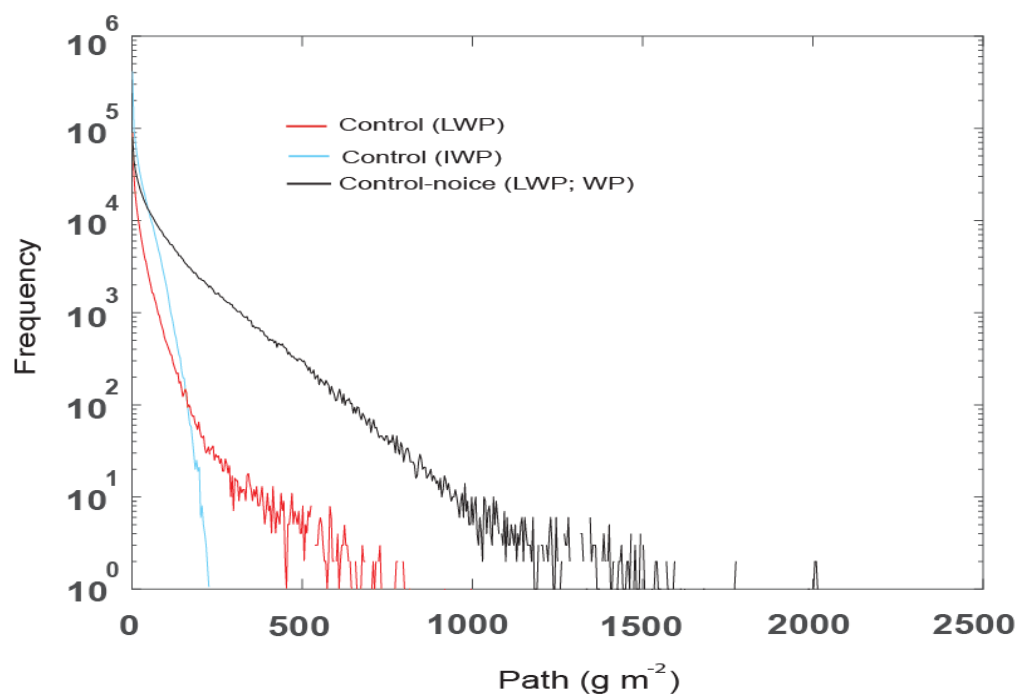
1765

**Figure 6b**

(a)



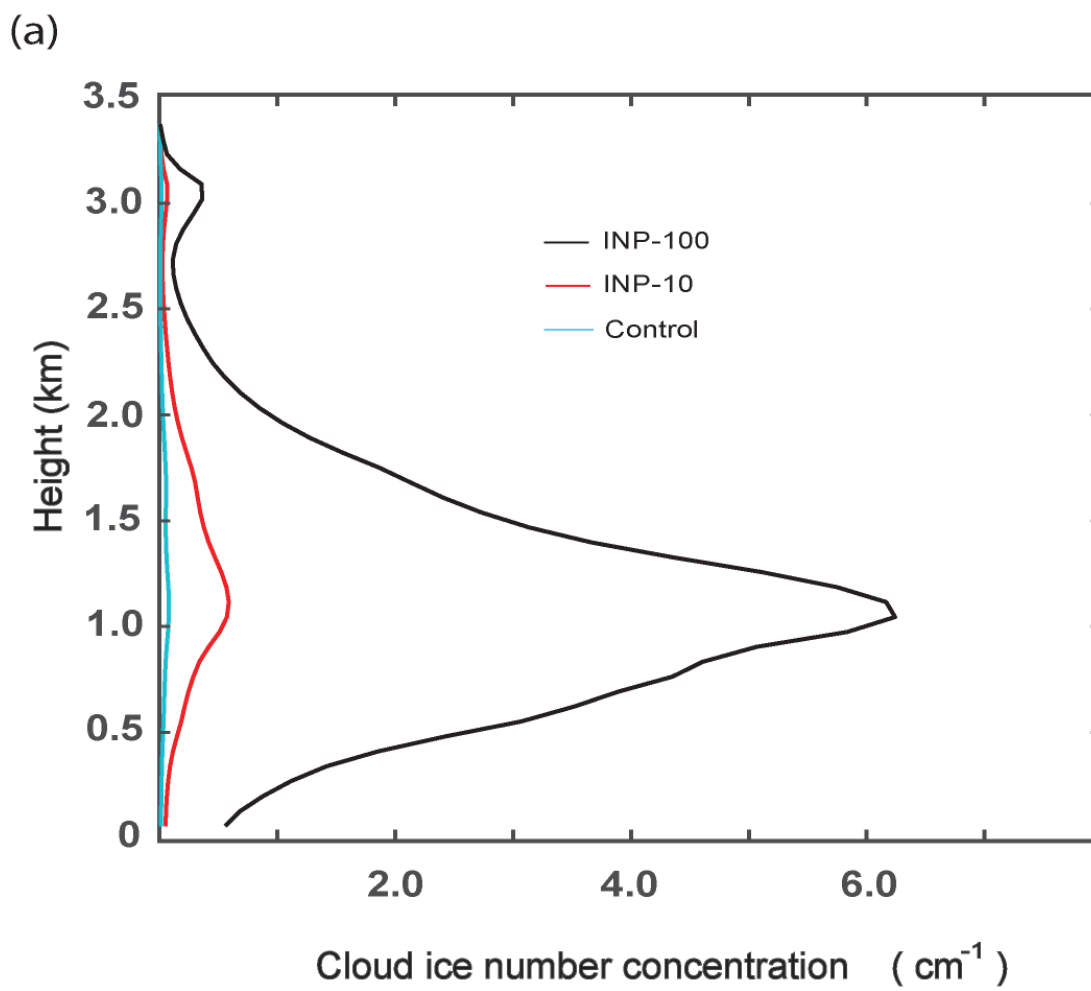
(b)



1766

1767

**Figures 7a and 7b**



1768

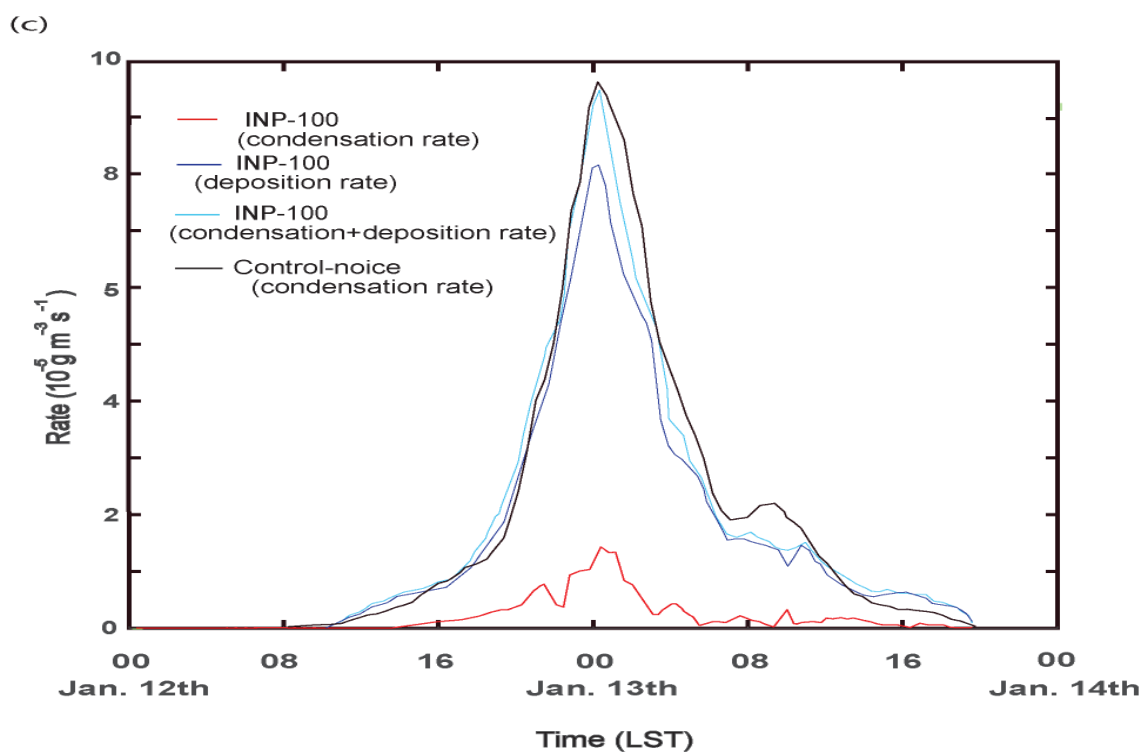
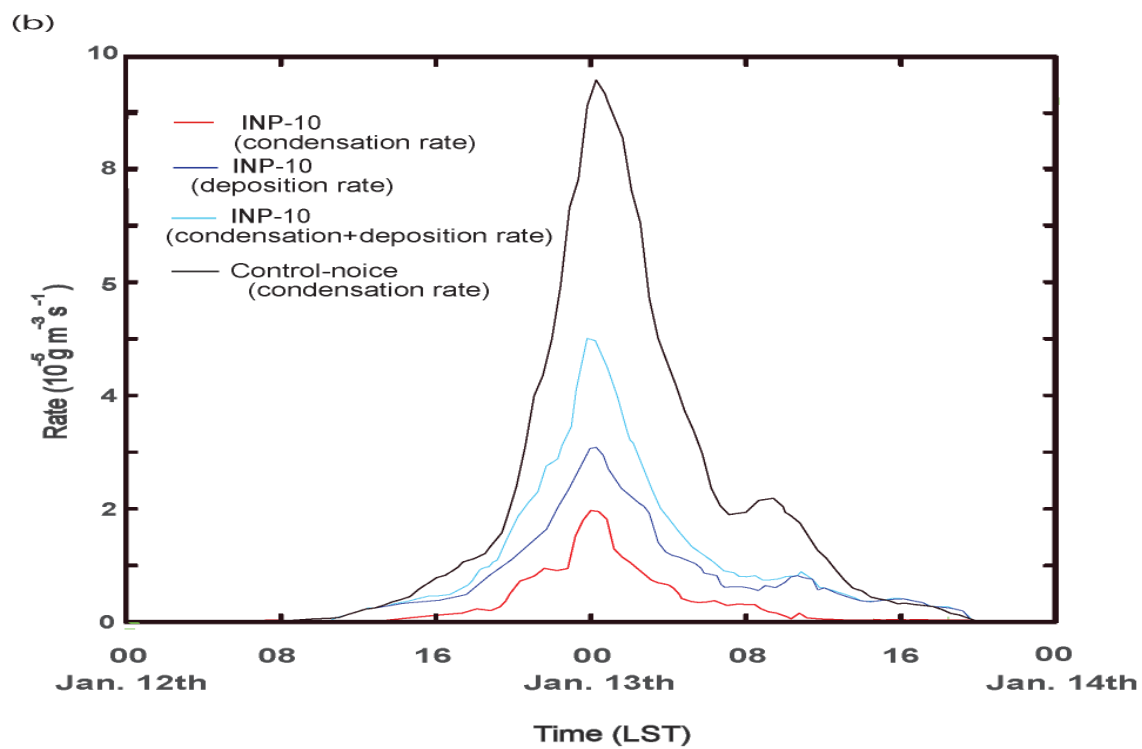
1769

1770

1771

1772

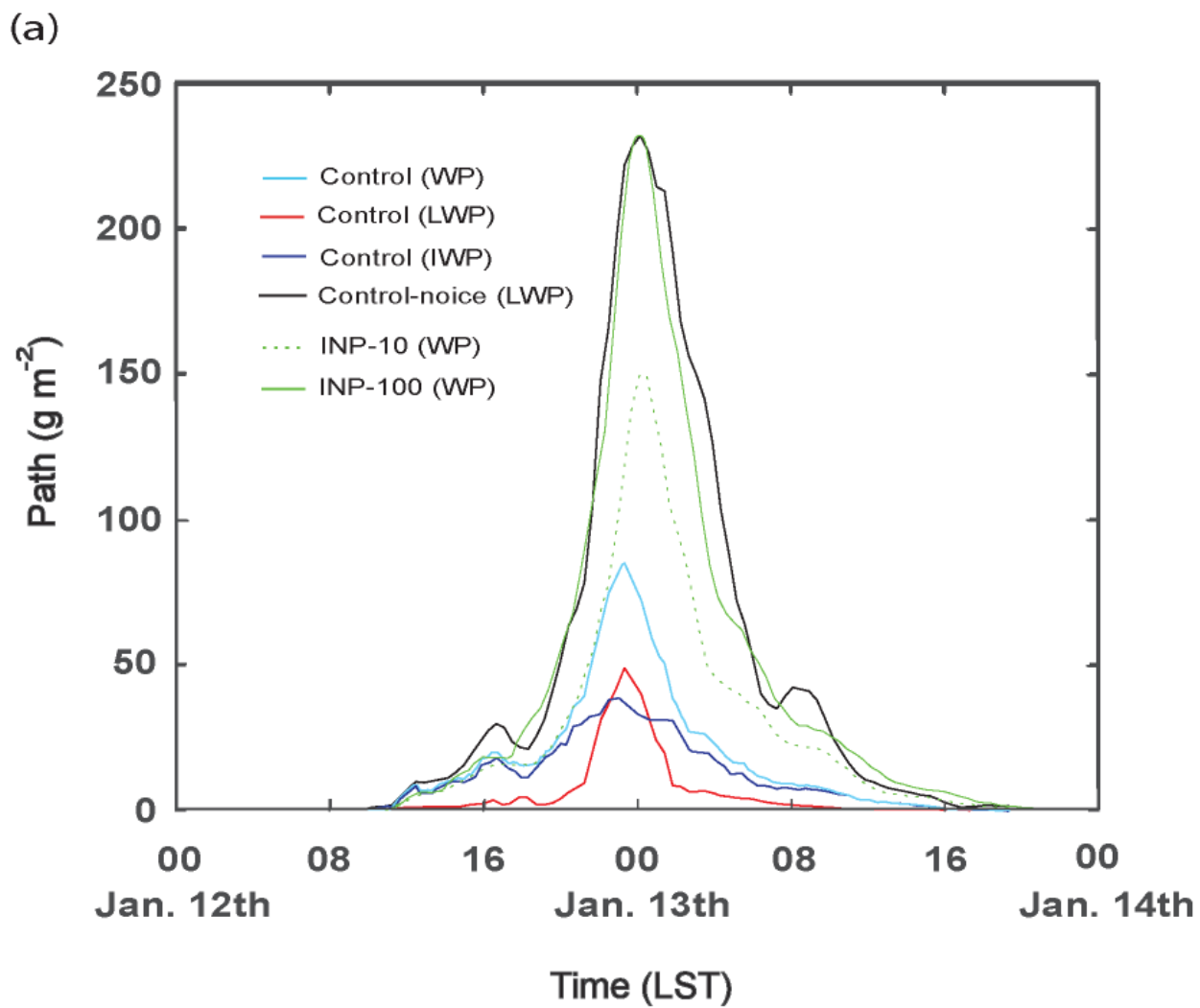
**Figure 8a**



1773

1774

**Figures 8b and 8c**



1775

1776

1777

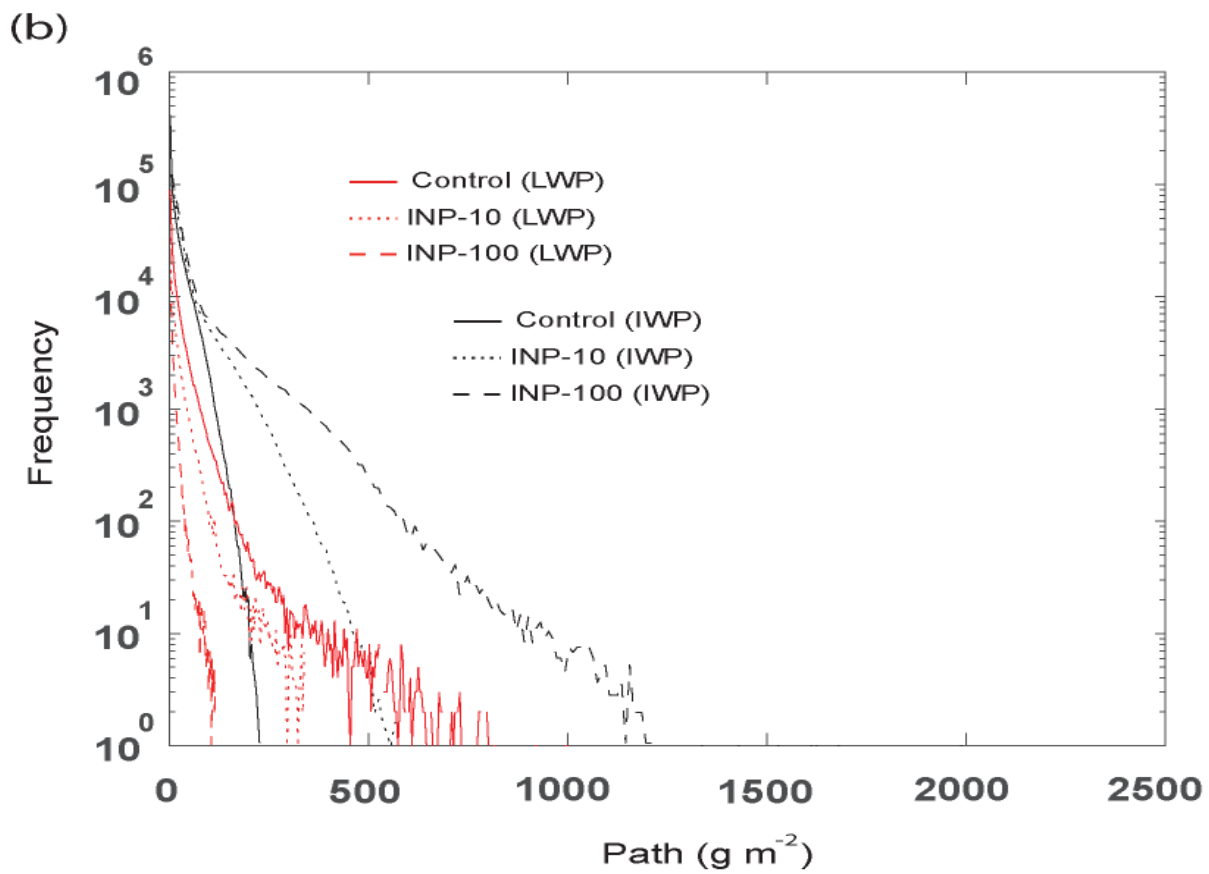
1778

1779

1780

1781

**Figure 9a**



1782

1783

**Figure 9b**

1784

1785

1786

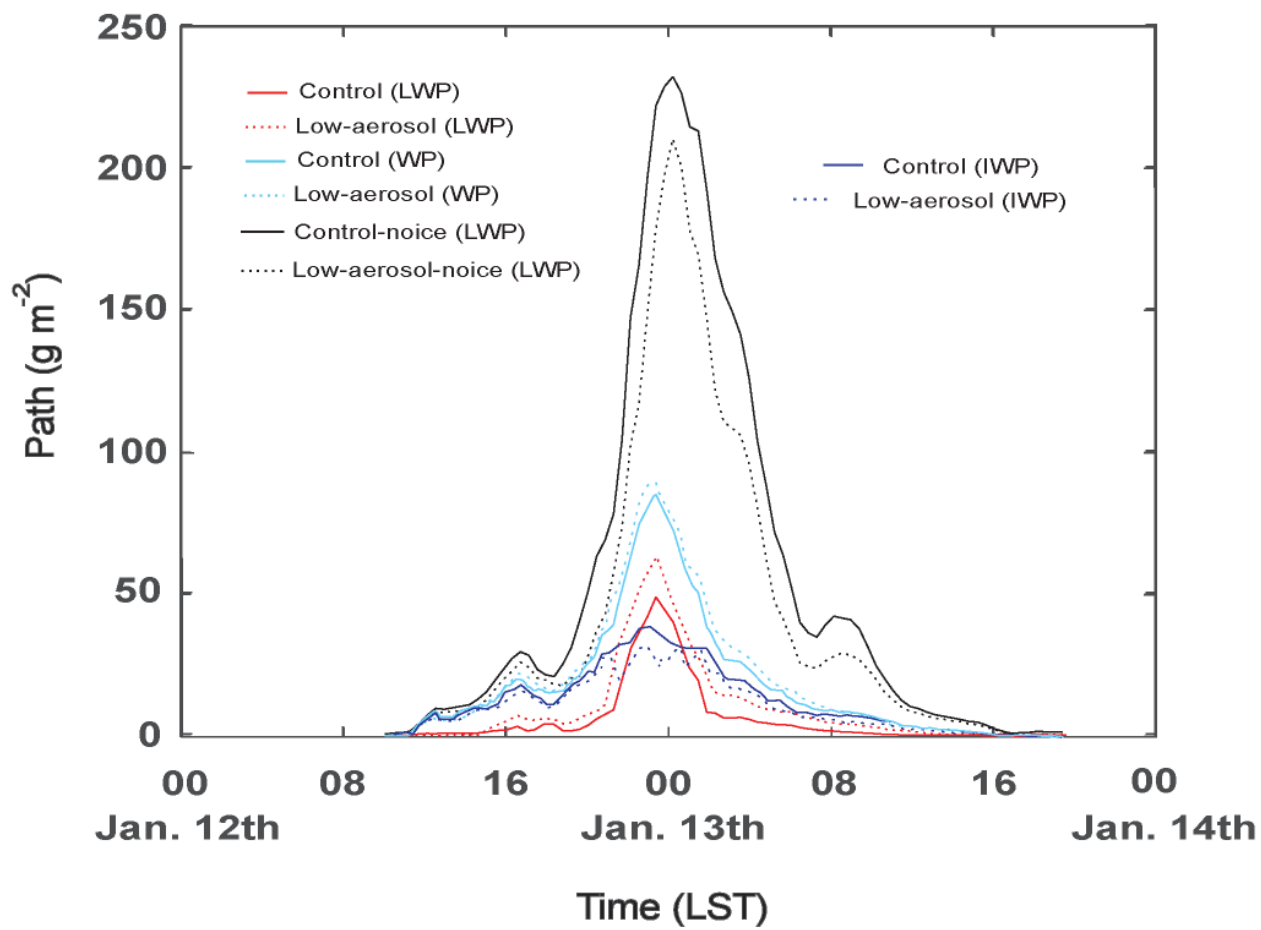
1787

1788

1789



(a)



1790

1791

**Figure 10a**

1792

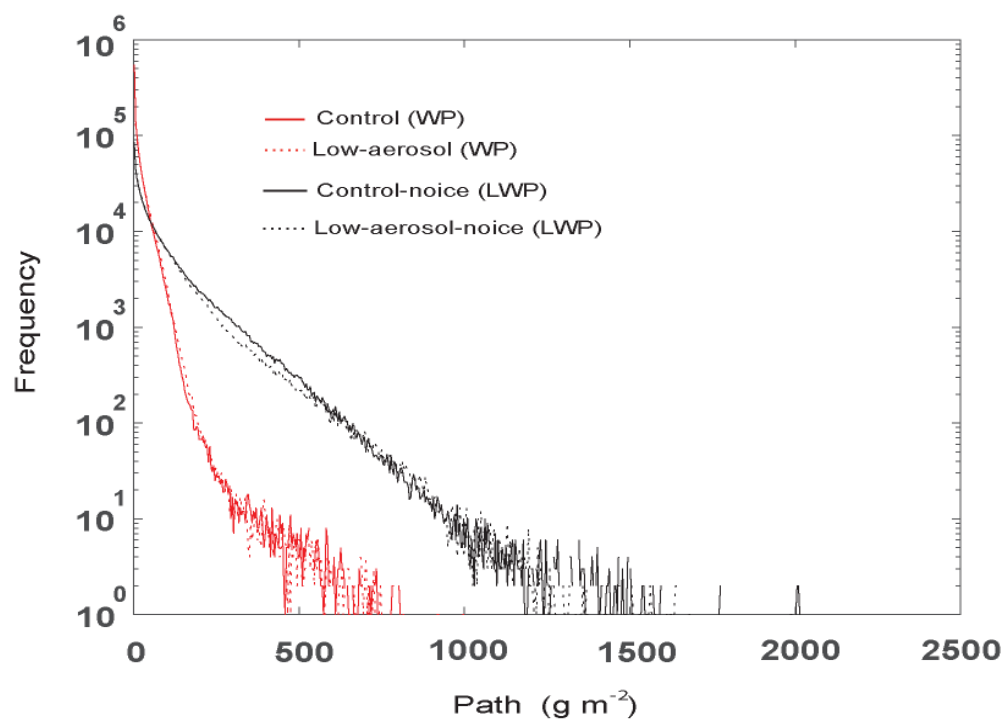
1793

1794

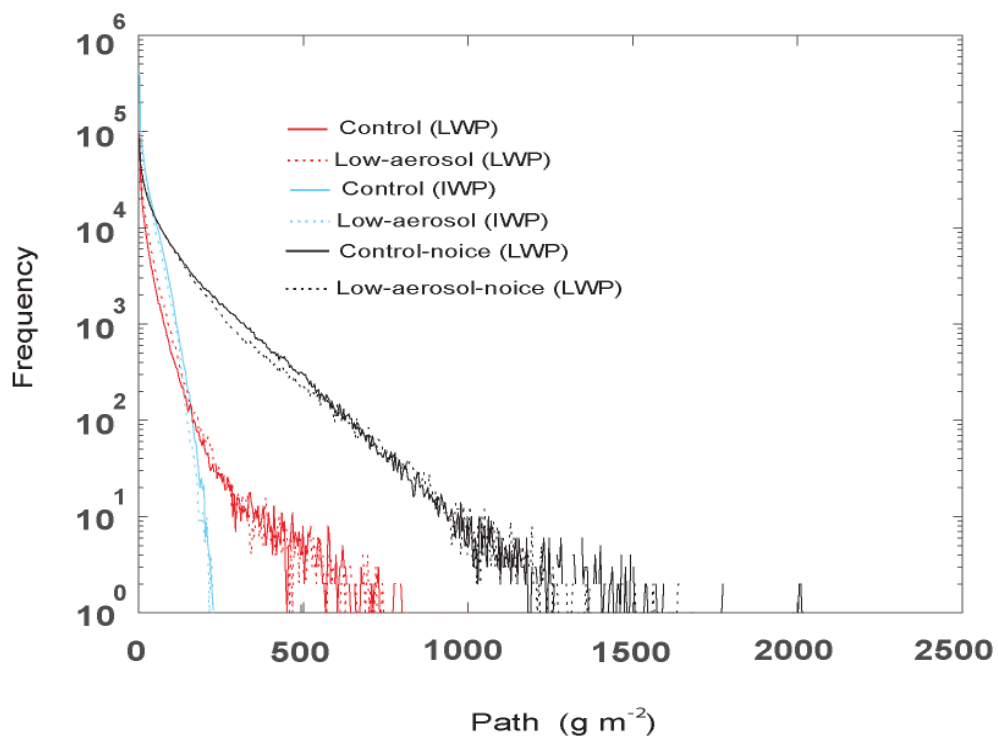
1795

1796

(b)



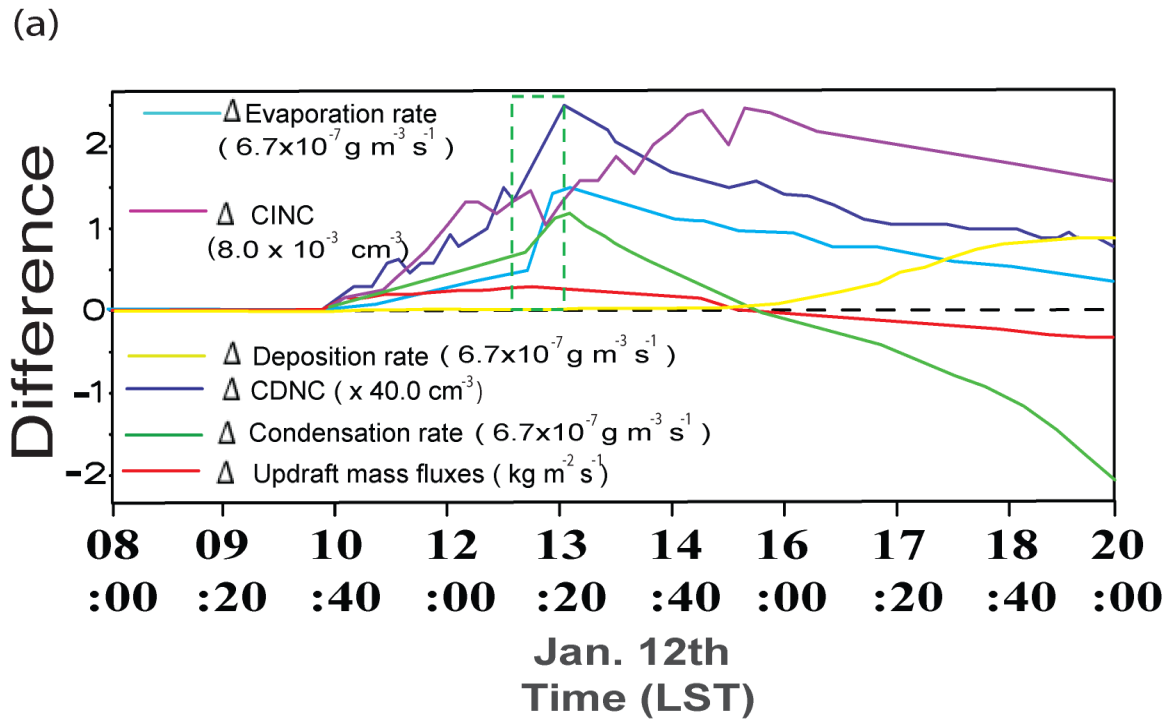
(c)



1797

1798

**Figures 10b and 10c**



1799

1800

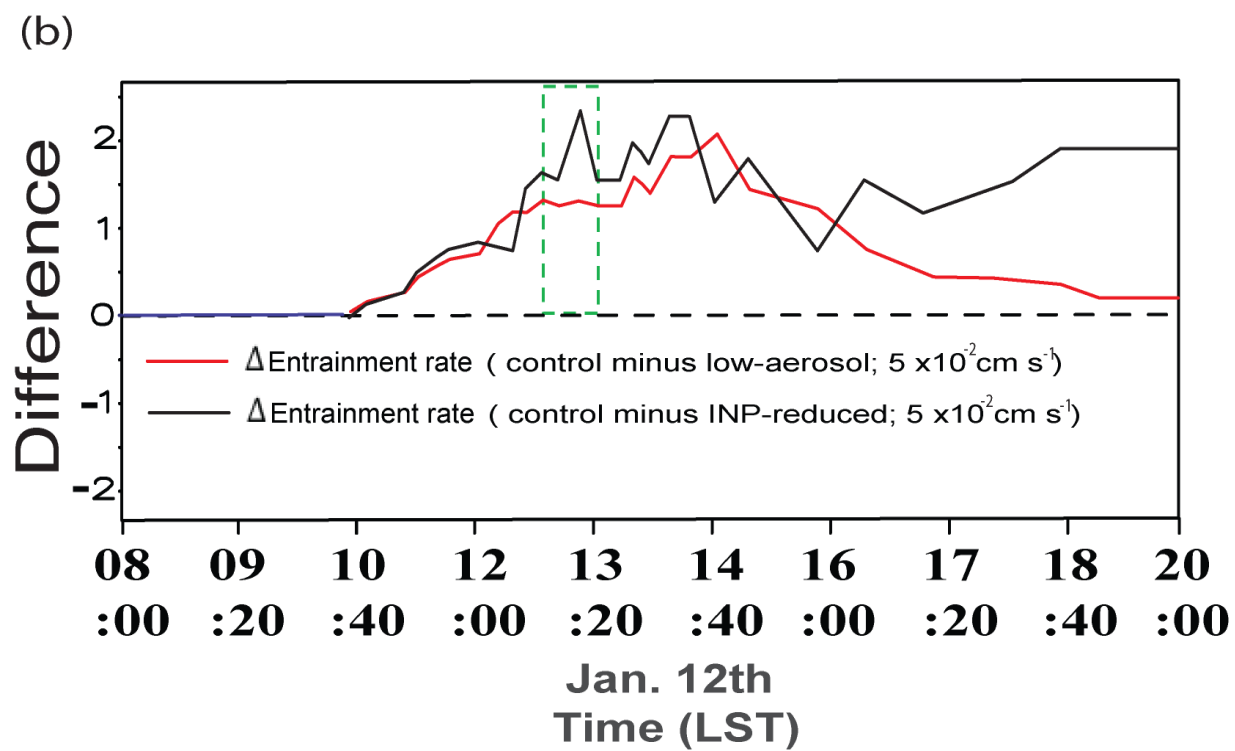
1801

1802

1803

1804

Figure 11a



1805

1806

Figure 11b

1807

1808

1809

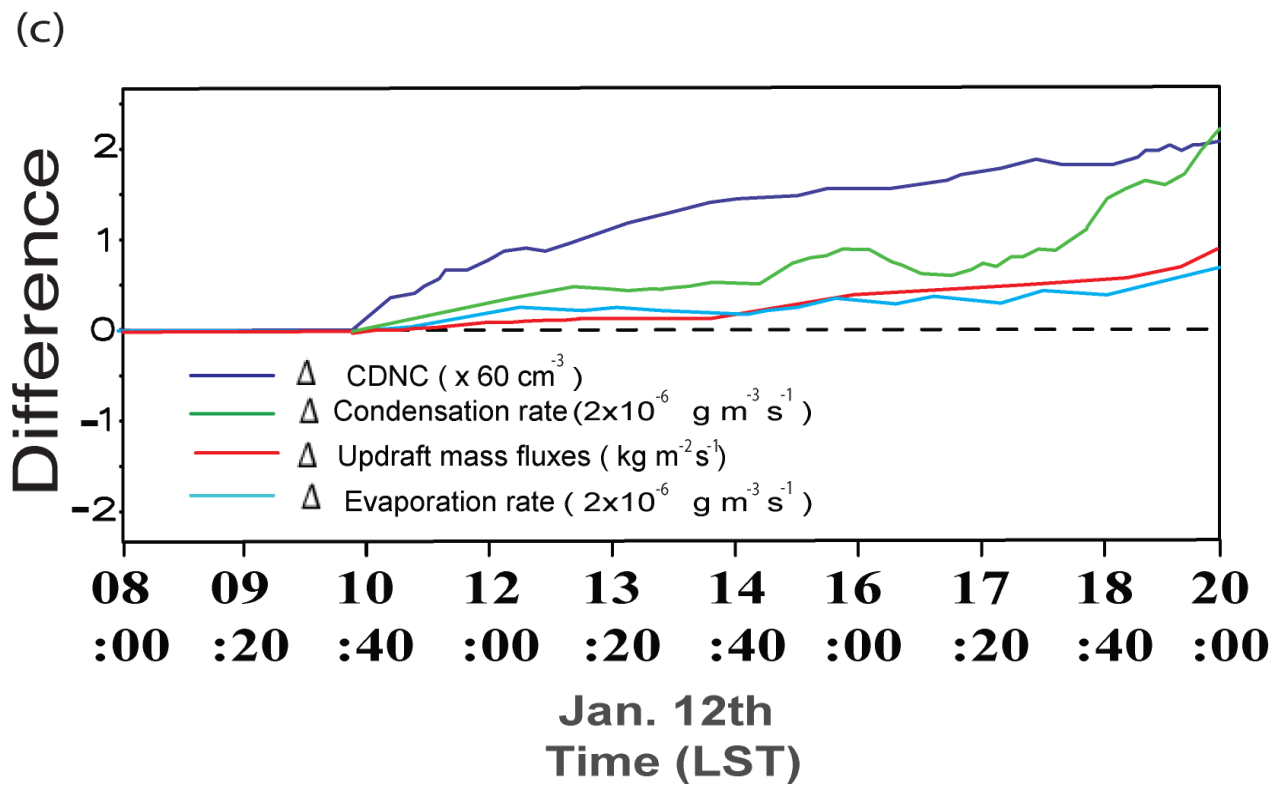
1810

1811

1812

1813

1814



1815

1816

Figure 11c

1817

1818

1819

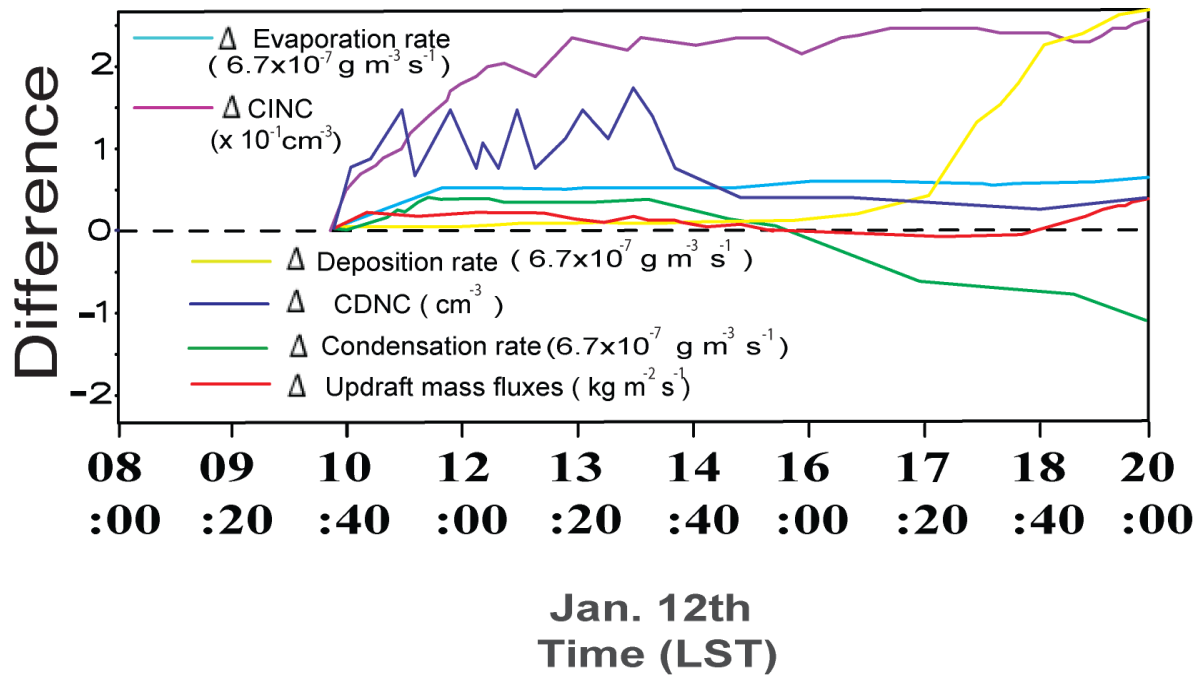
1820

1821

1822

1823

(d)



1824

1825

Figure 11d

1826

1827

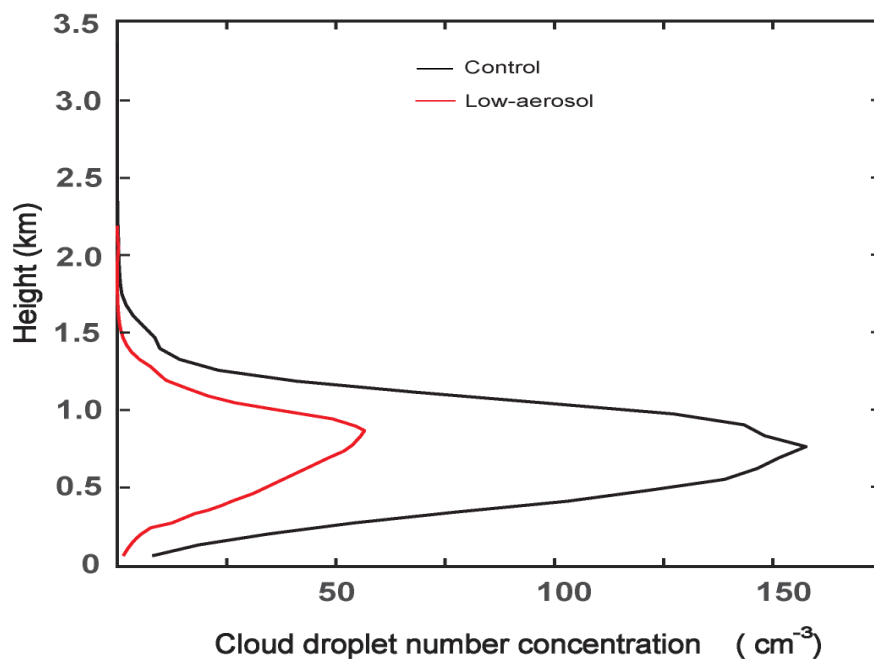
1828

1829

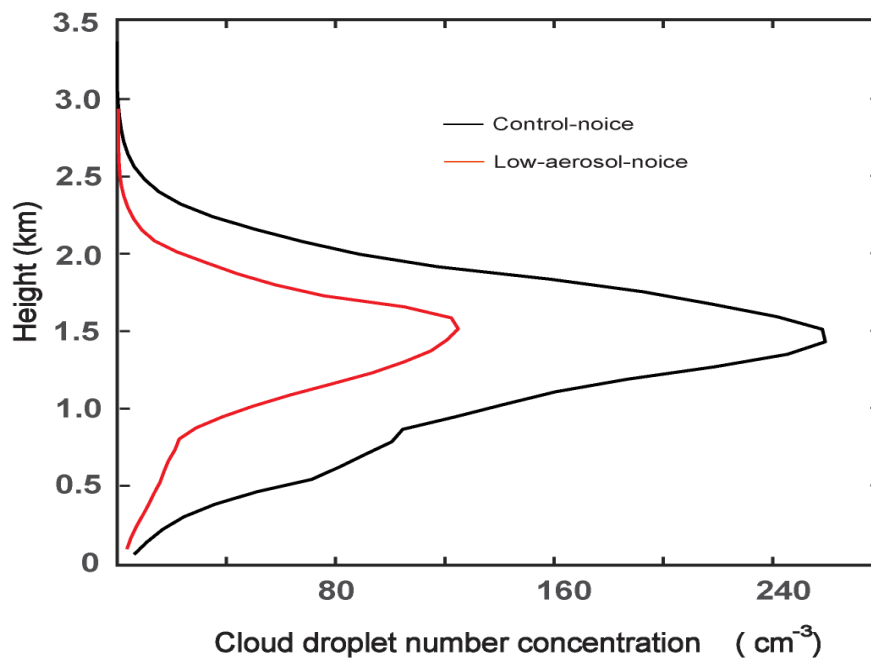
1830

1831

(a)



(b)

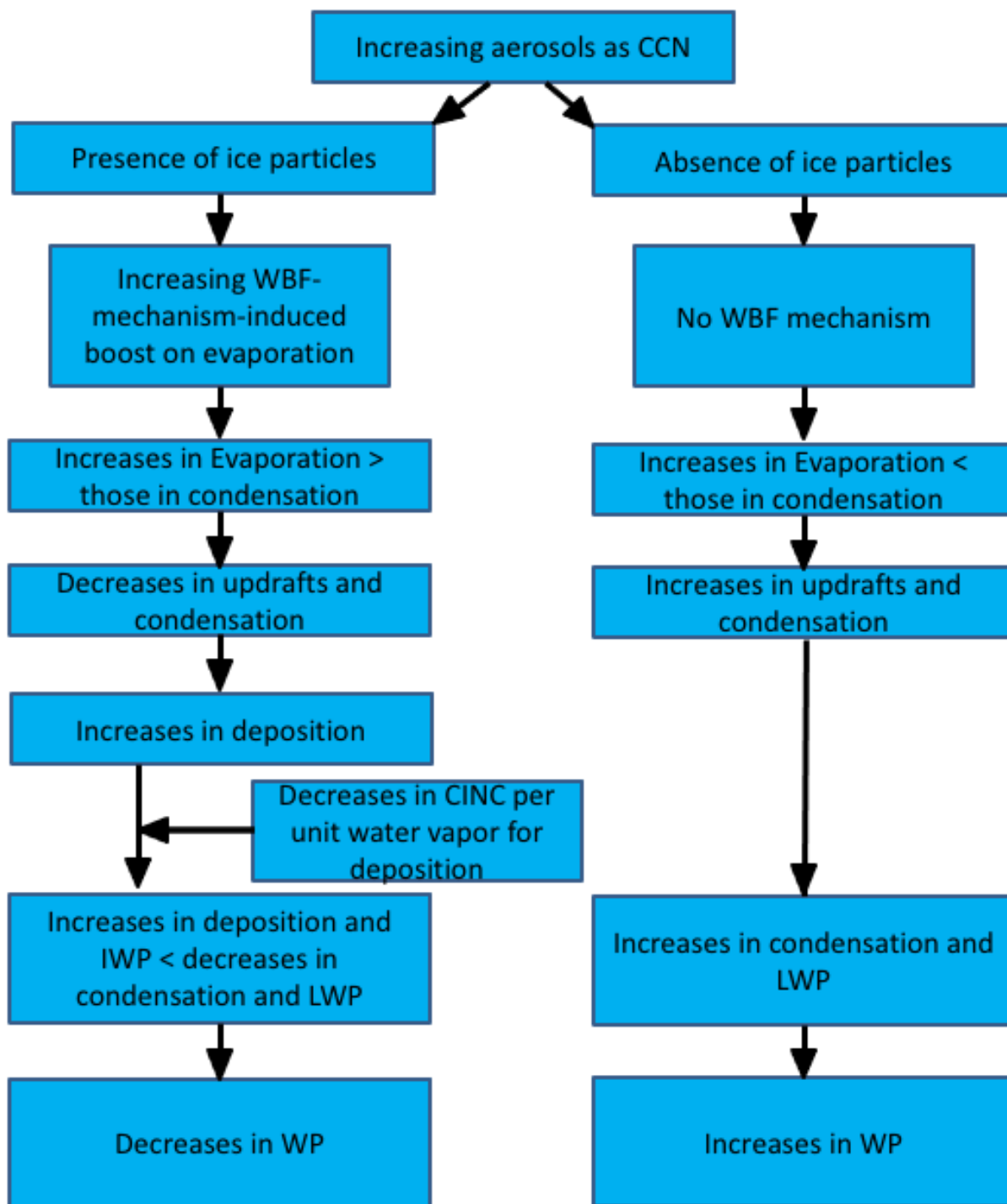


1832

1833

**Figures 12a and 12b**

1834

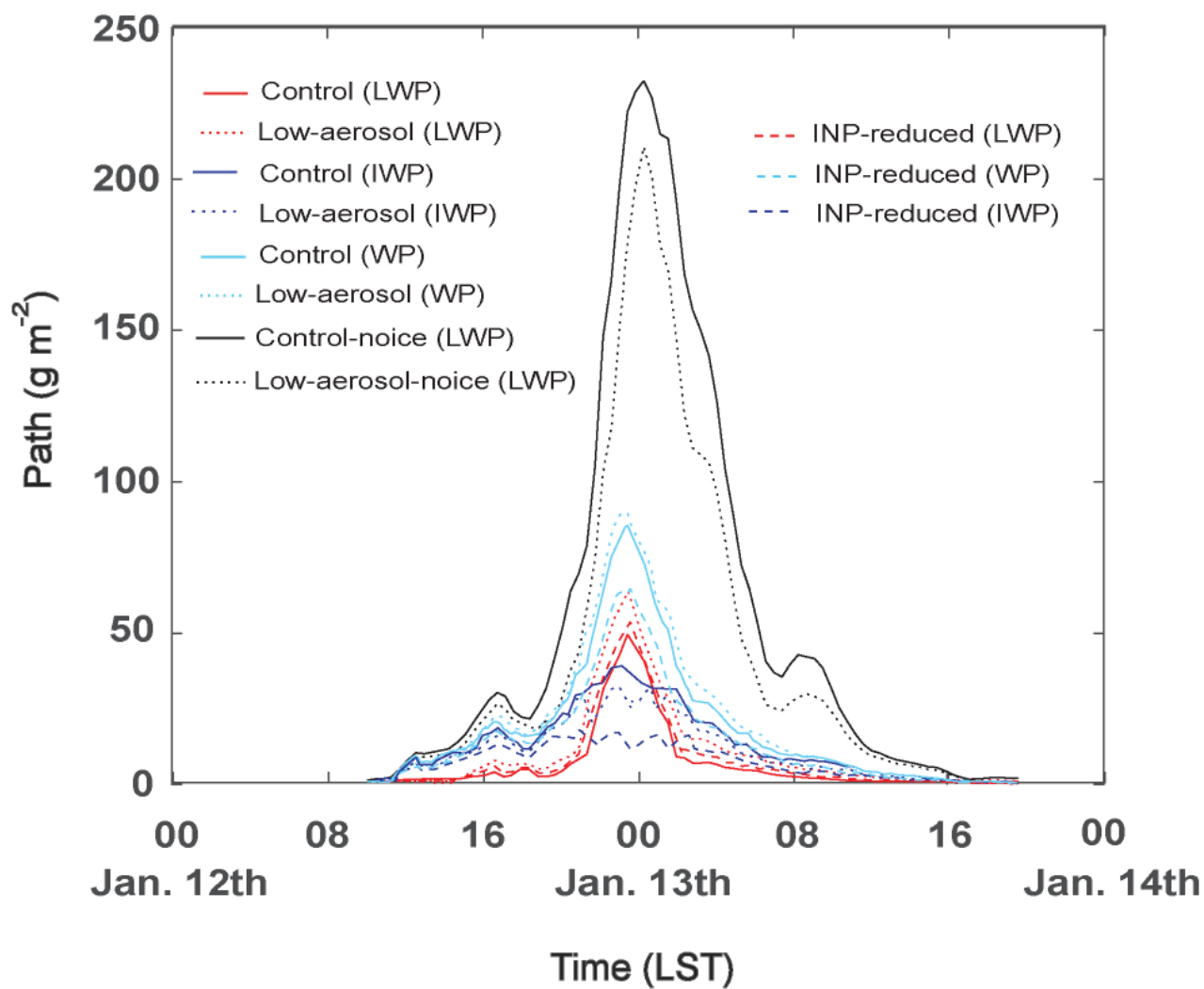


1835

1836

Figure 13





1837

1838

1839

1840

**Figure 14**